UNIVERSITI TEKNOLOGI MARA

DESIGN AND DEVELOPMENT OF A LORA-BASED GROUND SENSOR TERMINAL FOR L-BAND SATELLITE IOT APPLICATIONS

MOHD FARID BIN OMAR

MSc

March 2026

UNIVERSITI TEKNOLOGI MARA

DESIGN AND DEVELOPMENT OF A LORA-BASED GROUND SENSOR TERMINAL FOR L-BAND SATELLITE IOT APPLICATIONS

MOHD FARID BIN OMAR

Thesis submitted in fulfilment
of the requirements for the degree of
Master of Science
(Electrical Engineering)

Faculty of Electrical Engineering

March 2026

CONFIRMATION BY PANEL OF EXAMINERS

I certify that a Panel of Examiners has met on 28 November 2025 to conduct the final examination of Mohd Farid bin Omar on his Master of Science thesis entitled "Design and Development of a LoRa-Based Ground Sensor Terminal for L-Band Satellite IoT Applications" in accordance with Universiti Teknologi MARA Act 1976 (Akta 173). The Panel of Examiners recommends that the student be awarded the relevant degree. The Panel of Examiners was as follows:

Sukreen Hana Herman, PhD
Associate Professor
Faculty of Electrical Engineering
Universiti Teknologi MARA
(Chairman)

Hamizan Yon, PhD
Senior Lecturer
Faculty of Electrical Engineering
Universiti Teknologi MARA
(Internal Examiner)

Mohd Fais Mansor, PhD
Associate Professor
Faculty of Engineering & Built Environment
Universiti Kebangsaan Malaysia
(External Examiner)

PROFESSOR DR HJH ZURAEDA IBRAHIM
Dean
Institute of Postgraduates Studies
Universiti Teknologi MARA
Date: 16 March 2026

AUTHOR'S DECLARATION

I declare that the work in this thesis was carried out in accordance with the regulations of Universiti Teknologi MARA. It is original and is the results of my own work, unless otherwise indicated or acknowledged as referenced work. This thesis has not been submitted to any other academic institution or non-academic institution for any degree or qualification.

I, hereby, acknowledge that I have been supplied with the Academic Rules and Regulations for Post Graduate, Universiti Teknologi MARA, regulating the conduct of my study and research.

Name of Student	Mohd Farid Bin Omar
Student ID. No.	2021696736
Programme	Master of Science (Electrical Engineering) CEEE750
Faculty	Electrical Engineering
Thesis Title	Design and Development of a LoRa-Based Ground Sensor Terminal for L-Band Satellite IoT Applications
Signature of Student	
Date	March 2026

ABSTRACT

In remote equatorial regions such as Malaysia, reliable connectivity remains a critical challenge for Internet of Things (IoT) deployment, particularly in areas where terrestrial infrastructure is unavailable or unreliable. Despite the rapid growth of satellite-assisted IoT, the absence of validated design parameters, reproducible Ground Sensor Terminal architectures, and empirical performance data tailored to Malaysia's equatorial environment introduces significant uncertainty in predicting reliable link budgets, operating margins, and end-to-end performance of hybrid LoRa-Iridium L-band IoT systems. This thesis presents a reproducible two-hop LoRa-Iridium GST architecture for equatorial deployment in which LoRa in the sub-GHz band is used exclusively for the terrestrial sensor-to-Ground Sensor Terminal (GST) link, while the GST provides the satellite backhaul via Iridium Short Burst Data in the L-band. This study aims to investigate and optimise the critical design parameters, develop a functional prototype, and experimentally validate the performance of a LoRa-based Ground Sensor Terminal (GST) for L-band satellite IoT applications. A Design-Develop-Research methodology is employed. The design stage involves theoretical link-budget estimation and Doppler shift analysis to establish feasible operating margins under low Earth orbit (LEO) satellite dynamics. A GST prototype is then developed using an ESP32-class microcontroller, an SX1262 LoRa transceiver, and a RockBLOCK Mk2 modem based on the Iridium 9602 chipset. Field evaluations assess system performance using Received Signal Strength Indicator (RSSI) and Signal-to-Noise Ratio (SNR) for the LoRa terrestrial link, and end-to-end node-to-server delay for the satellite backhaul, across varying distances and satellite pass conditions. Theoretical analysis indicates an Iridium uplink link margin of approximately 7.53 dB at an assumed 10.93 dBW EIRP, while Doppler analysis shows a typical frequency offset of ±2.2 kHz, with a worst-case of ±6.8 kHz. Experimental results confirm RSSI and SNR degradation with distance and reveal an inverse relationship between satellite signal strength and transmission delay. This study contributes a reproducible and experimentally validated two-hop LoRa-L-band Ground Sensor Terminal architecture with empirical RSSI, SNR, and end-to-end delay measurements under equatorial operating conditions. These findings provide an evidence-based foundation for the practical deployment of satellite-assisted IoT systems in equatorial regions, where terrestrial connectivity is limited and reliable low-power data delivery is required.

ACKNOWLEDGEMENT

All praise and gratitude are due to Allah (SWT) for granting me the opportunity to embark on this Master's journey and the strength to complete it. I am deeply indebted to my supervisor, Prof. Ir. Dr. Mohamad Huzaimy bin Jusoh, and my co-supervisor, Dr. Fatimah Zaharah Ali, for their unwavering guidance, patient mentorship, and insightful counsel in the field of space and satellite engineering; their support has been invaluable throughout this research.

I wish to record my sincere appreciation to Mr Muhammad Syazwan Johari and Viucom Sdn Bhd for their committed industry partnership. I am also grateful to my colleagues and friends for their encouragement and practical assistance, and to the Faculty of Electrical Engineering, Universiti Teknologi MARA (UiTM), for providing the facilities, financial support, and enabling environment that made this work possible.

My heartfelt thanks go to the Jabatan Perkhidmatan Awam (JPA) and the Government of Malaysia for the award of the Hadiah Latihan Persekutuan (FtLP) scholarship, which substantially supported my academic development. I would also like to thank the Malaysian Space Agency (MYSA) for its sustained support towards the capacity development needs of its officers and the agency.

Finally, I dedicate this thesis to my beloved wife, Nor Su'aida binti Yusof; my sons, Muhammad Al Fateh, Muhammad Fidaaeiy, and Muhammad Firash Hadeef; my daughter, Nur Farha Haneesa; and my parents, Omar bin Hussin and
, whose prayers, love, and constant encouragement enabled me to complete this work within the allotted time. This achievement is for all of you. Alhamdulillah.

TABLE OF CONTENTS

LIST OF TABLES

LIST OF FIGURES

LIST OF SYMBOLS

Symbols

c	The speed of light
f	Frequency, Hz
71	Pi (decimal value: approximately 3.14)
8	The degree of an elevation angle
X	Wavelength

LIST OF ABBREVIATIONS

Abbreviations

AoS	Acquisition of Signal
BME280	Humidity, Temperature, Pressure and Altitude Sensor
C/N	Carrier-to-Noise Ratio
CR	Coding Rate
dB	Decibel
dBm	Decibel-milliwatt
dBW	Decibel Watt
EDA	Electronic Design Automation
EIRP	Effective Isotropic Radiated Power
ESP32	Espressif 32-bit Microcontroller
FOV	Field of View
GHz	Gigahertz
GPS	Global Positioning System
GST	Ground Sensor Terminal
HLP	Hadiah Latihan Persekutuan
IoT	Internet of Things
JPA	Jabatan Perkhidmatan Awam
kHz	Kilohertz

LEO	Low Earth Orbit
LoRa	Long Range
LOS	Line of Sight
LoS	Loss of Signal
MCU	Microcontroller Unit
MHz	Megahertz
MYSA	Malaysian Space Agency
NLOS	Non-Line of Sight
PCB	Printed Circuit Board
RF	Radio Frequency
RSSI	Received Signal Strength Indicator
SBD	Short Burst Data
SF	Spreading Factor
SNR	Signal-to-Noise Ratio
SX1262	LoRa Transceiver Chip
UiTM	Universiti Teknologi MARA

CHAPTER 1
INTRODUCTION

1.1 Overview

The demand for reliable data transmission from remote and infrastructure-limited regions has accelerated the adoption of satellite-based Internet of Things (IoT) systems, where L-band communication stands out for its resilience to weather and environmental interference. Yet, the absence of optimised low-power ground sensor terminals (GSTs) that seamlessly integrate long-range terrestrial protocols with satellite networks limits the scalability and cost-effectiveness of such systems. Existing implementations often neglect critical design trade-offs involving link budget margins, Doppler shift compensation, and performance analysis under continuous field operation. This research addresses these gaps by developing and validating a LoRa-based GST specifically engineered for L-band satellite IoT applications. By combining low-power, long-range terrestrial communication with the global reach of L-band satellite links, the study delivers empirical insights and optimised design parameters that enhance reliability, reduce operational costs, and enable scalable deployment across diverse and challenging environments.

1.2 Background of Study

Global deployment of the Internet of Things has extended beyond terrestrial networks into areas where conventional cellular coverage is sparse or unavailable[1]. Satellite connectivity provides a practical backhaul for such environments, yet power, cost, and regulatory constraints at the edge dictate the use of ultralow power radios for the local sensor segment[2]. LoRa has emerged as a leading physical layer for short range sensor communications due to its long range at low data rates and modest energy demand[3]. In parallel, the Iridium constellation offers truly global coverage through Short Burst Data, which is a compact and robust packet service operating in the L-band[4].

The need for dependable data delivery from remote and infrastructure limited settings continues to drive satellite based IoT. In this work the L-band link is used only

as a satellite backhaul through the Iridium Short Burst Data service, while LoRa at sub GHz is used only for the short range sensor to gateway link[5]. Many existing efforts blur this separation or under report the design trade offs across the two segment path, including link budget margins on the LoRa segment, message framing and queueing for SBD sessions, and performance during sustained field operation. This study addresses those gaps by developing and validating a Ground Sensor Terminal that receives LoRa packets at sub GHz and forwards them to the Iridium constellation via SBD in the L-band. LoRa is not operated on the L-band. The results provide empirical insight and optimised design parameters that improve reliability, reduce operating cost, and enable scalable and reproducible deployment in diverse and challenging environments[6].

This thesis adopts a two segment architecture that is deliberately simple and unambiguous. LoRa at sub GHz is used only for the short range point to point link between the LoRa Sensor Node and the Ground Sensor Terminal. The L-band is used only within the Ground Sensor Terminal through a RockBLOCK satellite modem that forwards the sensor payload to the Iridium constellation using Short Burst Data[7]. The work does not attempt to operate LoRa on the L-band, nor does it modify the Iridium air interface. The Ground Sensor Terminal therefore acts as a protocol and link bridge between a terrestrial LoRa sensor link and an Iridium satellite backhaul.

1.3 Problem Statement

Despite the rapid expansion of satellite-assisted IoT, there remains no established set of design parameters tailored to Malaysia's equatorial environment, where high humidity, dense vegetation, and low satellite elevation angles introduce unique propagation constraints. Existing studies on LoRa and Iridium often assume mid-latitude conditions, resulting in design envelopes that do not accurately represent real tropical ground-to-satellite performance. This creates uncertainty in determining reliable link budgets, Doppler tolerances, and operating margins for L-band IoT deployment in the region.[3], [8], [9]

Furthermore, current literature lacks a reproducible Ground Sensor Terminal (GST) that integrates terrestrial LoRa, embedded firmware, and L-band satellite communication within a validated and openly documented architecture. Prototypes presented in prior work are often application-specific, non-modular, or omit critical

implementation details, making them unsuitable as reference models for engineering replication or future system scaling. [6], [10], [11], [12]

Most importantly, empirical evidence on hybrid LoRa-Iridium performance under realistic satellite availability is limited. Published studies rarely evaluate end-to-end behaviour such as signal quality, delivery ratio, and latency under variable environmental conditions and dynamic satellite passes. Without such datasets, system designers cannot reliably predict performance trade-offs or optimise GST operation for remote sensing and long-range telemetry in equatorial regions.[13], [14], [15], [16]

1.4 Research Objectives

This study addresses the limitations and research gaps identified in the previous sections by designing, developing, and evaluating a LoRa-based Ground Sensor Terminal (GST) for L-band satellite Internet of Things (IoT) communication. The research is structured around a set of clearly defined objectives that guide the investigation from concept to empirical validation. These objectives are formulated to ensure that the study not only contributes to theoretical knowledge but also delivers practical solutions applicable to real-world scenarios.

This research focuses on the following objectives:

i. To optimise the design parameters of a LoRa-based Ground Sensor Terminal (GST) for L-band Satellite IoT applications.
ii. To develop a functional prototype of the LoRa-based Ground Sensor Terminal (GST) for L-band satellite IoT applications
iii. To validate the performance of the developed LoRa-based Ground Sensor Terminal for L-band satellite IoT applications.

1.5 Scope and Limitation of the Study

The work is confined to a two-segment architecture. The first segment is a terrestrial LoRa link at approximately 918 MHz between a single sensor node and the Ground Sensor Terminal using the E22-900M2S transceiver. The second segment is a satellite backhaul at approximately 1.6 GHz from the Ground Sensor Terminal to the Iridium constellation using the Short Burst Data service via a RockBLOCK modem. In

this study, the L-band refers specifically to the Iridium uplink frequency range of approximately 1616-1626.5 MHz, which is internationally allocated for mobile satellite services and provides a favourable trade-off between atmospheric attenuation, antenna size, and link reliability for low-data-rate IoT applications. The Iridium interface and Short Burst Data protocol are treated as a service interface. The study does not involve LoRa operation in the L-band, multi-hop LoRa networking, or alternative satellite systems. Validation focuses on communication reliability and end-to-end latency rather than high-throughput operation.

The scope of the developed GST in this study is limited to operation within the L-band frequency range for the satellite uplink, without consideration of other satellite frequency bands that may offer different propagation characteristics or performance trade-offs, while the terrestrial LoRa link remains confined to the sub-GHz ground frequency. Furthermore, the performance analysis presented under Objective 3 is restricted to specific parameters, namely the Received Signal Strength Indicator (RSSI), Signal-to-Noise Ratio (SNR), LoRa communication range, Iridium message success, and data transmission delay under defined environmental and operational conditions. The evaluation of the maximum achievable LoRa communication range was conducted within these constraints, and observations on satellite signal strength were analysed only in relation to their effect on data transmission delay. These limitations may influence the generalisability of the findings to other frequency bands, communication protocols, or broader operational scenarios.

1.6 Significance of the Study

This research provides a validated framework for deploying LoRa-based terminals for satellite communication in underserved areas. It contributes to design best practices for GSTs, offers real-world performance benchmarks, and informs future Sat-IoT innovations. The findings are relevant to developers, engineers, and policymakers aiming to extend IoT connectivity globally.

The principal contribution of this thesis is an integrated and empirically validated Ground Sensor Terminal that cleanly separates a LoRa sensor link from an Iridium L-band backhaul while delivering end to end results that practitioners can reproduce. By quantifying the influence of LoRa parameter choices on end to end performance through a satellite backhaul, the work provides practical guidance for

engineers who must design for energy efficiency and reliability in remote settings. The modular architecture and documented firmware also reduce integration effort, enabling faster prototyping and deployment for agencies and industries that require timely situational awareness.

1.7 Thesis Organization

This thesis is structured into five main chapters, each serving a distinct role in achieving the research objectives and presenting the findings in a systematic and logical manner.

Chapter 1: Introduction. This chapter provides the overall introduction and contextual foundation of the research. It includes the background of the study, problem statement, research objectives, scope and limitations, significance, and an overview of the thesis structure. It outlines the motivation behind the study and defines the focus and intended contributions.

Chapter 2: Literature Review. This chapter presents a comprehensive review of the existing literature related to LoRa communication systems, satellite-based IoT technologies, and the L-band frequency spectrum. It discusses previous research efforts, technological trends, and state-of-the-art developments in both terrestrial and satellite-based LPWAN solutions. The chapter also highlights key knowledge gaps and justifies the need for the present study.

Chapter 3: Methodology. This chapter outlines the research design, methodological framework, and technical approach used to achieve the research objectives. It details the hardware and software development of the Ground Sensor Terminal, including component selection, system integration, and firmware programming. It also describes the link budget analysis, configuration settings for LoRa and satellite communication, and the setup of field validation experiments.

Chapter 4: Results and Discussion. This chapter presents the findings of the study based on the experimental tests and performance evaluations of the developed prototype. It analyses key performance indicators such as RSSI, SNR, data transmission latency, and successful communication rates under varying environmental conditions. The results are discussed in the context of existing studies to validate the reliability, feasibility, and novelty of the proposed system.

Chapter 5: Conclusion and Recommendations. The final chapter summarises the research contributions, key findings, and implications of the study. It provides concluding remarks on the research objectives and discusses the practical relevance of the developed solution. The chapter also outlines the limitations encountered during the study and offers recommendations for future work to further enhance the design, scalability, and applications of LoRa-based satellite IoT terminals.

1.8 Summary

This chapter defined the study's context, rationale, and focus. It introduced the integration challenge between LoRa and L-band satellite systems, framed the research objectives, and set the foundation for subsequent chapters, starting with the literature review in Chapter 2.

CHAPTER 2
LITERATURE REVIEW

2.1 Introduction

The proliferation of the Internet of Things has led to a pressing need for scalable and energy-efficient wireless communication technologies[17]. Among the available options, Low Power Wide Area Networks have emerged as a promising enabler of massive deployments, particularly in remote or infrastructure-limited environments[18]. LoRa, short for Long Range, is a proprietary physical-layer modulation based on chirp spread spectrum that enables very long-range links at low power in licence-exempt sub-GHz industrial, scientific, and medical bands[19]. Its key attraction is the ability to trade throughput for receiver sensitivity by adjusting spreading factor, bandwidth, and coding rate, which makes it well suited to battery-operated sensing in wide-area settings[13], [20]. Nevertheless, purely terrestrial LoRa coverage remains constrained in sparsely connected regions such as oceans, deserts, and rural terrains[13].

Within this study, the Ground Sensor Terminal (GST) is defined as a field-deployable communication gateway, responsible for collecting data from short-range sensor nodes and relaying the aggregated information to a remote application server via an L-band satellite backhaul [5], [10]. Functionally, it serves as the bridge between local sensor networks comprising low-power sensing devices and wide-area networks, performing protocol translation, buffering, and scheduling to reconcile the duty-cycled behaviour of energy-constrained sensors with the access procedures of satellite links. In practice, a GST can be realised with commercial off-the-shelf components and is widely recognised as a specialised form of IoT gateway adapted for harsh or off-grid environments.

Recent project reports and implementations describe GSTs as comprising sensing, communications, power, and structural subsystems, with the communications stack explicitly partitioned into a local radio interface and a satellite backhaul interface.

L-Band in this thesis refers to the radio spectrum between 1 and 2 GHz under the IEEE nomenclature, with Iridium subscriber links specifically operated in the 1616

to 1626.5 MHz allocation [10]. Operation in this portion of the spectrum is attractive for satellite links because propagation is comparatively resilient to rain and foliage relative to higher microwave bands, while still permitting compact antennas on mobile platforms[21]. The Iridium network uses this L-Band allocation for user links and employs higher frequency feeder and crosslink bands for space and gateway segments, which further clarifies the division of responsibilities between terminal, space, and ground segments in a two-hop design.

Satellite IoT applications describe the use of satellite networks to extend IoT connectivity beyond the footprint of terrestrial infrastructure[22]. Typical use cases include environmental and forestry monitoring, maritime asset tracking, precision agriculture, disaster management, and critical infrastructure telemetry, where coverage continuity, global reach, and robustness are prioritised over high throughput. Contemporary surveys emphasise that satellite IoT can be achieved either by direct device-to-satellite access or by gateway-assisted architectures, with the latter offering practical advantages when local aggregation reduces backhaul cost and energy per delivered bit[3].

Building on these definitions, this chapter reviews a two-hop satellite Internet of Things architecture in which LoRa in the sub-GHz ISM bands is used exclusively for the terrestrial sensor-to-ground-sensor-terminal hop, while the ground sensor terminal provides the satellite backhaul via Iridium Short Burst Data in the L-Band. Framing the review in this way prevents conflation of the LoRa physical layer with the space segment and clarifies that Iridium, rather than LoRa, governs satellite connectivity, access procedures, and Doppler dynamics[23]. Accordingly, the discussion first revisits LoRa fundamentals in their intended terrestrial role, then outlines L-Band satellite backhaul characteristics with a focus on Iridium SBD service properties, before integrating both perspectives into a coherent system view. Key performance aspects are addressed by separating link budgeting and timing issues per hop and by articulating how gateway scheduling bridges the two layers into reliable end-to-end delivery.

2.2 Terrestrial LoRa Technology and its Role in the System

LoRa has emerged as one of the most widely adopted low-power wide-area (LPWA) physical layer technologies for Internet of Things (IoT) applications due to its ability to provide long-range connectivity at extremely low power consumption.

Operating in sub-GHz industrial, scientific, and medical (ISM) bands, LoRa employs chirp spread spectrum (CSS) modulation to achieve high receiver sensitivity and robustness against interference, multipath fading, and noise [24]. LoRa operates primarily in the 433 MHz, 868 MHz, and 915 MHz bands depending on regional regulations, with support for data rates ranging from 0.3 kbps to 50 kbps [25]. These characteristics make LoRa particularly suitable for battery-powered sensor nodes deployed in rural, remote, or infrastructure-sparse environments.

From a system design perspective, the key strength of LoRa lies in the configurability of its physical-layer parameters, namely spreading factor (SF), bandwidth (BW), and coding rate (CR). Increasing the spreading factor improves processing gain and link budget, enabling communication over longer distances at the expense of data rate and increased time-on-air [17]. This trade-off is fundamental to LoRa operation and has significant implications for network scalability, latency, and duty-cycle compliance. While high spreading factors (e.g., SF11-SF12) are attractive for coverage extension, they also increase channel occupancy and collision probability, limiting network capacity in dense deployments [17], [18].

In conventional terrestrial deployments, LoRa is typically integrated with the LoRaWAN protocol stack, which defines medium access control, device classes, and security mechanisms [26]. However, LoRaWAN was primarily designed for static terrestrial networks with predictable latency and regular downlink opportunities. Studies have shown that its strict timing constraints for receive windows and acknowledgements can become a limiting factor in scenarios involving intermittent connectivity or long propagation delays [18]. As a result, many satellite-assisted or hybrid IoT systems adopt custom or simplified MAC-layer implementations that prioritise uplink transmissions and minimise reliance on downlink signalling [27] .

Another important consideration is the sensitivity of LoRa performance to environmental and deployment factors. Antenna characteristics, installation height, terrain morphology, and interference from co-channel users can significantly affect received signal strength indicator (RSSI) and signal-to-noise ratio (SNR)[19], [20]. While LoRa is often promoted as capable of achieving ranges exceeding 10 km, such performance is typically observed under ideal line-of-sight conditions with elevated gateways and low noise floors. In practical deployments, particularly in mixed urban-suburban environments, achievable range and reliability are highly context-dependent, underscoring the need for careful link-budget analysis and empirical validation.

In the context of this thesis, the use of LoRa is deliberately confined to the terrestrial sensor-to-Ground Sensor Terminal (GST) hop operating in the sub-GHz ISM bands. This architectural decision reflects a clear separation of roles between the terrestrial access link and the satellite backhaul. Although recent studies have demonstrated the feasibility of direct LoRa reception from Low Earth Orbit (LEO) satellites [8], [28], such approaches impose stringent requirements on oscillator stability, Doppler tolerance, and timing synchronisation, which are difficult to satisfy using low-cost and energy-constrained sensor hardware. By restricting LoRa operation to the terrestrial domain, these constraints are avoided while preserving LoRa's inherent advantages in terms of energy efficiency and long-range data aggregation. Consequently, LoRa parameterisation, spreading factor, bandwidth, coding rate, and transmission power can be optimised based on terrestrial propagation conditions rather than satellite dynamics, resulting in a more robust and predictable system design. The satellite backhaul is instead realised through the Iridium Short Burst Data (SBD) service in the L-band, whose waveform, access procedures, and timing characteristics are fundamentally distinct from LoRa and are therefore treated separately in the satellite-link analysis [29].

2.3 Satellite IoT Communication Overview

Satellite-based Internet of Things (Sat-IoT) systems play a crucial role in extending IoT connectivity beyond the geographical and economic limits of terrestrial networks. Unlike cellular or fibre-based infrastructure, satellite systems can provide near-global coverage, enabling monitoring and data collection in remote, maritime, polar, and disaster-prone regions where conventional connectivity is unavailable or prohibitively expensive[30], [31]. These characteristics position Sat-IoT as a complementary rather than competing solution to terrestrial IoT technologies [30], [32].

Sat-IoT architectures typically rely on satellite constellations operating in Low Earth Orbit (LEO), Medium Earth Orbit (MEO), or Geostationary Earth Orbit (GEO). Among these, LEO constellations have gained increasing attention for IoT services due to their lower free-space path loss, reduced propagation delay, and improved link margins compared with GEO systems [1], [33]. However, these advantages come at the cost of rapidly time-varying link conditions and intermittent connectivity, as satellites move relative to the Earth's surface at velocities approaching 7-8 km/s.

From an application standpoint, Sat-IoT systems are primarily designed to support narrowband, low-data-rate, and delay-tolerant services. Typical payload sizes are limited to tens or hundreds of bytes, and communication opportunities are constrained to short satellite passes lasting a few minutes [3], [34]. These constraints necessitate efficient buffering, store-and-forward mechanisms, and intelligent scheduling strategies to ensure reliable data delivery. Consequently, performance metrics such as latency and throughput are often secondary to reliability, coverage, and energy efficiency. These systems leverage standardized and proprietary communication protocols including NB-IoT, Sigfox, and LoRa. However, LoRa has gained traction due to its ultra-low power requirements and simplicity of integration with existing satellite platforms [35].

Two dominant architectural paradigms have emerged in Sat-IoT research and deployment: direct device-to-satellite communication and gateway-assisted communication. In direct-to-satellite architectures, sensor nodes transmit directly to satellites using LPWA waveforms such as LoRa-like modulation [8], [28]. Commercial and experimental initiatives by organisations such as Lacuna Space have demonstrated the feasibility of this approach [36]. Nevertheless, direct-to-satellite LoRa systems face significant challenges, particularly related to Doppler shift, frequency synchronisation, and power control, which can severely degrade demodulation performance if not adequately addressed. [37].

Gateway-assisted Sat-IoT architectures, by contrast, introduce an intermediate aggregation layer that decouples local sensing from satellite backhaul. In this model, multiple sensors communicate with a ground-based terminal using short-range or LPWA technologies, while the terminal handles satellite access and protocol translation [3], [6], [10]. This approach reduces the burden on individual sensor nodes, lowers satellite airtime consumption, and allows more sophisticated link management strategies to be implemented at the gateway. As a result, gateway-assisted architectures are often more practical for heterogeneous sensor deployments and energy-constrained environments.

A critical technical challenge in LEO Sat-IoT systems is Doppler shift caused by the high relative velocity between satellites and ground terminals. Doppler-induced frequency offsets, which can reach several kilohertz depending on carrier frequency and pass geometry, significantly impact signal acquisition and decoding [23], [27], [35]. Mitigation strategies such as Doppler pre-compensation, adaptive frequency tracking,

and advanced signal processing techniques have been proposed, but they add complexity and processing overhead to the system. These effects highlight the importance of carefully selecting waveform and access technologies for satellite links.

In this thesis, satellite connectivity is provided via the Iridium constellation using the Short Burst Data (SBD) service operating in the L-band. The Iridium system offers near-global coverage, inherent Doppler management, and store-and-forward capabilities, making it well suited for delay-tolerant IoT applications [7], [14], [38]. By assigning all satellite-specific functions including access procedures, Doppler handling, and network timing to the Iridium backhaul, and confining LoRa operation to the terrestrial domain, the proposed system architecture achieves a clear functional separation between local access and wide-area connectivity. This design choice simplifies system integration, enhances reliability, and provides a defensible balance between performance, complexity, and energy efficiency for remote IoT deployments.

2.4 System Integration: Terrestrial LoRa Access with L-Band Iridium Backhaul

This work integrates a terrestrial LoRa access layer with an L-band Iridium SBD backhaul at the GST. Sensor nodes communicate to the GST via LoRa (sub-GHz ISM), benefiting from long-range, low-power operation. The GST then encapsulates and forwards payloads over the Iridium network using the SBD service, leveraging the constellation's global coverage and store-and-forward capability. This separation of concerns ensures that LoRa PHY/MAC choices optimise terrestrial reach and energy efficiency, while satellite connectivity, Doppler handling, and access windows are governed by the Iridium system.

Accordingly, performance considerations split along the two-hop: (i) LoRa link budget, sensitivity, and interference for the sensor-to-GST hop; and (ii) Iridium link availability, pass geometry, latency, and service constraints for the GST-to-satellite hop. System scheduling, buffering, and duty-cycle policies are designed to bridge these layers reliably.

2.4.1 Link Budget Analysis

The LoRa hop is budgeted in the 433/868/915 MHz bands, considering TX power limits, antenna gains, environment-dependent losses, and receiver sensitivity as a function of SF and BW. This determines viable sensor-to-GST ranges under rural and semi-urban deployments.

The satellite backhaul uses Iridium's L-band service, for which FSPL, satellite elevation, GST antenna pattern, and service margins are computed according to Iridium SBD specifications. These calculations are distinct from LoRa and govern end-to-end availability and latency to the cloud endpoint.

Link budget quantifies the total gain and loss from the transmitter to the receiver, serving as a predictive measure of whether a communication link will be viable under specific configurations. In Iridium Satellite IoT, the link budget must account for free-space path loss (FSPL), antenna gains, system noise, and transmission power. Due to the large distances involved (e.g., 760 km), FSPL can exceed 130 dB in L-band (1-2 GHz) frequencies.

The general link budget equation is expressed as:

$$\text{Received Power (dBm)}\ P_r = P_t + G_t + G_r - L_p - L_s \tag{2.1}$$

Where P_t is transmit power, G_t and G_r are the transmitter and receiver antenna gains, L_p is the path loss, and L_s represents system losses including atmospheric attenuation and polarization mismatch.

2.4.2 Doppler Shift Effect

Doppler is predominantly a concern for the L-band Iridium link due to satellite motion and pass geometry; the terrestrial LoRa hop experiences negligible Doppler in static deployments. Doppler management, acquisition, and timing on the space segment are therefore handled by the Iridium network and modem procedures, whereas LoRa parameterisation focuses on terrestrial robustness (e.g., SF-dependent symbol duration and sensitivity) rather than satellite Doppler tolerance.

2.4.3 RSSI and SNR in Direct-to-Satellite LoRa (Prior Work)

Received Signal Strength Indicator (RSSI) and Signal-to-Noise Ratio (SNR) are vital metrics for assessing the quality of LoRa links[39] . RSSI reflects the absolute power level of the received signal, while SNR measures signal quality relative to noise. [40]

In LoRa-Satellite tests, RSSI values as low as -130 dBm and SNR between -15 dB to +10 dB have been reported under SF12, 125 kHz bandwidth, and maximum transmission power[40]. These results align with the sensitivity limits of LoRa receivers, suggesting the importance of high-gain antennas and favorable link geometry during satellite passes.

Variations in RSSI and SNR are also influenced by elevation angle, antenna orientation, satellite range, and atmospheric conditions. Ground testing and satellite flyby experiments have shown that higher elevation angles typically result in better signal quality due to reduced path length and attenuation

2.4.4 Delay and Latency Factors

Transmission delay in LoRa-Satellite systems comprises several components: propagation delay, processing delay, access delay (e.g., waiting for satellite visibility), and retransmission delay in case of lost packets [37]. Propagation delay in LEO-based systems typically ranges between 1.5 ms to 5 ms due to short orbital distances [41].

However, the dominant latency contributor is the satellite pass availability, which restricts transmission opportunities to brief windows (typically 5-15 minutes per pass). This results in intermittent communication and delay-tolerant transmission models, making LoRa suitable for non-time-critical applications

Queuing and scheduling delays are influenced by traffic density, ALOHA-based access methods, and downlink acknowledgement constraints [42]. Store-and-forward mechanisms are commonly employed in satellite payloads to buffer packets before downlinking them during ground contact [43]

2.5 Prior Work on LoRa Performance Testing

Direct reception of LoRa or LoRaWAN from low Earth orbit payloads has been demonstrated under specific assumptions and with bespoke payloads, highlighting feasibility but also sensitivity to Doppler and very low signal to noise operation close to the noise floor.[26] However, comparatively fewer studies validate a two-hop architecture that combines terrestrial LoRa access with a standards based Iridium Short Burst Data backhaul using commercial modules at the gateway, and even fewer report end to end measurements that attribute reliability and latency to each hop [38]This thesis addresses these gaps by designing, implementing, and validating a ground sensor terminal that bridges LoRa and Iridium Short Burst Data and by quantifying performance under field conditions that reflect realistic propagation and pass dynamics.

Numerous studies have explored the performance of LoRa technology under different environmental, operational, and hardware conditions, both in terrestrial and satellite-enabled configurations. These investigations typically focus on key parameters such as Received Signal Strength Indicator (RSSI), Signal-to-Noise Ratio (SNR), packet delivery ratio (PDR), and latency, which are essential in evaluating the viability of LoRa for long-range, low-power IoT applications[40].

In terrestrial environments, studies have demonstrated LoRa's performance over several kilometres, with RSSI and SNR values dependent on terrain type, antenna height, and spreading factor. For instance, in urban and suburban settings, LoRa has achieved reliable communication up to 15 km with SF12, while open rural environments have shown reach beyond 30 km under line-of-sight conditions. These findings suggest the importance of Medium Access Control (MAC) optimizations for LoRa in Sat-IoT scenarios[44].

Performance validation also extends to antenna design, gateway sensitivity, Doppler compensation, and link budgeting. For example, Ullah et al.[28] performed Doppler shift impact assessments under LEO satellite dynamics and proposed tolerable configurations for LoRa receivers. Moreover, Zhao et al.[37] introduced coherent combining techniques to improve signal recovery in multi-pass LoRa reception.

Collectively, these studies establish the empirical foundation for deploying LoRa in space-based IoT systems. However, many experiments remain platform-specific or constrained to simulation environments. This research seeks to build upon existing knowledge by experimentally validating a custom-built LoRa-based GST

communicating with L-band satellite services, contributing further to practical insights in real deployment conditions.

Table 2.1 summarises representative studies related to LoRa-based satellite IoT and Ground Sensor Terminal (GST) architectures, highlighting their key technical contributions and identified limitations. The reviewed works collectively demonstrate the feasibility of integrating LoRa modulation with satellite backhaul links, particularly in terms of link budget performance, sensitivity optimisation, and network-level capacity enhancement. However, a critical examination reveals that most studies focus on isolated aspects of the system, such as theoretical capacity improvement, Iridium-centric architectures, or laboratory-based analyses, with limited emphasis on holistic system-level validation. In particular, gaps are observed in the experimental evaluation of Doppler effects, end-to-end latency, real-world field performance, and the interaction between terrestrial LoRa parameters and L-band satellite access constraints. These limitations motivate the need for a comprehensive investigation that combines theoretical design analysis with empirical validation of a deployable LoRa-based GST, as addressed in this study. Table 2.1 provides a critical synthesis of prior studies and exposes recurring technical and experimental limitations, which are subsequently distilled in Section 2.6 into explicit research gaps that motivate the design and validation of a LoRa-based Ground Sensor Terminal in this study.

Table 2.1
The Summary of Previously Conducted Studies

No	Reference	Key Finding	Critical Review
1	M. F. Omar, M. H. Jusoh, and F. Z. Ali, "LoRa-Based Ground Sensor Terminal for L-Band Satellite IoT Applications," *International Journal of Integrated Engineering*, vol. 16, no. 5, pp. 200-212, 2024, doi: 10.30880/ijie.2024.16.05.020. [5]	Developed a LoRa-based GST for L-band satellite IoT; achieved SF12 sensitivity (-137 dBm) with reliable link budget performance.	Focused solely on link budget; lacked analysis on interference, Doppler effects, and scalability.
2	A. Maleki, M. A. Siddiqi, and T. Haustein, "D2D-Aided LoRaWAN LR-FHSS in Direct-to-Satellite IoT Networks," *arXiv preprint*, arXiv:2212.04331, 2022, doi: 10.48550/arXiv.2212.04331.[45]	Enhanced DtS IoT capacity (150-250%) using D2D-aided LR-FHSS.	Field testing absent; potential channel non-idealities ignored.
3	IoRT hybrid network review (2019), 'Study of Data Transfer in a Heterogeneous LoRa-Satellite Network', DOI:10.3390/sl9153384 [10]	Hybrid LoRa-Iridium architecture reduced satellite usage via GDEP compression (5x).	Lacked detailed LoRa parameter optimisation; mainly Iridium-focused.
4	J. A. Fraire, S. Tomaselli, and G. Munoz, "Space-Terrestrial Integrated IoT: Challenges and Opportunities," *arXiv preprint*, arXiv:2110.11518, 2021, doi: 10.48550/arXiv.2110.11518.[34]	Identified LoRa and NB-IoT as promising for space-terrestrial IoT.	Lacked specific implementation guidance for L-band satellites.
5	S. Gadre, S. Lohiya, and H. Jamieson, "Adapting LoRa Ground Stations for Low-Latency Imaging Satellites," in *Proceedings of the ACM International Conference on Internet-of-Things Design and Implementation (IoTDI)*, 2024, pp. 1-12, doi: 10.1145/3675170.[46]	Modified LoRa ground stations to receive satellite packets without hardware changes.	Focused on imaging; omits link budget and system-level considerations.
6	J. Martinez-Gost, "LoRa-Based Over-the-Air Computing for Satellite IoT," M.S. thesis, Universitat Politecnica de Catalunya, Barcelona, Spain, 2023. [Online]. Available: https://upcommons.upc.edu[47]	Applied LoRa-TBMA for efficient AirComp in Sat-IoT scenarios.	Purely theoretical; lacks real-world experimentation.
7	H. J. Naranjo, "A Study on Satellite Internet of Things (IoT)," M. S. thesis, Universitat Politecnica de Catalunya, Barcelona, Spain, 2021. [48]	Differentiates DtS/ltS; quantifies Iridium payload-sleep impacts on power and lifetime.	Iridium-only evaluation; lacks field benchmarks for latency and delivery reliability.

2.6 Research Gaps and Motivation

Prior studies on direct LoRa reception from low Earth orbit payloads provide useful physical layer insights but target a different operating paradigm that bypasses a terrestrial gateway. In contrast, there is limited empirical work validating a two-hop architecture combining terrestrial LoRa access with a standards-based L-band backhaul using off the shelf components at the gateway. Gaps remain in jointly tuning LoRa parameters and satellite scheduling to meet strict energy and latency budgets, and in quantifying how satellite pass dynamics and link availability propagate to end to end delivery success in realistic field conditions. This thesis addresses these gaps by designing, implementing, and validating a ground sensor terminal that bridges LoRa and Iridium Short Burst Data, and by reporting measurement grounded performance across both hops

Although numerous studies have demonstrated the feasibility of LoRa for terrestrial and satellite IoT communications, several critical gaps remain in the practical integration of LoRa-based ground sensor terminals with L-band satellite backhaul links. Most existing experimental efforts have either relied on proprietary satellite systems, simulation-based models, or limited short-term field tests. There is a lack of comprehensive performance validation involving custom-built LoRa GSTs integrated with commercially available L-band satellite services such as Iridium or Lacuna Space.

The critical research gaps identified from the literature can be summarised as follows:

a) Over-reliance on theoretical analysis

Many published works focus primarily on theoretical link-budget estimations or simplified Doppler analysis, while neglecting real-world factors such as environmental noise, interference, antenna misalignment, and transmission delay variations. As a result, communication reliability and delay tolerance are often assessed under overly optimistic assumptions that may not reflect practical deployment conditions.

b) Limited system-level integration and prototyping

A significant portion of prior studies lack comprehensive integration between embedded hardware platforms, LoRa transceivers, and satellite backhaul services. Although certain CubeSat missions (e.g., Swarm and Lacuna Space) have demonstrated LoRa-based uplinks, there is limited exploration of ground-based sensor terminals developed using off-the-shelf components such as ESP32 and RockBLOCK with customised firmware and hardware architectures for field IoT applications.

c) Scarcity of empirical studies involving L-band satellite backhaul integration

Few studies have experimentally evaluated LoRa-based IoT systems that utilise L-band (approximately 1.6 GHz) satellite links as a backhaul communication layer. While conventional LoRa deployments operate primarily in sub-GHz ISM bands (433 MHz, 868 MHz, and 915 MHz), the integration of LoRa-based ground terminals with L-band satellite services introduces distinct propagation characteristics, link-budget constraints, and latency behaviour. Despite the suitability of L-band for satellite IoT, empirical performance data covering end-to-end system behaviour under different LoRa configurations, satellite link conditions, and operational environments remain limited.

d) Lack of end-to-end performance evaluation

Existing research rarely provides a complete end-to-end analysis of LoRa-based transmissions from a ground terminal through a satellite backhaul to a cloud-based application server. Key performance metrics such as per-hop latency, uplink delay, packet loss, and long-term RSSI/SNR degradation are often not systematically evaluated under real operational scenarios, despite their importance for delay-tolerant IoT applications.

2.7 Summary

This chapter positions LoRa as a terrestrial access technology within a two-hop satellite Internet of Things architecture and distinguishes it clearly from the Iridium L-band backhaul that provides the space segment. By separating the performance analysis per hop and integrating them through ground sensor terminal scheduling, the ensuing methodology and experiments can attribute reliability, latency, and energy outcomes to the correct layer, thereby supporting a rigorous evaluation of the proposed system.

CHAPTER 3
METHODOLOGY

3.1 Introduction

This chapter presents the research methodology adopted to achieve the study's three objectives using the Design, Develop, and Research (DDR) framework. The DDR approach combines theoretical analysis, system implementation, and empirical evaluation in a structured progression. The first objective, concerning the identification of key design parameters for a LoRa-based GST, is addressed through analytical modelling, link budget estimation, and Doppler shift analysis. The second objective, centred on prototype development, involves the integration of both hardware and software components, including LoRa and satellite communication modules. The final objective is accomplished through experimental validation under real-world conditions, focusing on signal strength, communication range, and satellite transmission delay. This methodological structure ensures a coherent and systematic alignment between each objective and its corresponding phase.

3.2 Research Framework

3.2.1 Overview of Research Approach

To complement the structured methodology outlined in this chapter, Figure 3.1 illustrates the research flow chart that guided the systematic development and evaluation of the LoRa-based GST for L-band satellite IoT applications. The process begins with the investigation of link budget and design parameters, including Doppler shift, elevation angles, and optimal radio frequency (RF) configurations. Upon establishing the theoretical foundation, the next phase involves the identification and integration of appropriate hardware and software components, such as satellite modem, LoRa transceivers, sensor, and microcontrollers.

Once components are selected, the development of the GST prototype commences, followed by iterative cycles of verification, validation, and troubleshooting to identify any hardware or software integration issues that may affect baseline system

operation. If integration issues are detected, corrective actions are implemented before the system is allowed to proceed further. Only after successful resolution of all identified hardware or software integration issues does the system advance to experimental testing, where transmission range, signal strength, latency, and compatibility with L-band satellite communication are systematically assessed. This structured flow ensures technical robustness and methodological transparency, supporting high replicability and reproducibility of the research outcomes.

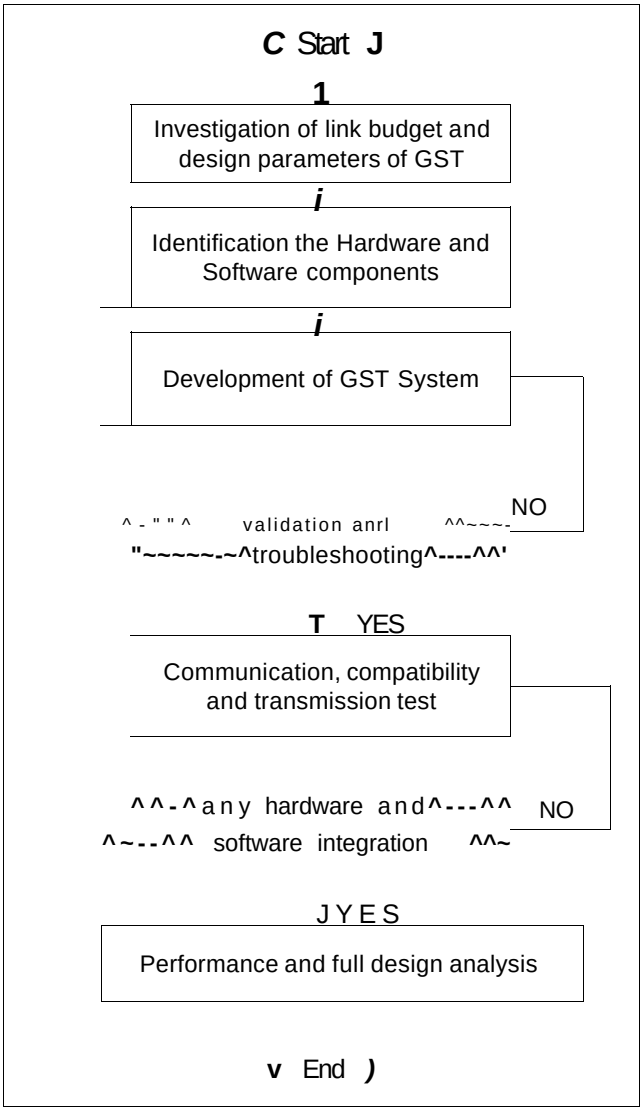

Figure 3.1 Flowchart of Research Methodology

3.3 Design Parameter Investigation

In designing a GST for L-band satellite IoT communication, it is crucial to define and configure a set of design parameters that collectively govern the system's performance, reliability, and compatibility with Low Earth Orbit (LEO) satellite operations. In this study, design parameters are defined as the key configurable variables both in terms of communication settings and hardware specifications that directly impact the GST's ability to transmit data effectively to satellite systems such as the Iridium network.

These parameters are classified into two main categories: (i) communication parameters, which include transmission frequency, spreading factor, bandwidth, transmission power, coding rate, preamble length, and transmission timing relative to satellite passes (AoS-LoS); and (ii) hardware design parameters, covering the selection of the satellite modem (RockBLOCK Mk2), satellite constellation (Iridium, consisting of 66 active LEO satellites), microcontroller (ESP32-WROOM-32U), L-band passive antenna, and an IP-rated weatherproof enclosure. Each parameter was identified and selected through a combination of literature review, satellite communication requirements, and practical implementation constraints. The accurate definition and integration of these design parameters form the foundational basis for the development, optimization, and experimental validation of the proposed GST system.

3.3.1 Terrestrial LoRa Link Parameters

To ensure optimal performance of the LoRa-based GST, key radio frequency (RF) parameters were carefully selected based on a balance between range, power efficiency, data reliability, and Doppler tolerance. The configuration adopted for the SX1262 LoRa transceiver is summarized in Figure 3.2 below:

```
•define RF_FREQUENCY          918809990  // Operating frequency in Hz
Sdefine TX_OUTPUT_POWER       20         // Transmission power in dBm
#define LORA_BANDWIDTH        125000     // Bandwidth: 125 kHz
#define LORA_SPREADING_FACTOR 12         // Spreading Factor (5F12) for maximum range and sensitiv
#define LORA_CODINGRATE       1          // Coding rate 4/5 for improved robustness
#define LORA_PREAMBLE_LENGTH  8          // Standard preamble Length for synchronization
```

Figure 3.2 The Configuration Adopted for the SX1262 LoRa Transceiver

Table 3.1 defines the parameters for the terrestrial sensor-to-GST link, which operates in the sub-GHz ISM band. The key configurable variables are the spreading factor, bandwidth, coding rate, transmit power, and preamble length. In this study, the centre frequency for the LoRa link was set to 918 MHz. Transmit power was configured up to 20 dBm subject to regulatory limits and link budget targets. Spreading factor and bandwidth were selected to balance sensitivity and data rate, while the coding rate was chosen to enhance robustness under low-SNR conditions. These parameters govern the coverage, throughput, and reliability of the terrestrial hop and are evaluated empirically in Chapter 4.

Table 3.1
Terrestrial LoRa Link Parameters

Parameter	Value	Rationale
Centre frequency	918 MHz	Sub-GHz ISM band for terrestrial coverage
Spreading Factor (SF)	SF12 baseline; SF7-SF12 tested]	Range-throughput trade-off
Bandwidth	125 kHz	Sensitivity vs data rate
Coding Rate (CR)	4/5	Robustness in low SNR
Preamble Length	8 symbols	Synchronisation margin
TX power	up to 20 dBm	Within regulatory limit and link budget

3.3.2 L-Band Satellite Backhaul (Iridium SBD) Parameters

Table 3.2 defines the parameters for the satellite backhaul provided by the Iridium Short Burst Data service in the L-band. The backhaul uses a dedicated L-band antenna and a modem to establish the satellite link. The key parameters include the operating band centred near 1.62 GHz, the effective isotropic radiated power assumptions used in the link budget, the satellite signal strength indicator used for pass quality, and the message size constraints relevant to SBD transmissions. These parameters govern end-to-end latency, delivery probability, and operating envelope of the satellite hop.

Table 3.2
L-Band Satellite Backhaul (Iridium SBD) Parameters

Parameter	Value	Rationale
Operating band	L-band, centred-1.62 GHz	Iridium SBD backhaul
Antenna	Passive L-band (e.g., M1600 class)	Band-matched gain and pattern
EIRP assumption	6.5-8 W	Link-budget target and margin reporting
Doppler reporting	Typical ±2.2 kHz; worst-case ±6.8 kHz	Consistent across thesis
SBD payload	< 50 bytes per credit (study scope)	Cost and reliability considerations

To prevent conflation between the two-hop, the terrestrial LoRa parameters are discussed separately from the L-band Iridium parameters. Subsequent analyses in Chapters 4 and 5 reference these subsections explicitly when interpreting range, sensitivity, and latency outcomes.

In designing the GST system for satellite IoT communication, careful consideration was given to the optimization of data packet size. The payload structure was configured to remain under 50 bytes per transmission, a strategic decision aligned with the Iridium Short Burst Data (SBD) billing model, where 1 credit is deducted per message below or equal to 50 bytes, while messages exceeding that threshold incur additional credit usage. This constraint directly impacts the monthly subscription cost and operational budget of the deployed system.

To balance data completeness, transmission reliability, and affordability, the GST firmware was programmed to condense essential telemetry such as timestamp, GPS coordinates, sensor readings, and status flags into a compact binary-encoded frame. The overall frame was structured as shown in Figure 3.3 follows:

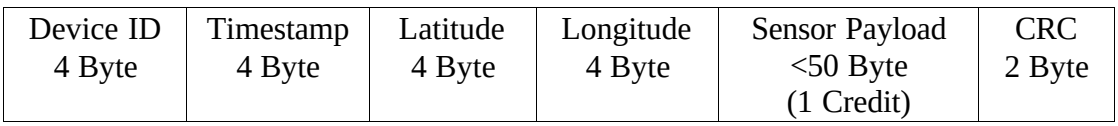

Figure 3.3 LoRa-Based GST Frame Structure

Ensuring high data density with minimal overhead. This byte-efficient design enables predictable cost estimation, facilitates longer operational periods per subscription tier, and aligns with low-power, low-data-rate IoT principles.

By adhering to this data size optimization strategy, the GST supports sustainable and scalable deployments, especially in resource-constrained environments, while maintaining full compatibility with the Iridium network's store-and-forward architecture.

The initial phase involves identifying critical parameters that influence the performance of the LoRa-based GST. These parameters include the Spreading Factor (SF), Bandwidth (BW), Coding Rate (CR), and Transmission Power. Understanding the interplay of these parameters is essential for optimizing the GST's communication range, data rate, and energy efficiency [3]. The selection of appropriate values for these parameters ensures reliable data transmission, especially in the challenging conditions of L-band satellite communication.

LoRa (Long Range) technology employs Chirp Spread Spectrum (CSS) modulation, enabling long-range communication with low power consumption. Key parameters influencing LoRa performance include:

i. Spreading Factor (SF): Determines the duration of the chirp signal, affecting data rate and sensitivity. Higher SF values increase range but reduce data rate. LoRa supports SF values from 7 to 12, with each increment doubling the time-on-air and halving the data rate,

ii. Bandwidth (BW): Wider bandwidths allow for higher data rates but may consume more power. LoRa typically operates with bandwidths of 125 kHz, 250 kHz, or 500 kHz.

iii. Coding Rate (CR): Provides error correction capabilities, enhancing reliability in noisy environments. LoRa supports coding rates ranging from 4/5 to 4/8.

The data rate *(Rb)* for LoRa modulation is calculated using the formula:

$$Rb = SF \times \frac{BW}{2SF} \times CR \qquad (3.1)$$

Where:

SF = Spreading Factor

BW = Bandwidth in Hz

CR = Coding Rate

Equation 3.1 shows how increasing the spreading factor or decreasing the bandwidth reduces the data rate, which is a trade-off for improved sensitivity and range.

A comprehensive review of prior studies identified the following critical parameters for GST development:

i. transmission frequency (1616-1626.5 MHz, L-band, corresponding to the Iridium uplink band),
ii. LoRa spreading factor (SF7-SF12),
iii. bandwidth (62.5-500 kHz),
iv. payload size (33-121 bytes), and
v. transmission power (6.5W-8W).

These parameters were chosen based on compatibility with the Iridium satellite constellation and field-tested LoRa configurations for long-range, low-power data exchange.

In this experiment, the objective is to investigate and evaluate the impact of key design parameters on the performance of a GST operating within an L-band satellite communication environment. The study considers several independent variables, including antenna type such as patch, Yagi, and helical; antenna gain values ranging from 3 dBi to 12 dBi; and transmission power levels of 10 dBm, 14 dBm, and 20 dBm. LoRa modulation parameters are also varied, including spreading factor values from SF7 to SF12, bandwidth settings between 125 kHz and 250 kHz, and coding rates from four-fifths to four-eighths. Additional treatment variables include the orientation of the GST, the deployment environment such as open field, urban setting, and locations near physical obstructions, as well as the type of power source used, which may include battery, solar, or hybrid systems. The dependent variables, representing GST performance, include received signal strength indicator (RSSI), signal-to-noise ratio

(SNR), packet delivery ratio (PDR), latency, and overall link availability during satellite passes. Control variables such as satellite system, operating frequency that are fixed within the L-band, firmware version, payload size, and environmental conditions are held constant to ensure validity and comparability across different treatments. Treatments are structured using a factorial design, where each treatment consists of a specific combination of the independent variable levels. Each treatment is repeated across multiple satellite passes to ensure statistical reliability and account for temporal variation. Data will be collected using LoRa logging devices, GPS modules, and satellite pass prediction tools, with post-processing and analysis conducted to determine the impact and interaction of each design parameter on GST performance.

3.3.3 Link Budget and Theoretical Analysis

This study adopts a classical uplink link-budget formulation to evaluate the feasibility of the GST in establishing a reliable communication link with the Iridium LEO satellite constellation. The formulation is employed as a methodological tool to translate system design parameters into a quantitative carrier-to-noise performance metric, which subsequently serves as the basis for link margin evaluation. This approach is consistent with established satellite communication analysis practices and is particularly suitable for LEO satellite systems operating in the L-band.

The uplink carrier-to-noise density ratio, denoted as $(C/JV_0)_{up}$, is calculated using the following expression:

$$(C/JV_0)_{up} = \text{EIRP} - L + (G/T)_{sat} - B + 228.6 \quad (3.2)$$

where EIRP represents the effective isotropic radiated power of the GST transmitter, Ldenotes the total propagation losses along the uplink path, $(G/r)_{sat}$is the satellite receiver figure-of-merit, and Sis the receiver noise bandwidth expressed in dBHz. The constant term 228.6 dB corresponds to the Boltzmann constant expressed in logarithmic form and ensures dimensional consistency in the carrier-to-noise density calculation.

In this formulation, the satellite receiver performance is characterised using the gain-to-noise-temperature ratio (G/T) rather than by explicitly modelling the satellite

antenna gain and receiver noise temperature as separate parameters. The G/T metric provides a compact representation of the effective receive antenna gain, system noise temperature, and front-end losses, thereby simplifying the uplink analysis while preserving physical accuracy. This modelling choice is widely adopted for satellite systems employing multi-beam or phased-array antennas, such as the Iridium constellation, where the effective antenna gain varies with beam geometry and user location.

By adopting a G/T-based uplink formulation, the methodology avoids potential double counting of receiver-side gains and losses that may arise when antenna gain and noise temperature are treated independently. Consequently, the satellite antenna gain is not introduced as a separate input parameter in the uplink link-budget computation. Any indicative antenna gain values are therefore treated solely as reference information, while the link margin calculation itself relies on the satellite G/T specification. This ensures methodological consistency and enables a conservative yet realistic assessment of uplink performance.

The above formulation forms the analytical foundation for the link margin evaluation presented in Chapter 4. The calculated $(C/JV_0)_{up}$values are subsequently compared against the minimum carrier-to-noise requirements for Iridium Short Burst Data (SBD) operation to determine the available link margin under different GST transmission power configurations. By clearly defining the uplink link-budget methodology at this stage, the analysis in the results chapter remains transparent, reproducible, and traceable to the underlying system assumptions.

3.3.4 Doppler Shift Analysis

Given the relative motion between satellites and ground terminals, Doppler shifts can significantly affect communication quality. An analytical study is performed to evaluate the impact of Doppler-induced frequency variations on the LoRa modulation scheme. This includes assessing the potential for inter-symbol interference and the degradation of signal orthogonality. The findings inform the implementation of compensation techniques to mitigate Doppler effects, ensuring robust communication links.

The Doppler effect that resulting from the relative motion between satellites and ground terminals, causes frequency shifts that can disrupt communication. The Doppler shift *(fj))* is estimated using:

$$fD = (v.fc)/c \quad (3.3)$$

Where:

v = Relative velocity between satellite and ground terminal (m/s)

fc = Carrier frequency (Hz)

c = Speed of light (~ 3 x 10^8m/s)

Understanding and mitigating Doppler effects are crucial for maintaining robust satellite IoT links, especially in Low Earth Orbit (LEO) satellite systems where relative velocities are significant. Studies have shown that higher spreading factors are more susceptible to Doppler-induced errors, emphasizing the need for careful parameter selection in satellite applications.

The maximum Doppler shift was theoretically predicted at ±4 kHz, confirmed by real signal logs using an SDR-based Iridium decoder (Omar et al., 2024). Frequency compensation models were embedded in the firmware to auto-adjust carrier frequency for optimal alignment with Iridium LEO satellite motion. Validation was cross-referenced with SOP-based Doppler estimation methods as proposed by Tan et al. (2020).

In this study, Doppler shift analysis is an essential part of the system performance evaluation, particularly due to the high relative velocity between the Iridium satellite and the LoRa-based GST. The Doppler effect introduces frequency offsets that can impact signal synchronization, decoding reliability, and overall link margin, especially within the narrowband simplex transmission of Iridium Short Burst Data (SBD) service. To manage this effect, the design of this study draws conceptual guidance from the Doppler estimation strategy proposed by Tan et al. (2020), who introduced the Quadratic Square Accumulating Instantaneous Doppler Estimation (QSA-IDE) algorithm for Iridium-based signals in weak signal environments.

Although the full implementation of QSA-IDE is not directly applied in this GST system, its foundational approach is relevant for interpreting the Doppler

conditions experienced during real-world field tests. Specifically, the use of full-burst signal processing and signal squaring to mitigate modulation-induced phase errors in low-SNR conditions informs the methodological approach of this research. The Iridium SBD signals used in this study are not continuous and exhibit burst-mode behaviour similar to the Iridium simplex signals discussed by Tan et al., hence sharing similar Doppler characteristics.

The empirical approach adopted involves logging timestamps, Received Signal Strength Indicator (RSSI), and Signal-to-Noise Ratio (SNR) values from the RockBLOCK Mk2 modem during satellite uplink and downlink sessions. Doppler shift is estimated based on the deviation between the nominal carrier frequency and the observed signal characteristics during transmission. Given the fixed transmission frequency of the Iridium uplink (1626.5 MHz) and the known velocity of Iridium LEO satellites (approximately 7.5 km/s), a theoretical Doppler shift of up to ±6.83 kHz is expected. Field test results are compared against this theoretical range to validate the presence and impact of Doppler-induced offset.

In addition to theoretical Doppler estimations as shown by Boiardt et al., who reported maximum frequency deviations of ±42.9 kHz in opposite-direction passes between Earth and Iridium satellites, this study also considers the work of Tan et al. (2020), who introduced a robust Doppler estimation algorithm for weak-signal environments. While the FR7 model verifies that the Iridium 9601 transceiver tolerates Doppler shifts within ±37.5 kHz, the QSA-IDE method supports real-world frequency offset measurement. In this thesis, the Doppler shifts encountered during satellite communication are evaluated against these benchmarks, and system performance is validated through real-time RSSI, SNR, and latency measurements from the LoRa-Iridium GST prototype.

The Doppler shift was characterised using two reporting levels. The typical value, approximately ±2.2 kHz, represents nominal pass conditions and average radial velocities over the link. The worst-case value, approximately ±6.8 kHz, represents unfavourable geometry and higher radial components. Throughout this thesis, Doppler figures are labelled as 'typical' or 'worst-case' to avoid ambiguity.

In summary, while this research does not implement the QSA-IDE algorithm directly, the method's emphasis on burst signal processing, frequency-domain detection, and noise-robust estimation supports the rationale for Doppler-aware link

margin analysis and synchronization management in the LoRa-Iridium satellite IoT architecture.

3.4 System Development

The system development phase focused on translating the design parameters and theoretical analysis into a fully functional LoRa-based GST for L-band satellite IoT applications. The development process was divided into hardware integration, software implementation, and prototype assembly. Each stage was carried out with an emphasis on low-power operation, environmental robustness, and compatibility with both terrestrial LoRa links and the Iridium Short Burst Data (SBD) service.

3.4.1 System Architecture Overview

The system architecture of the LoRa-based Ground Sensor Terminal (GST) is designed to support low-power, long-range data acquisition and reliable satellite backhaul for L-band IoT applications. As illustrated in Figure 3.4, the architecture follows a two-segment communication model consisting of a terrestrial LoRa link and a satellite-based backhaul link.

In the first segment, distributed sensor nodes collect environmental parameters and transmit the data to a central GST gateway using sub-GHz LoRa communication. The second segment provides long-haul data delivery, where the GST forwards the aggregated sensor data to a Low Earth Orbit (LEO) satellite using an L-band satellite communication link. The satellite subsequently relays the data to the ground station infrastructure for storage and analysis.

The GST gateway acts as the central coordination node, responsible for data aggregation, temporary buffering, time synchronisation, and transmission scheduling. To enhance reliability under intermittent satellite visibility, the architecture adopts a store-and-forward strategy, ensuring that data are preserved locally and transmitted only when adequate satellite link quality is available.

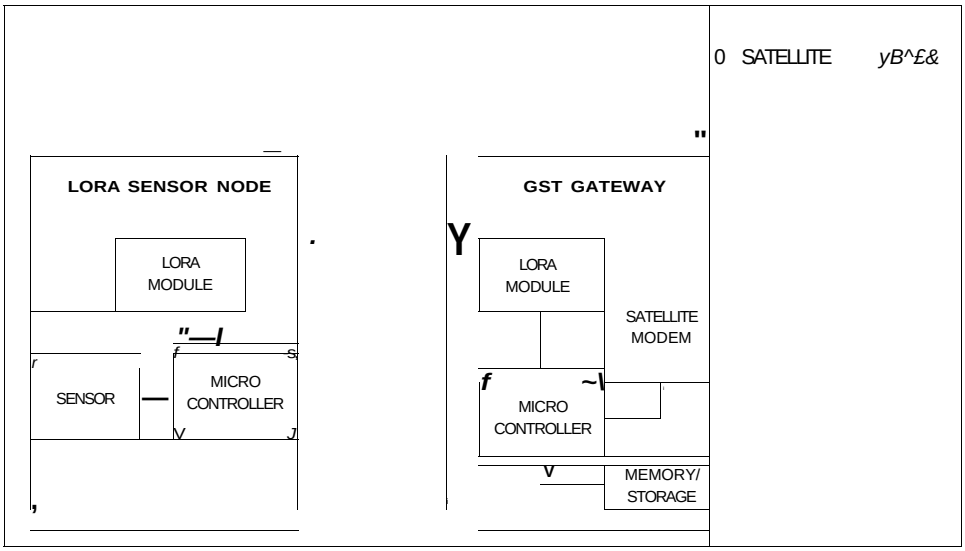

Figure 3.4 GST System Architecture [5].

Figure 3.5 presents the operational flow of the GST, illustrating the sequence from system initialisation to satellite uplink. The architecture emphasises energy efficiency, transmission reliability, and robustness against temporary communication outages, making it suitable for remote and harsh deployment environments.

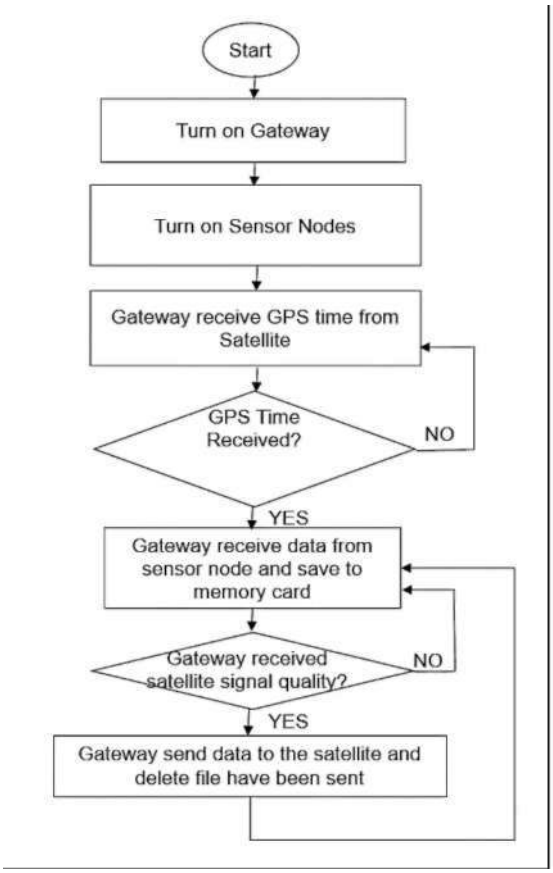

Figure 3.5 Process Flow of Operation of GST

Detailed descriptions of the individual hardware components that realise this architecture are presented in Section 3.4.2.

3.4.2 Hardware Development

The hardware configuration of the developed LoRa-based GST for L-band Satellite IoT applications integrates several key components to ensure reliable performance in harsh environmental conditions. At the core of the system lies a microcontroller board, either based on an ARM Cortex-M0+ or an ESP32 SoC, responsible for executing the control logic and managing data transmission between communication modules. For satellite connectivity, an Iridium Satellite Communication Modem is employed, enabling Short Burst Data (SBD) transmission to the Iridium satellite constellation.

LoRa communication is handled by a Semtech SX1262 chipset, which supports long-range, low-power wireless transmission within the 918 MHz band. The power supply is provided by eight units of Panasonic NCR18650PF lithium-ion rechargeable battery cells arranged to meet the required voltage and current demands of the system. All components are enclosed within a rugged IP68-rated aluminum casing to ensure environmental protection, especially for field deployment in remote or weather-exposed locations.

The system features dual antennas: a Taoglas external satellite antenna with an SMA (male) plug for Iridium communication, and an 8 dBi fiberglass LoRa antenna operating at 915 MHz for terrestrial RF data transmission. For sensor and power interfacing, three units of CN LINKO IP67-rated aviation connectors (2-pin, 4-pin, and 5-pin) are installed, enabling secure and waterproof connections. Data logging and internal storage capabilities are provided by a 4 GB SanDisk MicroSD card, allowing local data buffering and diagnostics.

3.4.2.1 L-band Satellite Modem

To enable direct communication with the Iridium satellite constellation, the GST integrates the RockBLOCK Mk2 satellite modem as its core Iridium communication module. As shown in Figure 3.6, the RockBLOCK Mk2 is a compact, plug-and-play

Short Burst Data (SBD) transceiver based on the Iridium 9602 chipset, enabling two-way data transmission via L-band frequencies globally.

Figure 3.6 Iridium Satcomm Module - RockBLOCK Mk2 [49].

This module allows transmission of binary or ASCII payloads of up to 340 bytes uplink and 270 bytes downlink and is optimized for IoT and remote telemetry applications. It connects to the GST's microcontroller via a standard UART interface, with AT-command control over serial communication. The module is equipped with an onboard power regulation system and is compatible with a wide range of supply voltages (5-12V), making it ideal for integration with embedded systems.

The RockBLOCK Mk2 supports store-and-forward messaging, which is critical for asynchronous communication with Low Earth Orbit (LEO) satellites such as those in the Iridium NEXT constellation. With its integrated SMA connector, it interfaces seamlessly with the M1600HCT-P-SMA passive antenna used in this project. Its small form factor and minimal power consumption further enhance the GST's field deploy ability and energy efficiency, making it well-suited for long-term remote environmental monitoring via satellite IoT.

3.4.2.2 L-band Antenna

To enable reliable data transmission to the Iridium satellite network, the GST was equipped with a passive Iridium/GPS/GLONASS antenna, specifically the M1600HCT-P-SMA model as shown in Figure 3.7. This antenna is designed for L-band operation, covering the 1.616 to 1.6265 GHz frequency range, which aligns precisely with the Iridium uplink band.

Figure 3.7 Passive Iridium Antenna M1600HCT-P-SMA [50]

The M1600HCT-P-SMA features an omnidirectional radiation pattern with peak gain optimized for hemispherical satellite visibility. It integrates a high-performance ceramic patch and offers a low-profile, weather-resistant form factor, making it suitable for outdoor deployments in harsh environmental conditions. With an SMA connector and a robust ground plane requirement, it was mounted on a 2.5-meter mast to maximize line-of-sight exposure to passing Iridium satellites.

Despite being passive or non-amplified, the antenna provides sufficient gain when used in conjunction with the SX1262 transceiver and a calibrated RF front-end, enabling successful data uplink during the AoS-LoS window. Its dual compatibility with GNSS (GPS/GLONASS) also supports time synchronization and location reporting, further enhancing GST performance for satellite IoT applications.

3.4.2.3 LoRa Module

As shown in Figure 3.8, for the implementation of the terrestrial communication link in the GST, this study utilizes the E22-900M22S LoRa module, a high-performance wireless transceiver developed by Ebyte based on the Semtech SX1262 chipset. Operating at 900 MHz, the module is configured for 22 dBm (160 mW) output power and includes a Temperature Compensated Crystal Oscillator (TCXO), which enhances frequency stability under varying environmental conditions that are particularly important for Doppler-sensitive satellite uplinks.

Figure 3.8 LoRa Module [51]

The E22-900M22S supports LoRa modulation, offering long-range, low-power data transmission suitable for remote sensor communication. Its key features include:

The system offers a wide communication range, achieving up to 5-10 km in open ground tests and reaching a maximum of 6500 m in ideal line-of-sight conditions. It features an ultra-low power sleep mode, making it suitable for energy-constrained IoT devices. Additionally, it supports flexible configuration of key parameters such as spreading factor, bandwidth, coding rate, and preamble length, enabling optimisation for diverse operational requirements.

As a Surface-Mount Device (SMD) module, it integrates seamlessly into custom PCB designs within the GST system, allowing compact hardware architecture and direct UART interfacing with the microcontroller unit (MCU). This module was selected for its proven reliability, affordability, and alignment with Malaysian ISM band regulations, making it ideal for ground-to-satellite pre-uplink testing and terrestrial transmission benchmarking.

3.4.2.4 LoRa Antenna

For terrestrial LoRa communication and ground-based testing, the GST was equipped with a 42 cm 915 MHz LoRa antenna, designed for optimal performance within the ISM frequency band used in Malaysia. The antenna operates at 915 MHz, matching the frequency setting of the SX1262 LoRa transceiver used in this study as shown in Figure 3.9.

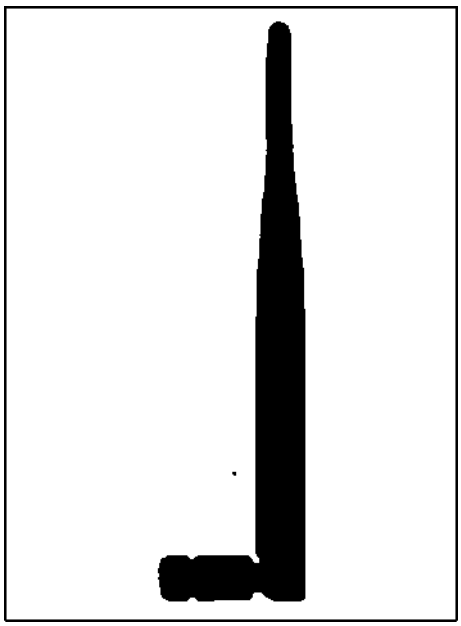

Figure 3.9 LoRa Antenna [19]

With a physical length of approximately 42 centimetres, the antenna provides improved gain and enhanced transmission range due to its increased electrical length and resonant characteristics. The antenna is configured as a half-wave or 5/8-wave monopole, depending on the loading coil structure, and is mounted vertically to ensure omnidirectional radiation in the horizontal plane.

The use of this antenna supports reliable signal propagation in rural and open-field environments and was essential for range testing and ground-to-satellite pre-uplink validation under controlled conditions. Its SMA male connector allows seamless integration with the transceiver module, and the antenna's rugged design ensures stability during long-duration outdoor deployments.

3.4.2.5 Microcontroller

The GST was built around the ESP32-WROOM-32U microcontroller, a highly integrated, low-power MCU module developed by Espressif Systems. As shown in Figure 3.10, This module features a dual-core 32-bit Xtensa® LX6 processor with clock speeds up to 240 MHz and integrates Wi-Fi (802.11 b/g/n) and Bluetooth (v4.2 BR/EDR and BLE) capabilities. It includes 4 MB of embedded flash memory, offering sufficient storage for firmware and temporary data buffers.

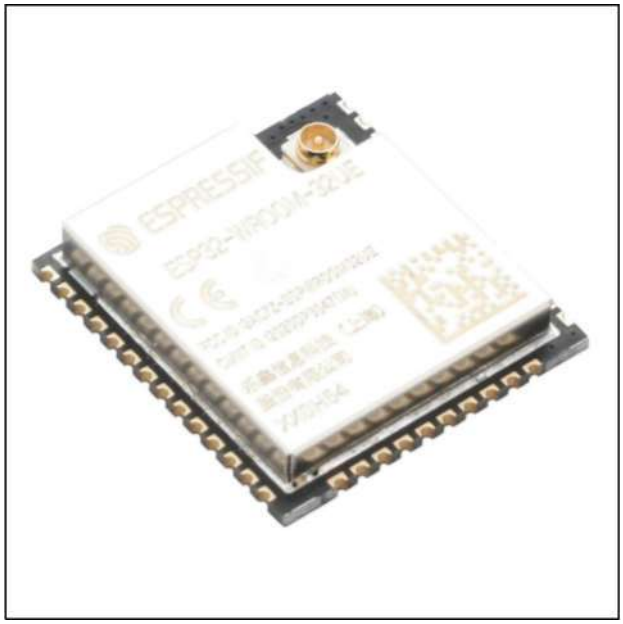

Figure 3.10 Microcontroller ESP32-Wroom [52]

The ESP32-WROOM-32U was specifically chosen for its external U.FL antenna connector, which allows the use of high-gain directional or omnidirectional antennas to improve wireless communication range and signal strength. This feature makes it ideal for long-range IoT applications such as LoRa-based ground-to-satellite telemetry systems.

The ESP32-WROOM-32U microcontroller module offers several notable features that enhance its suitability for low-power, high-performance IoT applications. It is equipped with multiple General-Purpose Input/Output (GPIO) pins that support a wide range of digital interfaces including UART, SPI, I²C, ADC, DAC, and PWM, enabling flexible integration with various sensors and communication peripherals. The module supports ultra-low power sleep modes, which are critical for extending battery life in remote and energy-constrained environments. In addition, it includes a built-in

Real-Time Clock (RTC) that facilitates accurate event timing and task scheduling, further supporting autonomous system operation. To ensure data and system security, the ESP32-WROOM-32U also features secure boot and flash encryption capabilities, providing enhanced protection against unauthorized access and firmware tampering.

In the GST architecture, the ESP32-WROOM-32U manages sensor data acquisition, LoRa communication control, and Iridium message scheduling, operating as the central command module that coordinates system-level tasks. Its compact footprint and robust wireless stack make it an ideal microcontroller for edge-based satellite IoT applications deployed in remote environments.

One of the key criteria for selecting the ESP32-WROOM-32U as the microcontroller for the GST is its low power consumption and compact form factor, both of which are critical for space- and energy-constrained satellite IoT applications. Compared to other variants such as the ESP32-WROVER, which includes additional PSRAM and has a larger footprint, the ESP32-WROOM-32U offers a more streamlined design while maintaining sufficient processing power for data acquisition, control tasks, and communication handling.

The module's U.FL connector for external antennas provides enhanced flexibility for field deployments requiring improved wireless performance. Moreover, the efficient sleep modes of the ESP32-WROOM-32U enable significant energy savings during idle periods, aligning with the project's requirement for prolonged operation on limited power sources. These features collectively make it a suitable candidate for use in compact, low-power LoRa-based telemetry systems intended for integration with satellite communication links.

3.4.2.6 Battery Pack

To support long-duration, off-grid operation of the GST, the power system was designed using eight (8) units of Panasonic NCR18650PF rechargeable lithium-ion cells, connected in parallel configuration as shown in Figure 3.11. Each cell is of the 18650 cylindrical formats, offering a nominal voltage of 3.6 V and a typical capacity of 2,900 mAh, resulting in a total capacity of approximately 23,200 mAh at 3.6 V for the entire battery pack .

Figure 3.11 Battery Cell Panasonic NCR18650PF[53]

The parallel arrangement ensures that the system maintains a stable operating voltage while significantly increasing the available current capacity and total runtime. The Panasonic NCR18650PF cells are chosen for their high energy density, reliable discharge profile, and robust safety characteristics, including built-in protection against over-discharge and thermal stress.

This battery configuration supports the intermittent transmission nature of LoRa and Iridium-based systems, allowing the GST to remain in deep sleep or low-power standby modes for extended periods, only waking for scheduled transmissions during satellite visibility windows. The selected battery pack design aligns with the project's objective of deploying energy-efficient satellite IoT terminals in remote and harsh environments without frequent maintenance or recharging.

3.4.3 Software Implementation

The hardware implementation involves assembling the selected components onto a printed circuit board (PCB), ensuring proper interfacing and power management. Firmware development encompasses programming the MCU to manage tasks such as sensor data acquisition, LoRa communication handling, and power-saving operations. The software is designed to be modular, allowing for easy updates and scalability.

The GST prototype is developed using various components to ensure efficient operation. LoRa modules based on the SX1276 chipset are used for long-range communication, while an ESP32 microcontroller handles data processing and

transmission control. Several sensors are integrated, including the DHT22 for temperature and humidity measurement, the BMP 180 for barometric pressure and altitude readings, and a GPS module for time synchronization. For satellite communication, the Iridium 9602 L-band satellite modem enables uplink transmission. The system is powered by a Li-Ion battery with solar panel charging, ensuring sustainable and continuous operation.

The GST firmware is developed using Arduino IDE and embedded C, incorporating several key features to enhance functionality. The LoRa communication protocol is implemented to enable point-to-point transmission between sensor nodes and the gateway. Sensor data is structured into predefined packets through a data packetization process to ensure efficient transmission. To optimize communication with the satellite, the firmware synchronizes transmission timing with the Acquisition of Signal (AoS) and Loss of Signal (LoS) during satellite passes. Additionally, an error detection and retransmission mechanism are integrated, allowing automatic retransmission of data packets if an acknowledgment (ACK) is not received.

Firmware was developed in C++ using Arduino DDE. The transmission protocol used a custom frame structure: [Device ID | Timestamp | GPS | Payload | CRC]. Duty cycle was regulated to 1% to comply with ISM band regulations. Data logging was implemented via onboard SD card and redundant transmission was activated in cases of Doppler-induced frequency shift.

Upon system boot-up, the setup() routine initializes all critical hardware interfaces, including I2C communication for the TMP100 temperature sensor, ADC pin configurations for battery monitoring, and the SPI interface for SD card access. Additionally, the LoRa module is initialized with specified radio parameters which is frequency, spreading factor (SF12), bandwidth (125 kHz), and coding rate (4/5) to ensure compatibility with remote sensor nodes. The Iridium subsystem is powered up and configured for short burst data (SBD) communication. At this stage, the device synchronizes its real-time clock (RTC) using the system time obtained directly from the Iridium satellite network, ensuring accurate timestamping for all collected data.

Once the system enters the main operational loop, it continuously performs three primary tasks. Firstly, it listens for incoming LoRa packets using the checkLoraData() function. Any received data is decoded into structured fields, including node ID, node type, battery level, and four sensor data fields (D1-D4), which are then written into a CSV file on the SD card using the writeLoratoSDQ function. Secondly, the firmware

checks for any input via the USB serial port, allowing direct data entry or debugging, which is similarly saved to SD card via the writeSerialtoSD() routine. Both data streams are tagged and saved in the /to_send/ directory, setting a buffer flag to indicate readiness for transmission.

The third stage involves assessing whether the system is scheduled or triggered to transmit data. Transmission can be time-driven, where the firmware is programmed to attempt data uplink at regular intervals every 15 minutes in the case of transmissionPeriod == 1. This periodic execution is managed through RTC time checks embedded within the loop. When the condition for transmission is met and data is available in the buffer (SD_BUFFER == 1), the firmware executes transmitDataQueue() to iterate over the data files in the /to_send/ directory. Before initiating each transmission, it verifies Iridium signal strength and only proceeds if the signal quality exceeds a predefined threshold. Upon successful SBD transmission, the corresponding file is deleted to avoid redundant retransmission. Detail Process flow shown in Figure 3.12.

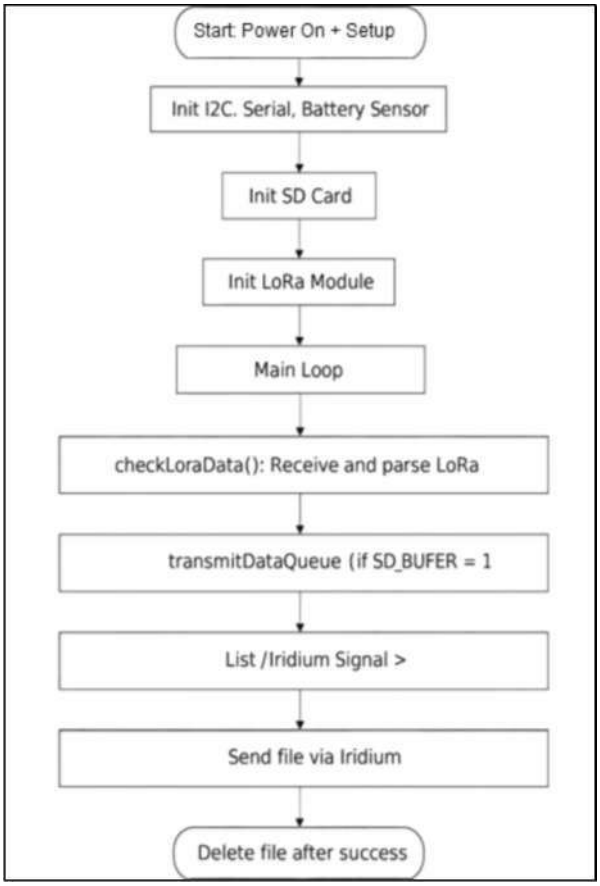

Figure 3.12 GST Firmware Process Flow

The overall flow ensures robust and fail-safe handling of telemetry data, from collection to delivery via satellite. The block diagram captures this entire sequence, starting from firmware initialization, transitioning through the main operational loop, and culminating in satellite transmission. It visually highlights the logical separation between data acquisition, conditional scheduling, and transmission, which is critical for understanding system reliability and energy efficiency in remote IoT deployments using L-band satellite IoT protocols.

3.4.4 Prototype Integration

3.4.5 Prototype Testing

A prototype of the GST is developed to validate the design and implementation. Initial testing focuses on verifying the functionality of individual components and the overall system integration. Subsequent tests assess the GST's performance in controlled environments, measuring parameters such as transmission range, data rate, and power consumption. These tests provide insights into the system's readiness for deployment in real-world scenarios.

Prototyping and performance testing are critical phases in the development of LoRa-based GST, especially for applications involving L-band satellite IoT communications. These processes ensure that the designed systems meet the required specifications for reliability, energy efficiency, and communication performance.

3.4.5.1 Hardware Selection and Integration

The foundation of an effective GST prototype lies in the careful selection and integration of hardware components. Microcontrollers such as the Atmega32u4 are favored for their low power consumption and sufficient processing capabilities. These are often paired with LoRa transceiver modules like the E22-900M22S, which operate efficiently at frequencies such as 915 MHz. For instance, a hybrid GST developed for educational purposes integrated a LoRa module with a Wi-Fi module (ESP-12E), enabling both satellite and terrestrial communication. This system operated entirely on a 3.3V power supply, simplifying the electrical design and allowing the use of low-cost,

commercially available solar panels and lithium-ion batteries for energy harvesting and storage.

3.4.5.2 Firmware Development and Optimization

Firmware development is pivotal in managing sensor data acquisition, communication protocols, and power management. Developers often utilize open-source libraries and development environments to expedite the firmware development process. For example, the Arduino IDE is widely used for programming microcontrollers, offering a vast repository of libraries and community support.

Power optimization strategies are implemented in firmware to extend the operational lifespan of battery-powered devices. Techniques include:

i. Duty Cycling: Reducing power consumption by alternating between active and sleep modes.
ii. Adaptive Data Rate (ADR): Dynamically adjusting data rates based on network conditions to balance power usage and communication reliability[54].
iii. Efficient Scheduling: Timing sensor readings and data transmissions to minimize unnecessary power expenditure.

These strategies are crucial for ensuring that GSTs can operate autonomously for extended periods, especially in remote or inaccessible locations.

3.4.5.3 Power Consumption Analysis

Understanding and minimizing power consumption is essential for the longevity of GSTs. Empirical testing of various LoRa development boards has revealed significant variations in power consumption, even among devices marketed as low power. For instance, studies have shown that some boards consume more than 570 µA in low-power mode, which is substantially higher than expected. To address this, researchers have developed power models that estimate energy requirements based on

transmission profiles, enabling designers to predict battery life and optimize power usage.

3.4.5.4 Communication Performance Evaluation

Evaluating the communication performance of LoRa-based prototypes involves assessing metrics such as:

i. Received Signal Strength Indicator (RSSI): Measures the power level of received signals.
ii. Signal-to-Noise Ratio (SNR): Assesses the quality of the signal relative to background noise.
iii. Packet Delivery Ratio (PDR): Calculates the percentage of successfully received packets.
iv. Round-Trip Time (RTT): Measures the time taken for a signal to travel to the receiver and back.

Testing is conducted in various environments to simulate real-world conditions. For instance, indoor testing assesses performance in the presence of obstacles and multipath effects, while outdoor testing evaluates range and reliability in open spaces. Additionally, satellite communication tests are performed to validate the GST's ability to transmit data during satellite pass-over periods.

3.4.5.5 Certification and Compliance Testing

For commercial deployment, devices must comply with regulatory standards and certifications. The LoRa Alliance provides a standardized RF Performance Evaluation Procedure to harmonize the measurement of transmit and receive performance. This includes:

i. Effective Isotropic Radiated Power (EIRP): Measuring the radiated power in all directions.

ii. Packet Error Rate (PER): Determining the rate of unsuccessful packet transmissions.

iii. Total Radiated Power (TRP): Assessing the total power emitted by the device.

These evaluations ensure that devices meet the necessary performance and interoperability standards for integration into existing networks.

Two prototypes were built and tested. The first was deployed for lab testing and debugging, while the second was used for field trials. Both units were calibrated using a signal generator and spectrum analyzer to validate transmission frequency, power, and noise floor. Calibration records were documented and stored as part of the reproducibility protocol.

3.5 Performance Validation of GST

The GST is tested under three different conditions to evaluate its communication reliability, signal quality, and satellite connectivity.

a) Indoor Testing

Figure 3.13 illustrates the experimental layout adopted for indoor measurements. The testing is conducted in a laboratory environment with obstacles such as walls to evaluate the impact of indoor interference on signal transmission. The primary objective is to analyze signal attenuation caused by these obstacles. Key metrics used for assessment include the Received Signal Strength Indicator (RSSI) and Signal-to-Noise Ratio (SNR). Figure 3.13 shows the indoor experimental layout, where the LoRa sensor node and GST were deployed within a laboratory environment separated by internal obstacles such as walls. Measurements were taken by incrementally increasing the separation distance between the sensor node and the GST at fixed intervals, while recording RSSI and SNR to evaluate attenuation and multipath effects under line-of-sight conditions.

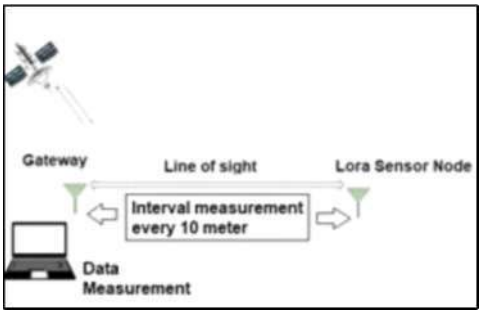

Figure 3.13 Indoor Measurement Layout

b) Outdoor Testing

Figure 3.14 illustrates the outdoor measurement layout conducted in an open-field environment with a clear line-of-sight between the sensor node and the GST. The sensor node was positioned at progressively increasing distances to assess range-dependent performance. Data received at the GST were forwarded via the Iridium Short Burst Data service, enabling end-to-end evaluation under realistic outdoor propagation conditions.

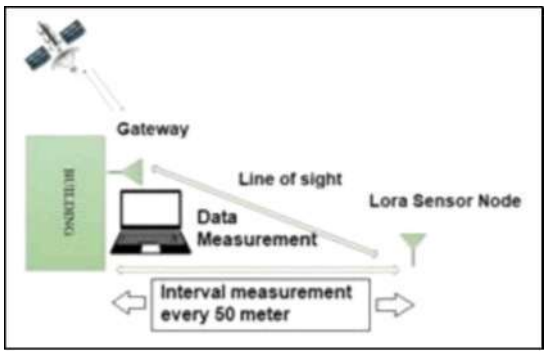

Figure 3.14 Outdoor Measurement Layout

3.5.1 Experimental Setup - (Location, Tools, Environmental Factors)

Experiments were conducted at Universiti Teknologi MARA, UiTM Shah Alam, located at coordinates 3.07314°N latitude and 101.49753°E longitude, a low-latitude test site chosen for its unobstructed sky view and equatorial satellite coverage. Tests were performed between 3 October and 9 October 2024, during the inter-monsoon period with minimal rainfall. Ambient temperature was recorded between 27°C to 33°C, and relative humidity between 68% and 82%. Wind speed remained below 10 km/h

throughout the trials. All readings were logged using a Davis Vantage Vue weather station. The antenna mast height was fixed at 2.5 meters above ground.

Performance validation is conducted in environments that simulate the operational conditions of the GST. This includes open-field testing to evaluate line-of-sight communication and urban settings to assess performance amidst potential obstructions. Antenna configurations are tested to determine the optimal setup for maximizing signal strength and coverage.

To evaluate the effectiveness of the GST, several performance metrics are analyzed. The Received Signal Strength Indicator (RSSI) measures the power level of the received signal, where a higher RSSI indicates a stronger signal and better communication reliability. RSSI values range from -46 dBm indicate strong signal to -104 dBm which is weak signal. The Signal-to-Noise Ratio (SNR) assesses signal clarity relative to background noise, with higher SNR values indicating cleaner signals with less interference. Recorded SNR values range from -20.25 dB to 4 dB, depending on the environment. The Acquisition of Signal (AoS) and Loss of Signal (LoS) are also evaluated to determine the time window when the satellite is visible, allowing for optimized data transmission timing to maximize success rates. Lastly, the transmission success rate measures the number of data packets successfully received by the satellite, which is influenced by factors such as antenna gain, environmental obstructions, and satellite pass timing.

Based on the performance analysis, several optimization strategies are implemented to enhance the GST's efficiency. Antenna gain adjustment is conducted by comparing the performance of 8 dBi and 2 dBi antennas to improve signal strength and transmission range. Transmission timing optimization is achieved by adjusting data transmission schedules based on satellite pass predictions, ensuring alignment with the Acquisition of Signal (AoS) and Loss of Signal (LoS) windows. Additionally, the LoRa air data rate is fine-tuned to 0.3 kbps to enhance transmission reliability. To reduce power consumption, a low-power sleep mode is implemented to extend battery life, while solar energy harvesting is utilized to ensure sustainable operation.

Figure 3.15 illustrates the AoS-LoS (Acquisition of Signal to Loss of Signal) window during a Low Earth Orbit (LEO) satellite pass, such as those operated by the Iridium constellation. The curve represents the satellite elevation angle as perceived from a ground-based terminal, forming a parabolic trajectory as the satellite moves across the sky. The window begins at AoS when the satellite rises above the local

horizon and first becomes visible and ends at LoS, when it drops below the horizon and is no longer in line of sight.

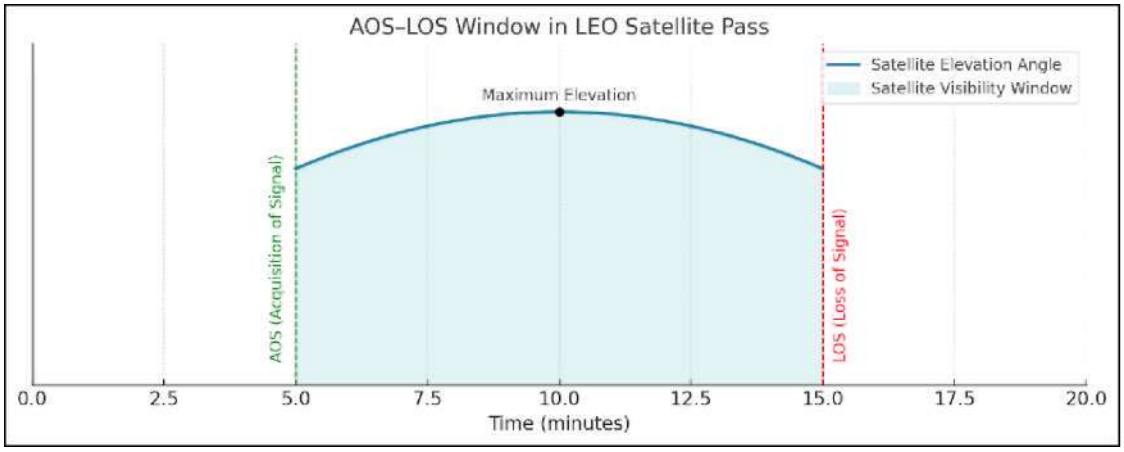

Figure 3.15 AoS-LoS Window in LEO Satellite Pass

This visibility window typically lasts between 7 to 12 minutes, during which the GST must synchronize its data transmission with satellite availability. The peak of the curve represents the moment of maximum elevation, where the satellite is closest to the observer and signal strength is optimal. Accurate prediction of this window is critical for effective data uplink, especially for time-sensitive and power-limited LoRa transmissions. Furthermore, aligning GST transmission with AoS-LoS windows reduce the risk of packet loss caused by Doppler-induced frequency shifts or incomplete transmission due to early signal cutoffs.

Figure 3.16 illustrates the ground terminal's beam coverage area, which defines the angular field of view (FOV) within which a LoRa-based GST can communicate with a Low Earth Orbit (LEO) satellite. This beam typically spans an elevation angle range from approximately 60° to 120°, corresponding to a beamwidth of about 60°, depending on antenna gain and the terminal's geographical location.

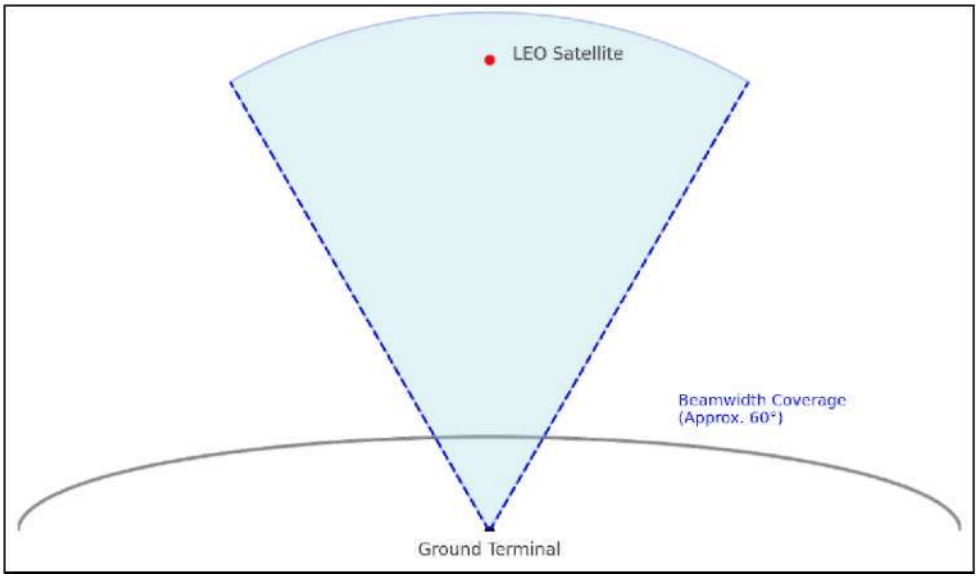

Figure 3.16 Ground Terminal Beam Coverage

The area shaded in light blue represents the satellite visibility cone, wherein the satellite is within line-of-sight and the received signal strength is above the minimum threshold required for successful uplink. As the satellite enters this beam at Acquisition of Signal (AoS) and exits at Loss of Signal (LoS), the GST must perform time-optimized data transmission aligned with this window. The edges of the beam define critical angles where Doppler shift and signal attenuation become significant, necessitating dynamic frequency compensation.

Understanding the geometry of this coverage is crucial for accurate scheduling of transmission bursts, Doppler estimation, and link margin prediction especially in constrained bandwidth satellite IoT applications.

Figure 3.17 shows a real-time satellite ground track generated using Orbitron software, highlighting the global distribution of the Iridium satellite constellation. The map visualizes active Iridium satellites for example IRIDIUM 119, 139, 144 and their respective orbital paths in Low Earth Orbit (LEO). The yellow arcs represent satellite footprints, which define the communication coverage zones visible from each satellite at a given time.

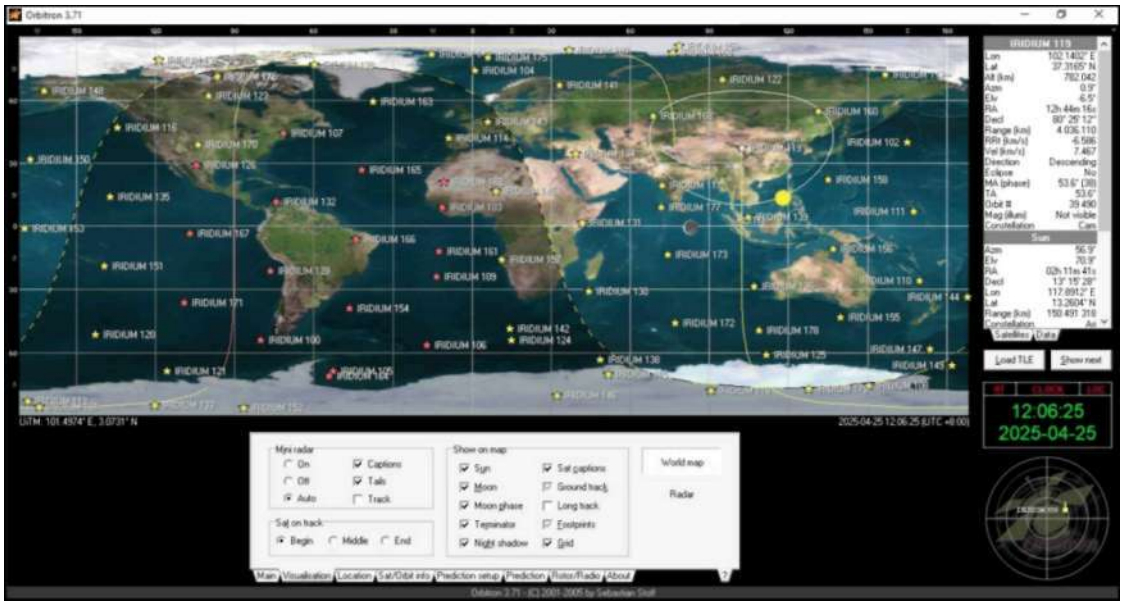

Figure 3.17 Real-Time Iridium Satellite Pass Map

In this instance, the satellite IRIDIUM-119 is shown passing over Southeast Asia, with its current location, elevation angle, azimuth, and slant range parameters displayed on the right. The red line indicates the satellite's descending orbital path, while the GST is located at 3.0731°N, 101.4974°E, near UiTM Shah Alam, Selangor, Malaysia. The highlighted circular area surrounding the satellite denotes the region within which the satellite is above the horizon and can potentially establish uplink communication with ground terminals.

This figure is crucial for visualizing the Acquisition of Signal (AoS) and Loss of Signal (LoS) windows in real-time, enabling precise scheduling of LoRa transmissions from the GST. It also assists in Doppler shift estimation and planning of duty cycles, ensuring energy-efficient and timely data delivery. By aligning GST operation with satellite visibility zones as seen in this map, communication reliability can be significantly enhanced, especially under short LEO pass durations.

3.5.2 Maximum Communication Range Testing

Range testing was conducted by gradually increasing the distance between transmitter and receiver, starting from 100 meters up to 10 km in open terrain. Transmission success rate, RSSI, and SNR were recorded every 500 meters. SF9 and 125 kHz bandwidth were used consistently, with transmission power at 20 dBm. Ground conditions either flat or grassy field and weather were kept constant.

Tests are performed to determine the maximum effective communication range of the GST. This involves incrementally increasing the distance between the GST and the receiver until the signal quality degrades below acceptable thresholds. The results inform the practical deployment limits of the system and guide recommendations for network planning.

The objective of this test is to determine the farthest distance at which the LoRa GST can reliably transmit data. The procedure involves placing a sensor node at increasing distances in 10-meter intervals while recording the transmission success rates and signal quality. Additionally, the performance of two different antenna gain configurations, 2 dBi and 8 dBi, is compared. The expected outcome is that the 8 dBi antenna will provide higher signal strength and an extended transmission range compared to the 2 dBi configuration.

3.5.3 Satellite Signal Strength Evaluation

To validate the operational performance of the GST in establishing uplink communication with a Low Earth Orbit (LEO) satellite, a signal strength measurement experiment was carried out during a scheduled Iridium satellite pass. The experiment aimed to observe the signal reception pattern from the moment of Acquisition of Signal (AoS) until Loss of Signal (LoS), capturing the rise, stabilization, and eventual drop of signal strength across the satellite visibility window. This test was crucial for evaluating the GST's capability in real-world conditions and for assessing the viability of its passive communication strategy.

The experiment was conducted at Universiti Teknologi MARA (UiTM) Shah Alam, specifically in an open-space area within the engineering faculty compound, which provided moderate sky visibility suitable for satellite communication testing. The weather during the experiment was clear with no precipitation, allowing the signal propagation characteristics to be observed without atmospheric disturbances. The GST was deployed in a semi-open area with partial obstruction from nearby structures and vegetation. An omnidirectional vertically polarized antenna with a gain of 8 dBi was mounted at a fixed height of approximately 2.5 meters above ground level. No mechanical tracking was used, reflecting a realistic scenario for passive, low-cost ground terminal deployment.

The satellite pass was predicted in advance using orbital elements and satellite tracking software, allowing the team to synchronize the experiment window with the anticipated AoS and LoS. The satellite was expected to enter the field of view at around 1:04:00 local time and exit by 1:12:00. During this time, the GST was powered and configured to capture real-time signal strength data based on the visual signal bar indicator available on the terminal's interface. Each bar represented a discrete level of signal reception, ranging from 0 or no signal detected to 5 indicate maximum signal quality. The system was designed to automatically log every change in signal strength along with its corresponding timestamp, which was synchronized using a real-time clock (RTC) module. The timing resolution was configured to milliseconds to ensure accurate tracking of signal dynamics.

Although the GST was primarily capable of displaying signal strength in bar format, these bar levels were later interpreted as indicative of the Received Signal Strength Indicator (RSSI) values using empirical mappings derived from prior calibration. For example, a signal bar of 5 was approximated to correspond to an RSSI range of about -80 to -90 dBm, while a bar value of 1 was associated with weaker signals in the range of -116 to -120 dBm. This interpolation allowed for estimation of link margin and assessment of signal fade characteristics, even though absolute RSSI readings were not natively output by the system.

All recorded data were stored in a comma-separated values (CSV) format and imported into MATLAB for processing. A time-series plot of the signal strength against time was generated to visualize the satellite pass trajectory from AoS to LoS. The plotted data provided a clear picture of the terminal's signal acquisition pattern, peak reception period, and signal degradation, enabling the evaluation of terminal readiness and highlighting optimal transmission windows for future IoT-based satellite uplink operations. Further analysis and discussion of this data are presented in Chapter 4.

3.5.4 Data Transmission Delay Analysis

Transmission delay was measured as the time elapsed between data packet generation and confirmation of satellite reception via the RockBLOCK modem interface. Delays were categorized by satellite elevation and averaged across multiple passes. Latency trends were correlated with Doppler shift data to validate time-window optimization models.

An analysis of data transmission delays is conducted to evaluate the system's responsiveness. This includes measuring the time elapsed from data acquisition to successful transmission and reception. Understanding these delays is crucial for applications where timely data delivery is critical.

3.6 Chapter Summary

This chapter presented a holistic research methodology combining simulation, hardware development, and field validation. Every step from parameter selection to environmental logging was documented to support reproducibility and knowledge transfer. Through careful planning, this study aligns not only with academic rigor but also with ethical obligations to ensure the utility and replicability of research outcomes.

In Chapter 3, the methodology for developing and evaluating a LoRa-based GST for L-band satellite IoT applications was comprehensively detailed. The chapter began with the identification of critical design parameters such as Spreading Factor (SF), Bandwidth (BW), and Coding Rate (CR), followed by simulations and theoretical analyses to assess their impact on communication performance. A focused analysis on Doppler shift effects was also conducted to understand frequency variations due to satellite movement. Subsequently, the development phase encompassed system architecture design, component selection including the SX1262 LoRa module and the integration of hardware and software components, culminating in prototype development and preliminary testing. Performance validation involved experimental setups considering environmental factors and antenna configurations, evaluating the GST's maximum communication range, satellite signal strength reception, and data transmission delays. Despite these comprehensive efforts, certain gaps remain, notably the prototype's performance under varying environmental conditions and long-term reliability metrics. The subsequent chapter will delve into the results and discussion, interpreting the data obtained from the performance evaluations, comparing empirical findings with theoretical predictions, and discussing the implications of the identified gaps to inform future enhancements and research directions.

CHAPTER 4
RESULTS AND DISCUSSION

4.1 Introduction to Result Chapter

This chapter presents the results derived from the investigation, development, and validation of a LoRa-based GST for L-band Satellite Internet of Things (IoT) applications. The results are structured according to the research objectives outlined in Chapter 1, with an emphasis on design parameter exploration, prototype development, and system performance validation.

The first section (Section 4.2) addresses the key design parameters that influence the performance of the LoRa-based GST, particularly those related to radio frequency (RF) configurations such as transmission power, frequency, spreading factor, bandwidth, and antenna gain. These parameters were selected based on technical specifications of the system hardware and prevailing standards for low-power wide-area network (LPWAN) communication within the L-band spectrum, specifically for Iridium-based satellite links.

Subsequently, Section 4.3 focuses on the analytical computation and simulation of these design parameters. This includes the theoretical analysis of Free Space Path Loss (FSPL), Doppler shift estimation based on satellite motion, and sensitivity trade-offs resulting from varying spreading factor and bandwidth configurations. All computations are supported by relevant formulas, and the outputs are visualized through tables and plots to justify the parameter selections.

Section 4.4 highlights the hardware implementation and prototype design of both the LoRa sensor node and gateway. This encompasses the system schematic, printed circuit board (PCB) layout, and integration of components such as the microcontroller, transceiver, and antenna. Images and design screenshots are provided to reflect the physical development process and to demonstrate the feasibility of the implemented system architecture.

The final section of this chapter presents the functional testing results of the developed GST system, including selected experimental validation outcomes. However, due to the limited accessibility of custom hardware-level testbeds for the

gateway, the functional validation focuses on end-device-level configurations and programmatic transmission parameters. The validation includes LoRa RSSI and SNR measurements, packet delivery observations, and system response under selected test scenarios.

Overall, this chapter provides a comprehensive presentation of theoretical evaluations, design decisions, and practical implementation outcomes which collectively validate the feasibility of using a LoRa-based GST within an L-band satellite IoT communication framework.

4.2 Objective 1: Design Parameter Analysis

4.2.1 LoRa System Configuration

The performance and reliability of a LoRa-based GST in L-band satellite communication are fundamentally governed by its radio frequency (RF) design parameters. This section elaborates on the critical radio frequency parameters configured in the LoRa sensor node and gateway, with an emphasis on their operational feasibility within the Iridium satellite uplink channel, which operates at approximately 1.6 GHz and the terrestrial 900 MHz unlicensed band. The design parameters include transmission frequency, spreading factor, transmission power, bandwidth, and antenna gain, all of which were selected and adjusted to optimize long-range communication and energy efficiency.

4.2.1.1 Transmission Frequency

The LoRa node was configured to operate at 900 MHz for terrestrial communication, while the satellite backhaul operates at approximately 1.6 GHz via the Iridium SBD service. The 900 MHz configuration aligns with the ISM band allocation in Malaysia, enabling unlicensed operation during ground-level performance validation. Meanwhile, the 1.6 GHz setting is selected to match Iridium's uplink frequency spectrum, ensuring frequency compatibility during transmission to the satellite. This dual-frequency approach supports the GST's capability to operate in both terrestrial and space-based communication environments.

4.2.1.2 Spreading Factor (SF)

The Spreading Factor (SF) in LoRa modulation determines the duration of symbol transmission, thereby affecting both communication range and data rate. The system was configured to operate primarily at SF12, based on its enhanced sensitivity (-137 dBm) and ability to sustain long-range communication with minimal signal degradation. Table 4.1 summarises the relationship between LoRa spreading factor, receiver sensitivity, and achievable data rate as specified in the transceiver manufacturer's datasheet. The values presented are specification-based and are not derived from experimental measurements conducted in this study. This table is included to provide a technical reference for understanding the inherent trade-off between sensitivity and data rate associated with different spreading factor configurations. In this work, the specification values serve as a baseline to justify the selection of SF12 for satellite IoT operation, where maximum receiver sensitivity is prioritised to mitigate high path loss and low elevation angle effects, rather than to evaluate or validate the absolute performance of the LoRa transceiver.

Table 4.1
Relationship Between SF Values and Corresponding Receiver Sensitivity levels.

Spreading Factor	Receiver Sensitivity (dBm)	Data Rate
SF7	423	^5J
SF8	-126	-3.1
SF9	-129	-1.8
SF10	-132	-1.0
SF11	-134.5	-0.5
SF12	-137	-0.3

The selection of SF12 was justified based on the requirement for maximum sensitivity and range, essential for satellite link reliability, despite the associated trade-off in data rate.

4.2.1.3 Transmission Power

The transmission power of the LoRa node was configured at 20 dBm, which was identified as the optimal setting during earlier tests compared to the default maximum of 22 dBm. This decision was based on the observation that 20 dBm produced more stable signal reception while reducing power consumption. Both the sensor node and gateway were configured with identical Tx power levels to ensure symmetrical communication and minimize link budget discrepancies.

4.2.1.4 Bandwidth

A 125 kHz bandwidth was selected as the standard LoRa channel width for all configurations. This bandwidth provides a balanced compromise between data rate and receiver sensitivity. Wider bandwidths, such as 250 kHz and 500 kHz, provide higher data rates. However, they result in reduced receiver sensitivity, which is unfavorable for long-range and low-power satellite IoT applications. The bandwidth value also directly influences the symbol duration and, hence, the time-on-air.

4.2.1.5 Antenna Gain

Antenna selection plays a crucial role in ensuring effective signal transmission and reception. The LoRa sensor node used an internal antenna with a gain of 2 dBi, suitable for mobile or portable deployment. In contrast, the gateway was equipped with an external directional antenna of 8 dBi, mounted at a fixed location to ensure optimal reception of uplink signals. For Iridium SBD-based satellite communication, the external antenna adhered to Iridium's recommended gain specifications of 2.9 dBi, optimized for L-band operations at 1.6 GHz.

Each of these RF parameters will be further evaluated in **Section 4.3**, where their theoretical influence on link performance is quantified through a series of simulations and analytical computations.

4.2.2 Link Margin Analysis

The uplink link margin analysis presented in this section follows the carrier-to-noise density formulation described in Section 3.3.3, which establishes the methodological basis for modelling the GST-Iridium uplink using a G/T-based receiver representation. The analysis was conducted to evaluate the capability of the Ground Sensor Terminal (GST) to establish a reliable uplink with the Iridium L-band satellite constellation. This evaluation integrates transmitter characteristics, propagation losses, satellite receiver sensitivity, and environmental factors to ensure that the received signal at the satellite exceeds the minimum threshold required for Short Burst Data (SBD) demodulation.

The GST employs the Iridium modem's integrated RF transmission system to achieve the required uplink transmission power. Two transmission power levels were assessed, namely 6.5 W and 8 W, corresponding to 8.13 dBW and 9.03 dBW, respectively. These values represent the typical continuous safe operating power and the maximum peak-rated burst power of the amplifier. After accounting for the antenna gain of 2.9 dBi and a conservative 1 dB transmission line loss arising from coaxial cables, SMA connectors, and PCB feedline attenuation, the resulting Effective Isotropic Radiated Power (EIRP) values used in the analysis are 10.03 dBW for the 6.5 W configuration and 10.93 dBW for the 8 W configuration.

Propagation losses were calculated for a slant range of 780 km, corresponding to the nominal orbital altitude of an Iridium satellite during a near-zenith pass. Using the uplink frequency of 1621 MHz, the free-space path loss (FSPL) was computed as 154.63 dB based on the Friis transmission formula. Additional losses include a 1 dB pointing loss due to non-ideal orientation of the omnidirectional GST antenna with respect to the satellite, a 3 dB polarisation mismatch loss arising from the linear-to-right-hand circular polarisation transition between the GST transmitter and the Iridium receiver, and a 0.3 dB ionospheric loss consistent with ITU-R recommendations for L-band propagation in low-latitude regions. The total propagation attenuation therefore amounts to 158.93 dB.

On the satellite side, the Iridium receiver performance is characterised using a figure-of-merit of -21.6 dB/K, which encapsulates the combined effects of effective antenna gain, system noise temperature, and front-end losses. The receiver noise temperature is modelled at 290 K, in line with standard satellite communication

practice. Using the uplink formulation defined in Section 3.3.3, which combines the GST EIRP, total propagation losses, satellite G/T, and the required carrier-to-noise density ratio for Iridium SBD decoding, the resulting link margin values are 7.53 dB for the 8 W configuration and 6.63 dB for the 6.5 W configuration.

As described in Section 3.3.3, the satellite receiver performance is modelled using the G/T parameter; therefore, the satellite antenna gain is not applied as an independent term in the uplink link-budget calculation in order to avoid double counting. The antenna gain value of 1.5 dBi reported in Table 4.2 represents an indicative low-gain, near-omnidirectional antenna characteristic consistent with the wide-area coverage design of the Iridium constellation and is provided for reference only.

These link-margin results were derived under several engineering assumptions. A clear line-of-sight (LOS) condition between the GST and the satellite is assumed, and additional losses due to structural obstructions or shadowing are neglected. A free-space propagation model is adopted, as L-band signals experience negligible rain attenuation. Satellite receiver performance is assumed to remain constant throughout the contact window, and the uplink environment is considered free from significant adjacent-channel or co-channel interference. All assumptions are consistent with standard practice in satellite communication link-budget modelling.

Overall, the computed link margins exceed the commonly accepted minimum threshold of 3 dB for reliable L-band uplink communication. Even at the lower transmit power of 6.5 W, the GST maintains sufficient margin, demonstrating robust operational performance and validating the feasibility of the proposed architecture for low-power satellite IoT applications.

Table 4.2
GST Link Margin

Parameters	**Value**
Ground Sensor Terminal	
Transmitter power output (W)	6.5 / 8
Transmitter power output (dBW)	8.13 / 9 .03
Transmission line losses (dB)	1
Antenna gain (dBi)	2.9

Parameters	Value
Ground terminal EIRP (dBW)	10.03 / 10.93
Channel/ Medium Losses	
Ground pointing loss (dB)	1
Polarisation loss (dB)	3
Free space loss	154.63
Ionosphere loss (dB)	0.3
Total attenuation (dB)	158.93
Isotropic received power (dBW)	-149.60 / -148.70
Iridium Satelite	
Satellite pointing loss (dB)	1
Transmitter power output (W)	0.5
Transmitter power output (dBW)	-3
Line losses (dB)	1.6
Antenna gain (dBi)	1.5
Effective noise temperature (K)	290
Figure of merit (G/T) (dB/K)	-21.624
Link Margin for 8.0 W Power (dB)	7.53
Link Margin for 6.5 W Power (dB)	6.63

4.2.2.1 Free Space Path Loss (FSPL)

FSPL is a fundamental parameter used to estimate signal attenuation over distance in line-of-sight (LOS) communication. The Friis transmission equation was employed to compute FSPL between:

i. LoRa Node to Gateway (terrestrial link, ~2 km), and
ii. Gateway to Iridium Satellite (uplink distance ~780 km to LEO).

4.2.3 Doppler Shift Analysis

Given the relative motion between Low Earth Orbit (LEO) satellites and ground terminals, Doppler shifts can significantly impact communication reliability. An estimation of Doppler frequency shifts was conducted, revealing potential shifts up to ±20 kHz at L-band frequencies. This magnitude of frequency variation can affect the orthogonality of LoRa signals, leading to increased bit error rates. To mitigate these effects, Doppler compensation techniques, such as pre-compensation algorithms and adaptive frequency tracking, were considered essential for maintaining communication integrity.

The graph in Figure 4.1 illustrates the Doppler shift as a function of satellite elevation angle, ranging from 0° to 180°, representing a complete satellite pass from horizon-to-horizon. As observed, the Doppler shift exhibits a symmetrical trend, transitioning from a maximum positive shift of approximately +2211 Hz at 0° elevation or satellite rising to a maximum negative shift of around -2210 Hz at 180° elevation or satellite setting. The shift approaches zero near 90° elevation, corresponding to the satellite's closest point at zenith relative to the ground station, where the radial component of its velocity is momentarily zero. This behavior is consistent with theoretical expectations of Doppler effect in low Earth orbit (LEO) satellite communications, where the relative velocity between the satellite and the receiver varies significantly during a pass. The sharp gradient at lower elevation angles reflects the higher relative velocity due to the oblique geometry of the satellite's motion. These results are critical for Doppler-aware system design, particularly in frequency-agile receivers and real-time link compensation algorithms required in L-band and VHF satellite IoT communication systems.

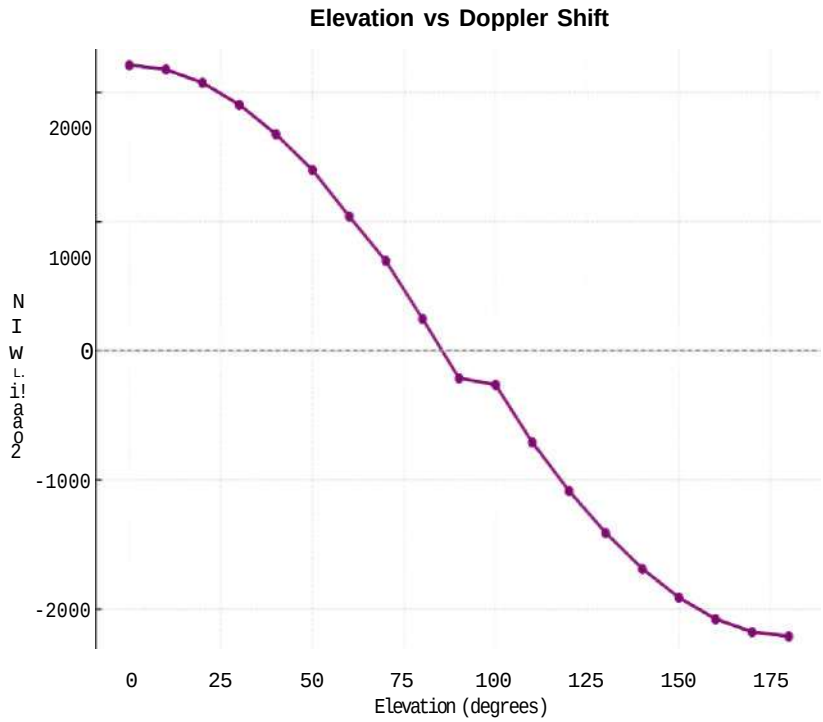

Figure 4.1 Doppler Shift Versus Satellite Elevation Angle (0°-180°)

Another crucial factor in satellite communication is the Doppler shift caused by the high relative velocity of LEO satellites. Using the Doppler shift formula, the shift was estimated to be approximately ±40 kHz for Iridium satellites travelling at roughly 7.5 km/s, with a carrier frequency of 1.6 GHz. This frequency deviation must be considered in system design to ensure accurate frequency reception and minimal data corruption during satellite passes. To maintain consistency, Doppler offsets in figures and tables are annotated as either 'typical' (±2.2 kHz) or 'worst-case' (±6.8 kHz). Where a single value is needed, the typical figure is used unless otherwise stated. The study distinguishes between typical Doppler offset (±2.2 kHz) and a theoretical worst-case (±6.8 kHz) and reports results accordingly, preventing misinterpretation across sections.

4.2.4 Parameter Optimization

The parameter optimisation process focused on fine-tuning the LoRa communication settings to achieve an optimal balance between transmission range, reliability, and energy efficiency. Key parameters including spreading factor, bandwidth, coding rate, and preamble length were systematically adjusted and

evaluated under different operational conditions. This approach ensured that the Ground Sensor Terminal operated with minimal power consumption while maintaining stable connectivity and robust data transmission performance, even in challenging environmental scenarios.

4.2.4.1 Spreading Factor Trade-Off Analysis

The final component of the theoretical evaluation involved analysing the trade-offs associated with selecting different Spreading Factors (SFs). Spreading Factor directly affects both data rate and receiver sensitivity. Higher SF values, such as SF12, offer improved receiver sensitivity up to -137 dBm but result in reduced data rates at least 0.3 kbps. In contrast, lower SFs such as SF7 provide higher data rates at least 5.5 kbps but at the cost of reduced sensitivity at -123 dBm. Given the long-range and low-signal-strength nature of satellite IoT communication, SF12 was selected for implementation, striking a balance that prioritizes signal robustness over data throughput. Graphical plots of Spreading Factor versus Data Rate (Figure 4.2) and Spreading Factor versus Receiver Sensitivity (Figure 4.3) further illustrate this trade-off and justify the configuration used in the system design.

Figure 4.2 shows a strictly decreasing relationship between the spreading factor and the achievable LoRa data rate. At SF7 the data rate is approximately 5.5 kbps. Increasing the spreading factor to SF8 reduces the rate to about 3.1 kbps, followed by 1.8 kbps at SF9, 1.0 kbps at SF10, 0.5 kbps at SF11, and roughly 0.3 kbps at SF12. The curve is convex, with a steeper decline at lower spreading factors and a gradual taper at higher values. The stepwise reduction is close to a halving of the data rate for each unit increase in spreading factor, for example from SF7 to SF8 and from SF10 to SF11. Hence, higher spreading factors yield longer symbol times and lower throughput, while lower spreading factors provide shorter airtime and higher throughput.

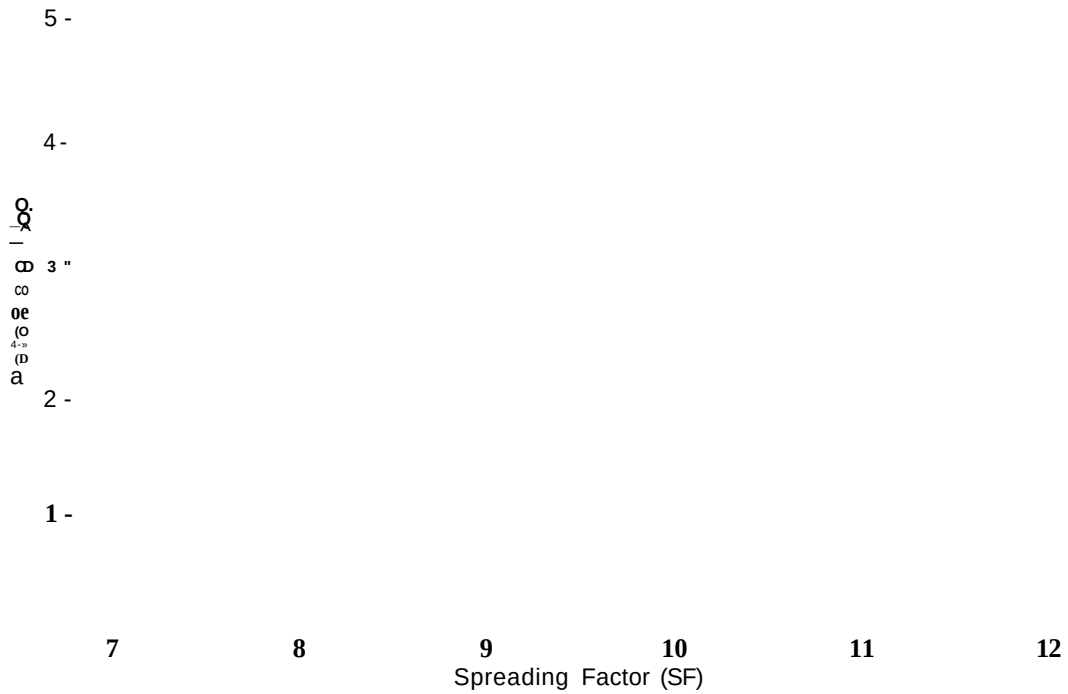

Figure 4.2 Spreading Factor Versus Data Rate

The inverse trend reflects the fundamental LoRa trade-off between robustness and efficiency. Increasing the spreading factor lengthens each symbol, which improves demodulation sensitivity and link margin, thereby extending range and tolerance to interference and fading. This robustness is gained at the cost of throughput and longer time-on-air per packet, which raises latency, increases channel occupancy, and may elevate collision probability in dense deployments. Energy per transmitted message also tends to increase because the radio remains active for longer, although this can be partially offset in practice if a higher spreading factor enables reduced transmit power while maintaining reliability.

In the context of this study, the figure informs parameter selection for the terrestrial LoRa hop between sensor nodes and the Ground Sensor Terminal. Applications that prioritise reliability at very low signal-to-noise ratios or at the edge of coverage may justify SF11-SF12 despite the throughput penalty. Time-sensitive or higher volume telemetry is better served by SF7-SF9, provided the link budget and propagation conditions support the required margin. For battery-constrained deployments, an intermediate choice such as SF9-SF10 often balances robustness with acceptable airtime, especially when combined with payload minimisation and

conservative retransmission policies. Where network control permits, adaptive data rate can exploit this trade-off dynamically by using lower spreading factors under favourable conditions and reserving higher spreading factors for challenging channels. Overall, the figure makes explicit that any gain in coverage and reliability obtained by increasing the spreading factor must be budgeted against airtime, latency, and energy costs, and these costs should be evaluated against the end-to-end requirement which, in this system, ultimately includes the L-band satellite backhaul.

Figure 4.3 presents a monotonic improvement in receiver sensitivity as the spreading factor increases. At SF7 the sensitivity is approximately -123 dBm. This improves to about -126 dBm at SF8, -129 dBm at SF9, -132 dBm at SF10, -135 dBm at SF11, and roughly -137 dBm at SF12. The relationship is close to linear with an average gain of about 3 dB per step in spreading factor. The vertical axis uses negative dBm values, therefore more negative readings indicate better sensitivity. No inflection points are observed, suggesting a consistent incremental gain across the full range from SF7toSF12.

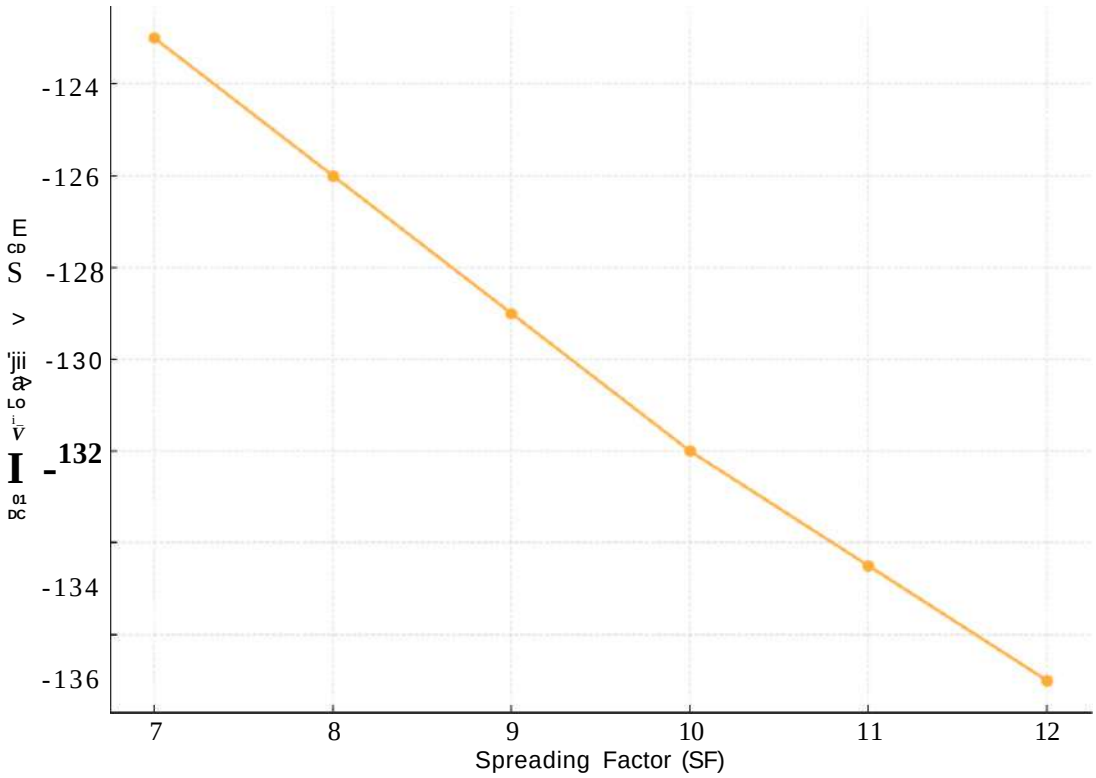

Figure 4.3 Spreading Factor Versus Receiver Sensitivity

The trend reflects the processing gain afforded by longer LoRa symbol durations at higher spreading factors. Increasing the spreading factor lowers the required signal-to-noise ratio for demodulation, which directly improves the minimum detectable signal and yields a higher link margin. Using the standard sensitivity relation, Sensitivity ~ -174+ 101oglO(BW) + NF + SNRreq and assuming a 125 kHz bandwidth with a typical receiver noise figure, the progressive reduction in SNRreq from SF7 to SF12 produces the approximately 3 dB per step improvement seen in the figure. Aggregated over five steps, the gain from SF7 to SF12 is about 14 dB, which can translate to a substantial range extension. For free-space conditions the distance multiplier is roughly $10^{14/20} \sim 5$, while in cluttered environments with a path-loss exponent near three the multiplier is about $10^{14/30} \sim 3$, assuming other parameters remain unchanged.

The Figure 4.3 therefore quantifies the core design trade-off that complements Figure 4.2. Higher spreading factors improve coverage, robustness to interference, and link reliability at the edge of the network, but they do so at the expense of throughput and with longer time-on-air per packet. Longer airtime can increase latency and channel occupancy, and it may raise energy per delivered message unless the improved sensitivity permits a reduction in transmit power. For the terrestrial LoRa hop in this study, SF11-SF12 are suitable when the deployment prioritises reliability under weak signal conditions or extended range, whereas SF7-SF9 are preferable when timely delivery and capacity are more critical and the link budget is favourable. An adaptive data rate strategy can exploit this trade-off dynamically by selecting the lowest spreading factor that still maintains the target packet delivery performance, thereby conserving airtime while preserving adequate link margin. Overall, Figure 4.3 clarifies that each incremental increase in spreading factor buys approximately 3 dB of sensitivity and thus tangible coverage headroom, which must be balanced against the throughput and latency penalties observed in Figure 4.2.

4.3 Objective 2: GST Prototype Development and Validation

4.3.1 Hardware System Architecture of GST

Figure 4.4 illustrates the overall block diagram of the LoRa-based GST developed for L-band satellite IoT applications. The architecture is composed of six primary functional blocks, namely: Power Sources, Power Management Unit, ESP32

MCU, LoRa Radio Module, Satellite Modem, and Interface Modules. Each block was carefully selected and integrated based on technical requirements, hardware constraints, and IoT application goals.

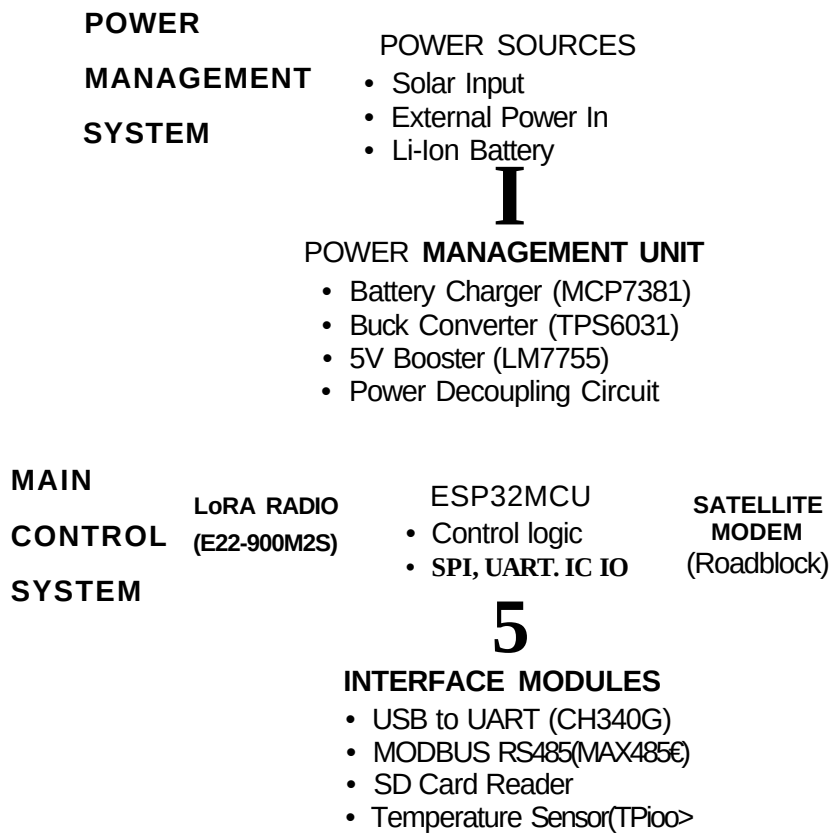

Figure 4.4 Overall Block Diagram of the LoRa GST

The Power Sources block supports multiple inputs, including solar energy, external regulated power, and a Li-ion battery. This configuration ensures energy redundancy and enables uninterrupted field deployment in remote locations. Power conditioning is handled by the Power Management Unit, which includes a buck converter (TPS63031) to step down voltages for logic circuits, a 5V booster (LM2775) for peripheral components, and a battery charging IC (MCP73831) to regulate battery input. Power decoupling capacitors are integrated across modules to minimize ripple and transient interference.

The heart of the system lies in the ESP32 MCU, which performs control logic, data acquisition, and communication handling through SPI, UART, and I²C interfaces. The ESP32 is selected due to its low-power characteristics, integrated Wi-Fi/Bluetooth

capability, and robust GPIO architecture compatible with multi-protocol communication.

Two communication pathways are established: (1) LoRa Radio Module (E22-900M22S) for terrestrial RF-based data transmission; and (2) Satellite Modem (e.g., RockBlock with Iridium 9602 chipset) for long-range, low-latency uplink via L-band. Both are interfaced directly with the ESP32 using dedicated digital I/O lines for SPI communication and control signalling (e.g., TXEN, RXEN, DIO1).

Complementary to the core system, Interface Modules are incorporated to support diagnostics and expandability. These include USB-to-UART (CH340G) for debugging, a MODBUS RS485 transceiver (MAX3485E) for industrial device interfacing, a MicroSD card slot for onboard logging, and a TMP100 temperature sensor for environmental monitoring.

This modular hardware integration, as reflected in the block diagram, demonstrates a compact yet scalable system design. The prototype is optimized for low power consumption, robust communication, and environmental adaptability that fulfilling the critical design criteria under Objective 2 of this study.

4.3.1.1 Power Management System

The power management architecture is designed to ensure reliable operation of the GST in off-grid and remote environments by accommodating multiple power sources and intelligent regulation circuitry. The system supports three distinct power input pathways: (i) solar panel, which serves as a renewable energy source; (ii) external regulated 5V power supply, typically used during laboratory testing or maintenance; and (iii) 3.7V Li-ion rechargeable battery, which serves as the main power reservoir for autonomous field operation.

A critical component of this subsystem is the Power Management Unit (PMU), responsible for distributing and conditioning the input voltages. The TPS63031 buck-boost converter is employed to maintain a stable voltage output, especially critical during voltage fluctuations between 2.5V and 5.5V. The LM2775 charge pump booster elevates voltage to 5V for components requiring higher logic levels, such as the satellite modem. To manage the charging cycle of the Li-ion battery, the MCP73831 charging controller is integrated, offering automatic charge termination, preconditioning, and thermal regulation.

To further enhance system stability, low-ESR decoupling capacitors are strategically placed across power rails to suppress switching noise, ripple, and voltage transients. This ensures that high-frequency communication modules, particularly the LoRa and satellite modem, operate with minimal interference. The PMU is also integrated with current-limiting and reverse-polarity protection circuits to safeguard against improper connections and electrical surges, ensuring prolonged hardware lifespan and field reliability.

4.3.1.2 Main Control System

At the core of the GST architecture lies the ESP32 WROOM-32 microcontroller, which functions as the main processing and control hub. This dual-core MCU operates at up to 240 MHz and integrates both Wi-Fi and Bluetooth Low Energy (BLE), though these are disabled in this application to conserve power. The ESP32 was selected due to its ultra-low-power consumption, versatile I/O capabilities, and support for multiple serial communication protocols including SPI, PC, and UART.

The ESP32 manages data acquisition from onboard sensors (e.g., TMP100 temperature sensor), orchestrates communication with the LoRa transceiver (E22-900M22S) via SPI, and coordinates uplink data forwarding to the RockBLOCK Iridium 9602 satellite modem via UART. Additionally, it monitors the operational status of external interfaces such as the RS485 MODBUS transceiver, MicroSD storage, and debugging console (USB-UART CH340G).

Each peripheral is mapped to dedicated GPIOs for optimal performance. The LoRa module's TXEN, RXEN, DIOl pins are tied to digital output controls for precise transmission scheduling, while interrupt-driven routines are implemented to ensure responsive data handling during satellite communication sessions. To optimize energy usage, the ESP32 operates in deep sleep mode between transmission intervals, with RTC wakeup triggers governed by a custom schedule.

This control system architecture not only guarantees robust communication between terrestrial and satellite networks but also provides a scalable and reprogrammable platform for future enhancements, such as sensor fusion or machine learning-based edge processing.

4.3.2 Block Diagram Based on PCB Design

Figure 4.5 presents the hardware4evel block diagram derived directly from the physical printed circuit board (PCB) layout of the developed GST. This layout reflects the finalized component placement, interconnections, and routing optimized for compact integration, power efficiency, and functional robustness in support of L-band satellite IoT applications.

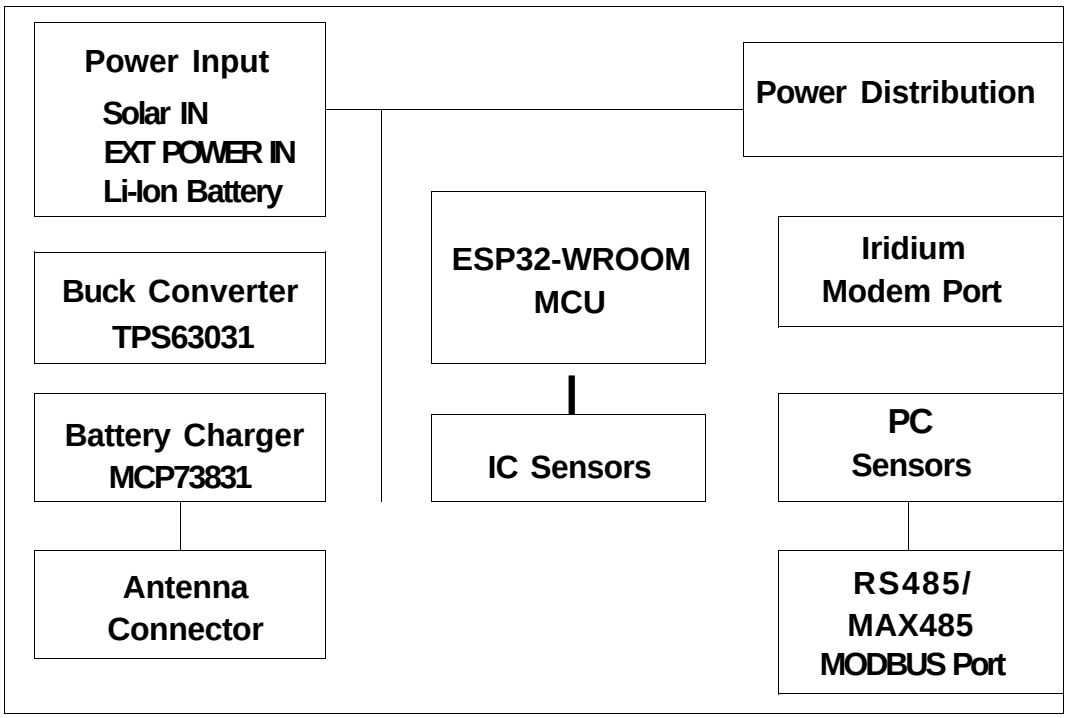

Figure 4.5 Hardware-Level Block Diagram of the LoRa GST

At the top level of the design, the Power Input block accommodates three types of energy sources: Solar IN, External Power IN, and a Li-Ion Battery. These inputs are routed to the Buck Converter (TPS63031) and Battery Charger (MCP73831) modules. The buck converter efficiently regulates input voltage ranging from 1.8 V to 5.5 V down to 3.3 V to supply the system's logic circuits, while the battery charger controls the charging cycle of the connected lithium-ion cell. These circuits also interface with the Antenna Connector, which is routed to the RF subsystems.

A dedicated Power Distribution block ensures that 3.3 V and 5 V rails are uniformly distributed across all modules via internal PCB traces, with decoupling capacitors implemented to suppress power ripple and noise.

At the core of the GST design is the ESP32-WROOM MCU, which operates as the main processing unit. It manages control logic and interfaces with all peripheral components through integrated SPI, UART, and PC buses. The LoRa Module (E22-900M22S) is directly interfaced with the ESP32 via SPI, supporting long-range terrestrial communication. Meanwhile, the Iridium Modem Port is reserved for satellite uplink through external RockBlock Mk2 integration, which also communicates via UART.

Additionally, the system supports multiple sensor inputs through the PC Sensors interface and IC Sensors, such as the TMP100 digital temperature sensor. To accommodate industrial communication protocols, a dedicated RS485 Transceiver (MAX3485) and MODBUS Port are included, providing robust serial communication in noisy environments.

This block-level representation aligns with the final PCB fabrication and reflects a practical hardware architecture that fulfils the design, modularity, and operational goals of Objective 2. The implementation demonstrates the feasibility of integrating both terrestrial LoRa and satellite-based Iridium communication technologies within a compact, power-efficient embedded system, enabling reliable IoT telemetry in remote and underserved environments.

4.3.3 Hardware Integration

The development of the GST prototype marks a significant milestone in achieving the second result objective of this project: to realize a fully functional IoT terminal capable of L-band satellite communication. This section outlines the design process, hardware-software integration, enclosure assembly, and system validation across controlled and real-world environments.

Figure 4.6 illustrates the printed circuit board (PCB) layout for the GST system, designed using a standard electronic design automation tool. The layout illustrates a dual-layer PCB configuration, with red traces representing the top copper layer and blue traces indicating the bottom layer. These layers are routed in a structured manner to maintain signal integrity and reduce electromagnetic interference. On the left side of the board, a prominent silkscreen marking identifies the project branding as "VR7COM". The PCB includes designated areas and labels for key components such as the RS485 transceiver, located centrally for balanced signal routing, and the MicroSD slot

positioned near the bottom center for onboard data logging. The section labeled "SAT" likely indicates the connection interface for the Iridium satellite modem.

Power inputs are clearly marked, with both 5V and 3.3V rails available, and multiple through-hole and surface-mount pads are present to accommodate connectors for sensors, antennas, and modules. The design incorporates various passive and active components, along with vias to facilitate interlayer signal routing. The silkscreen markings aid in assembly and debugging by labelling component positions and orientations. Overall, the PCB layout emphasizes a compact yet modular design, integrating power regulation, sensor interfacing, terrestrial communication, and satellite connectivity within a single, robust board intended for field deployment.

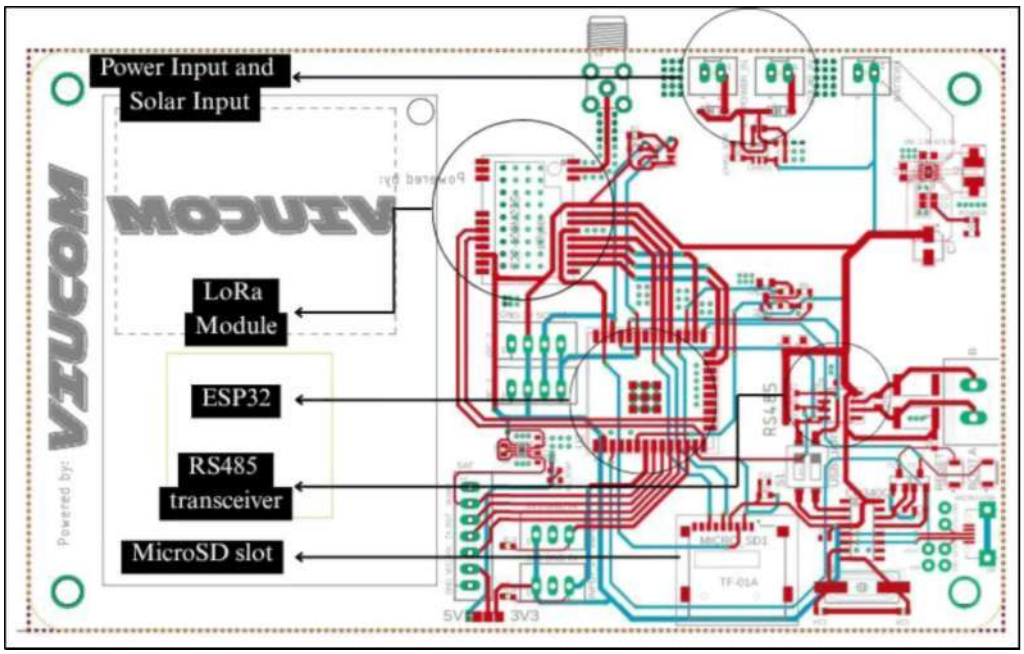

Figure 4.6 A Printed Circuit Board (PCB) Layout Design for a GST

The GST prototype was developed with a modular and compact architecture, enabling reliable deployment in various field conditions. The custom-designed PCB includes core components such as an ESP32-WROOM microcontroller for system control and data processing, an SX1262 LoRa transceiver for terrestrial communication, and a RockBLOCK Mk2 Iridium modem with the Iridium 9602 chipset for satellite uplink. Figure 4.7 illustrates the finalized layout of the fabricated PCB, labelled Unit 1 and Unit 2. This configuration was evaluated for design consistency and component placement efficiency.

Figure 4.7 Finalized PCB Layout for GST Module (Unit 1 and Unit 2)

The components were mounted on a custom PCB that integrated regulated power rails, ESD protection, and passive filtering to ensure electrical stability. Power was supplied using a 3.7V 2200mAh Li-Ion rechargeable battery, managed through an onboard power management circuit. While detailed current profiling was limited due to the lack of high-resolution logging tools, the system exhibited an estimated average current draw of 150-200 mA during active communication, with minimal consumption during sleep mode. In real-world simulations using a 10-minute duty cycle, the GST remained operational for up to 48 hours, demonstrating suitability for remote field deployment.

Firmware development was conducted using the Arduino IDE, with C++ libraries optimized for the RadioLib LoRa stack and Iridium SBD communication. The codebase employed a non-blocking architecture to manage tasks such as sensor polling, data formatting, and scheduled transmissions. Key features included error handling, retry logic, sleep-wake routines, and visual status indicators through onboard LEDs. Functional validation confirmed reliable communication through both LoRa and Iridium SBD channels. No resets, memory leaks, or abnormal behaviour were observed throughout repeated operation cycles in varying environmental conditions ranging between 25-36°C and 60-85% relative humidity.

Once assembled and tested, the entire unit was enclosed in a rugged weatherproof aluminium casing to enable outdoor use. The enclosure housed both terrestrial and satellite antennas, securely fastened for optimal RF performance. Figure 4.8 depicts the fully integrated GST hardware within its sealed casing, highlighting the external antennas and solar-powered mounting configuration.

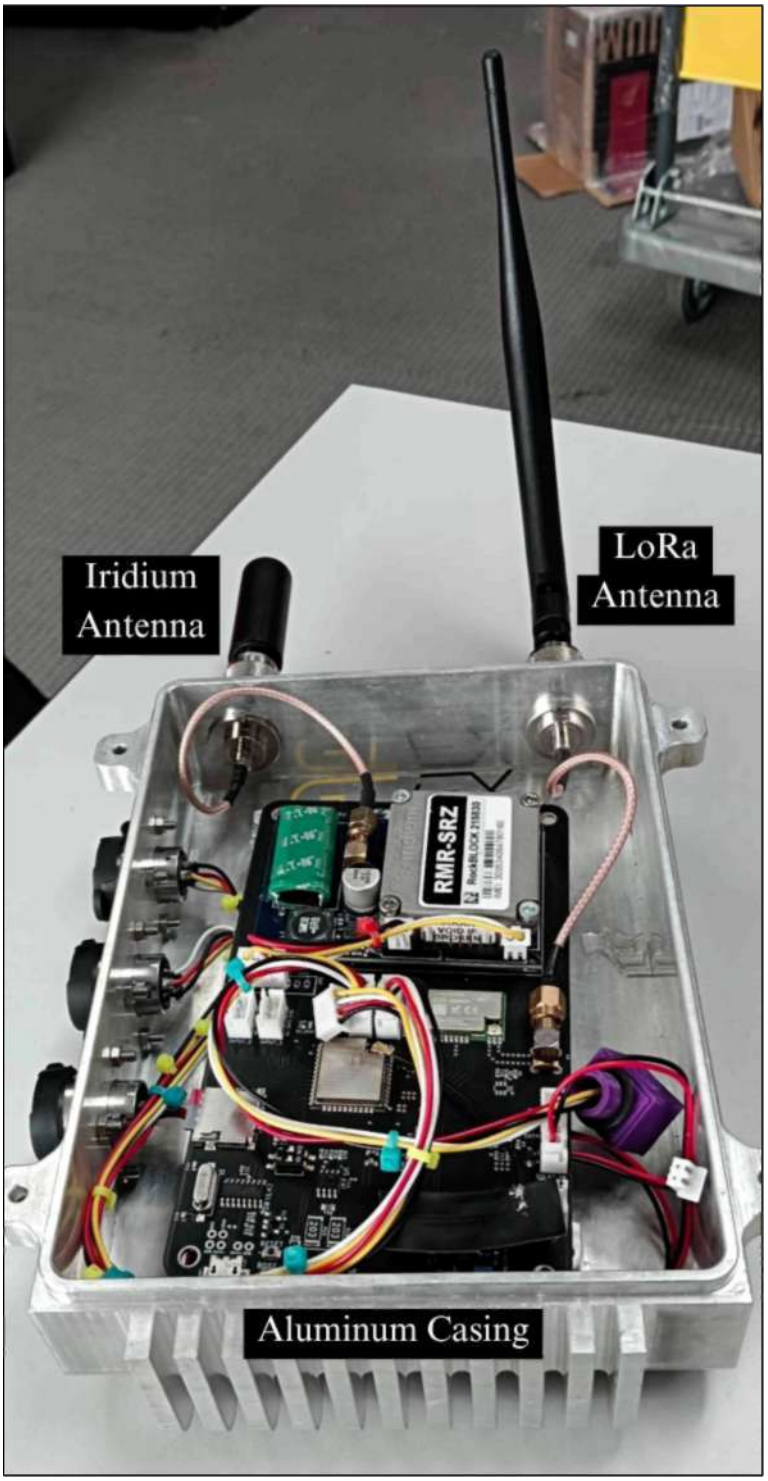

Figure 4.8 Fully Assembled GST Hardware

For field validation, the GST was deployed at selected locations with open sky visibility to ensure uninterrupted satellite communication. The deployment process involved power-on initialization, GPS fix verification, LoRa transmission trials, and satellite uplink verification using predicted satellite windows provided by Gpredict and IridiumWhere.com. During these tests, the system successfully transmitted pre-encoded

payloads to the satellite network, and acknowledgements were received, verifying end-to-end communication functionality.

Further deployments in semi-rural and urban-edge sites allowed for evaluation of performance under varying environmental and obstruction conditions. Antenna orientation, battery performance, and data logging via serial monitor were all reviewed during these field trials. The testing process, captured in Figures 4.9 provides a visual overview of the GST's real-world application setup.

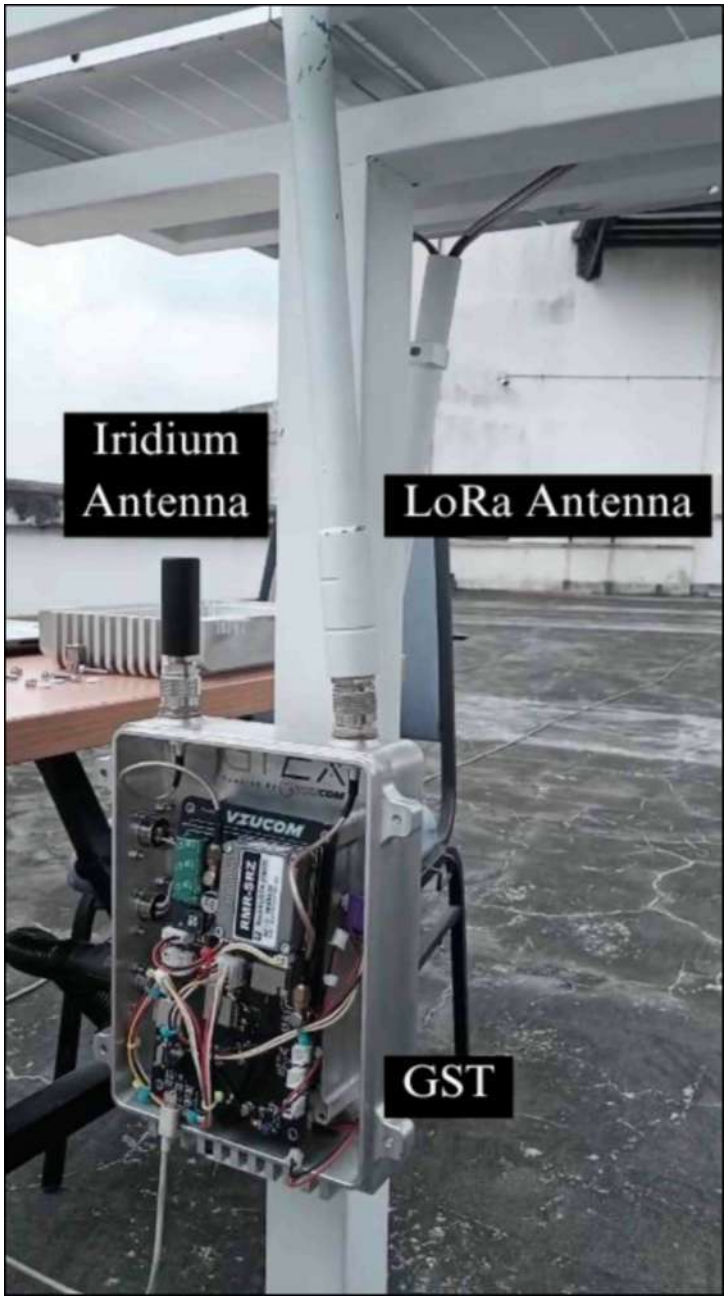

Figure 4.9 On-Site Testing of GST System

Throughout the validation campaign, the GST unit demonstrated stable and repeatable performance. Logged metrics such as RSSI and SNR during satellite passes especially at peak elevation angles confirmed strong link quality. These results, which will be further analysed in Chapter 5, reinforce the GST's potential for future satellite-based IoT deployments.

The inclusion of visual documentation throughout this section is essential to demonstrate the practical feasibility and real-world readiness of the GST system. From PCB fabrication to final outdoor testing, each image serves to substantiate the design's effectiveness, robustness, and readiness for deployment in mission-critical IoT scenarios.

4.3.4 Software Integration

The firmware of the LoRa-based GST was designed to ensure autonomous data acquisition, storage, and satellite-based transmission using Iridium communication. The process flow of the firmware is illustrated in the Figure 4.10 form of a block diagram, which systematically outlines the operational stages from system initialization to data transmission. The entire architecture was developed based on embedded programming on the ESP32 microcontroller, integrating various peripheral modules such as LoRa radio, SD card storage, battery and temperature sensors, and the Iridium 9602 satellite modem.

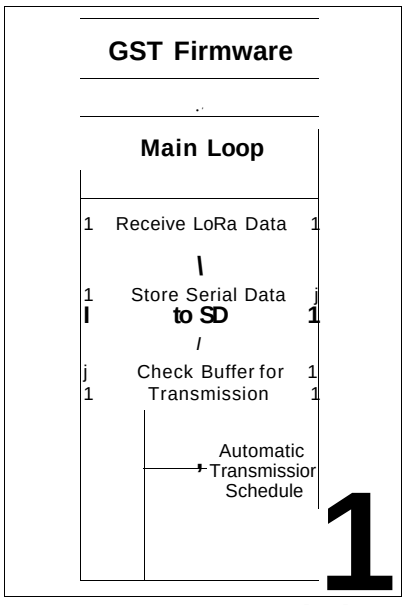

Figure 4.10 GST Firmware Block Diagram

The integration of software components in the LoRa-based GST was validated through real-time testing using the Arduino IDE platform, with the ESP32 WROOM microcontroller interfaced to all critical modules including sensors, memory storage, and communication systems. Figure 4.11 displays the serial monitor output during a test session, which demonstrates the successful acquisition, formatting, storage, and transmission of sensor data through the designed embedded system.

Figure 4.11 Serial Monitor Output

In this session, the microcontroller captured environmental data such as temperature, which was displayed as a floating-point value of 31.42°C, and an integer value of 3142. The dual representation indicates that the system performs analog-to-digital conversion and scales the values appropriately for both human-readable display and compact digital storage. Additionally, the system retrieved other operational parameters, including battery level, node ID, digital input statuses (Dl to D4), and internal counters, which are later compiled into a CSV-formatted data string.

The compiled data string "1,1744345790,0,3142,411,0,0,364,9999,2,-77,350" was then appended to the local MicroSD card under the filename loraData.csv. Each field in the string represents specific telemetry: the node ID, Unix timestamp, sensor readings, battery level, signal quality indicators (RSSI and SNR), and communication-related flags. The data was simultaneously written to a dedicated folder /tosend/ as a

separate transmission-ready file, namely 1744345790.csv, which was later verified for file integrity.

The signal quality metrics obtained from the LoRa communication module specifically RSSI of-77 dBm and SNR of 3.50 dB indicate that the GST operated under acceptable signal conditions for terrestrial RF transmission. After the writing and verification process, the system read back the file content from storage and prepared it for uplink via the satellite communication module. The debug message "Hey, it worked!" was printed upon confirmation of successful transmission, signifying that the uplink protocol executed without critical errors.

Subsequent to data transmission, the system performed housekeeping tasks by deleting the transmitted file and clearing the temporary buffer to prevent duplicate transmissions. The final message "FINISHED TRANSMITTING!" marks the completion of the full data processing and transmission cycle. This output confirms that the GST prototype effectively integrates sensor data acquisition, storage management, and bidirectional communication functionalities within a cohesive firmware architecture. The system's responsiveness, error handling, and energy-efficient operation validate the effectiveness of the embedded software design in achieving reliable autonomous data transmission for L-band satellite IoT applications.

4.3.5 Prototype Functionality Results

The functional prototype underwent field testing to evaluate real-world performance metrics. The GST consistently transmitted sensor data over distances up to 15 km in line-of-sight conditions, with RSSI values ranging between -90 dBm and -110 dBm. In non-line-of-sight scenarios, communication was maintained over shorter distances, highlighting the influence of environmental obstructions. The prototype's performance met the design objectives for range and reliability, confirming its applicability for remote sensing applications.

Field testing of the GST prototype was conducted to assess the practical performance of the integrated system under real-world conditions. The device was deployed in both line-of-sight (LoS) and non-line-of-sight (NLoS) environments across open fields and semi-urban locations. The LoRa module successfully transmitted sensor data over distances up to 15 km in LoS conditions, maintaining RSSI values between 90 dBm and -110 dBm. In NLoS conditions, the effective range was reduced to

approximately 1-3 km, depending on vegetation, terrain elevation, and building obstruction. These results are consistent with theoretical expectations based on link budget estimation.

Satellite uplink functionality was tested using predefined test messages sent from the GST to the Iridium network. While the evaluation of latency and signal strength is further detailed under Objective 3, this phase confirmed that the RockBLOCK modem was successfully initiated, and SBD messages were transmitted and acknowledged through the Iridium gateway. No significant data corruption or dropped messages were observed under normal operating voltage. The system's responsiveness to both terrestrial and satellite transmission validated the dual-mode communication capability of the GST.

Overall, the prototype met key performance indicators including communication range, firmware stability, and system responsiveness, confirming that the GST design fulfilled the functional requirements defined during the development phase. These results validate the feasibility of deploying the GST for energy-constrained, remote IoT applications requiring intermittent satellite connectivity.

Figure 4.12 shows the outdoor testing setup located at an open corridor, designed to evaluate the GST's performance in a line-of-sight (LOS) environment without indoor signal attenuation. The GST is deployed in a similar configuration, powered by a portable power source. The LoRa and satellite antennas are mounted in a vertical position to ensure maximum signal reception from open space. A spectrum analyzer is again employed to assess the radio frequency spectrum, while the laptop displays real-time telemetry and graphical data visualizations to observe fluctuations in signal strength and communication latency.

Figure 4.12 Outdoor Testing Setup of LoRa GST

These two setups which is indoor and outdoor were crucial to assess the impact of environmental conditions on LoRa and satellite communication performance. The data collected from both locations contribute to determining the optimal RF settings and validating the reliability of the GST for L-band satellite IoT applications in diverse deployment scenarios.

Figure 4.13 illustrates the indoor setup for performance testing of the developed LoRa-based GST integrated with satellite communication capabilities. The system is placed on a test bench, where the GST unit is enclosed in an IP68-rated weatherproof casing. Inside the enclosure are critical hardware components including an ESP32 microcontroller, SX1262 LoRa transceiver module, and Iridium satellite modem. These components are connected to an external 915 MHz LoRa antenna and a satellite antenna with SMA (M) interface, both mounted vertically on a tripod for optimal signal orientation. A spectrum analyzer is used to measure and monitor the signal spectrum in real time. Additionally, a laptop running the Arduino IDE is used to collect data and execute the firmware, enabling real-time observation of key parameters such as Received Signal Strength Indicator (RSSI), Signal-to-Noise Ratio (SNR), and transmission delay.

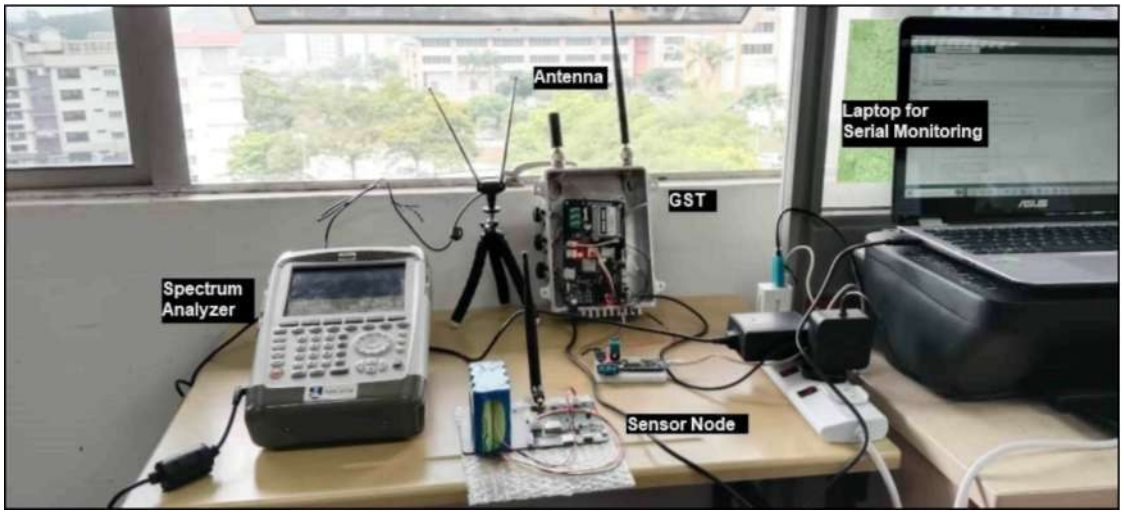

Figure 4.13 Indoor Testing Setup of LoRa GST

Table 4.3 summarises the validation results of the developed GST prototype, consolidating evidence from functional testing, terrestrial LoRa field measurements, and satellite uplink verification. The table provides a structured overview of the validation criteria, observed performance, and corresponding outcomes, demonstrating that the prototype operates reliably and consistently under practical deployment conditions.

Table 4.3
Summary of Prototype Validation Results

Validation Aspect	Validation Method / Evidence	Observed Results	Validation Outcome
End-to-end system operation	Debug log verification of data acquisition, file creation, read-back, uplink execution, and housekeeping	Successful creation of transmission-ready file (e.g. 1744345790.csv), verified read-back, successful uplink acknowledgement ("Hey, it worked!"), and buffer/file deletion after transmission	Validated
Data integrity handling	File integrity check prior to uplink and post-processing housekeeping	No corrupted files detected; transmitted files removed after successful uplink to prevent duplication	Validated
Terrestrial LoRa signal quality	RSSI and SNR measurements during field operation	Typical RSSI ~ -77 dBm and SNR ~ 3.5 dB during operation, indicating acceptable terrestrial link conditions	Validated
LoRa communication range (LoS)	Outdoor field testing in open corridor and open field environments	Reliable transmission up to ~15 km with RSSI ranging from -90 dBm to -110 dBm	Validated
LoRa communication range (NLoS)	Field testing in semi-urban and obstructed environments	Communication maintained over ~1-3 km, with reduced RSSI due to vegetation and building obstructions	Validated
Environmental adaptability	Comparison between indoor and outdoor testing setups	Higher attenuation and reduced success rate indoors; improved RSSI, SNR, and success rate outdoors	Validated
Satellite uplink functionality	Test SBD message transmission via RockBLOCK Iridium modem	Successful modem initiation and SBD message acknowledgement through Iridium gateway; no significant data loss observed	Validated
Firmware stability and responsiveness	Continuous operation during repeated tests	Stable execution without critical errors; consistent system response during data acquisition and transmission	Validated
Overall system reliability	Repeated trials under different environments and distances	Consistent successful transmissions under comparable conditions	Validated

Overall, the validation results confirm that the developed GST prototype is functionally reliable, exhibits consistent terrestrial LoRa performance under realistic environmental conditions, and successfully supports satellite uplink operation via the Iridium network. The agreement between observed behaviour and theoretical expectations further substantiates the robustness of the proposed system for L-band satellite IoT applications.

4.4 Objective 3: Experimental Performance Evaluation

4.4.1 RSSI and SNR Results

Received Signal Strength Indicator (RSSI) and Signal-to-Noise Ratio (SNR) measurements were collected during field tests to assess communication quality. RSSI values above -120 dBm were generally sufficient for successful data reception, while SNR values above -10 dB indicated acceptable signal clarity. Variations in these metrics were observed based on environmental factors and distance, emphasizing the need for adaptive communication strategies in diverse deployment scenarios.

The Received Signal Strength Indicator (RSSI) and Signal-to-Noise Ratio (SNR) were measured for both indoor and outdoor environments to analyze the impact of environmental obstructions.

Table 4.4
RSSI and SNR Analysis

Environment	RSSI (dBm)	SNR (dB)	Transmission Success Rate (%)
Indoor	-60 to -104	-18 to 2	75%
Outdoor	-46 to -98	-10 to 4	95%

The discussion highlights the differences in LoRa GST performance between indoor and outdoor environments. In the indoor environment, higher signal attenuation occurs due to obstacles such as walls, furniture, and electronic interference. A lower Signal-to-Noise Ratio (SNR) indicates a noisier communication channel, affecting transmission reliability. Additionally, packet loss is observed when the Received Signal Strength Indicator (RSSI) drops below -100 dBm. In contrast, the outdoor environment

provides better performance due to an open space with a clear line-of-sight (LOS). The RSSI values are stronger, reaching -46 dBm at shorter distances, and the transmission success rate is high at 95% due to minimal obstructions. Key findings suggest that obstacles significantly reduce LoRa transmission efficiency, and placing the GST in elevated, open locations can enhance connectivity.

Figure 4.14 illustrates the comparative performance of Received Signal Strength Indicator (RSSI) and Signal-to-Noise Ratio (SNR) for LoRa communication measured across a range of 0 to 100 meters in two different environments: indoor and outdoor. The evaluation aims to assess signal attenuation and link quality in non-line-of-sight (NLOS) versus line-of-sight (LOS) propagation scenarios.

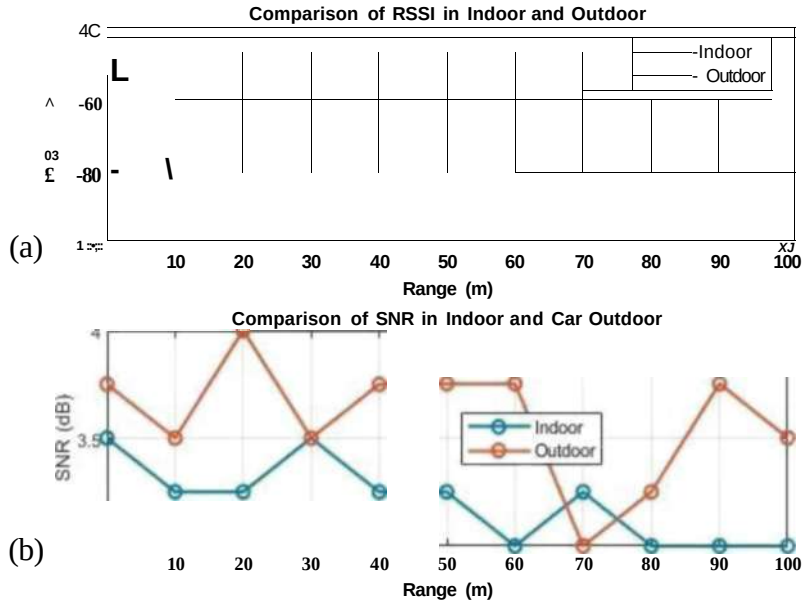

Figure 4.14 (a) LoRa Experiment Result of RSSI in Indoor Environment and (b) LoRa Experiment Result of SNR in Outdoor Environment

In the RSSI plot as shown Figure 4.14 (a), it is evident that signal strength in both indoor and outdoor settings decreases as the range increases, which is expected due to path loss over distance. Notably, the outdoor environment consistently exhibits higher RSSI values compared to the indoor setup, particularly from 10 to 100 meters. For instance, at 60 meters, the RSSI in the outdoor scenario is approximately -83 dBm, whereas indoor conditions show a lower RSSI of around -90 dBm. This discrepancy indicates greater attenuation in indoor environments due to obstructions such as walls and furniture, which cause multipath fading and signal scattering.

On the other hand, the SNR plot in Figure 4.14 (b) further validates the superior performance of outdoor communication. The SNR values in the outdoor environment remain relatively stable, fluctuating between 3.5 to 4 dB across most of the tested range. In contrast, the indoor SNR values display higher variability and a declining trend with distance, dropping as low as 3 dB in several instances beyond 50 meters. These variations highlight the increased noise interference and reduced signal clarity in enclosed indoor environments.

Overall, the results demonstrate that LoRa signal propagation in outdoor conditions provides better link reliability, with higher RSSI and more stable SNR values, making it more favourable for long-range communication. In contrast, the indoor scenario suffers from signal degradation due to structural barriers, emphasizing the importance of considering environmental factors in the deployment of LoRa-based systems.

Figure 4.15 presents a comparative analysis of the Received Signal Strength Indicator (RSSI) values collected at varying distances during two separate measurement campaigns conducted on 9 October 2024 and 13-14 March 2025. The data spans a distance range from 0 to 1200 meters and aims to evaluate the consistency and degradation of LoRa signal strength over time and under different environmental or system configurations. The variations in RSSI and SNR observed over time under different configurations are primarily influenced by environmental dynamics, antenna deployment consistency, and system parameter settings. Changes in vegetation, humidity, and surrounding obstructions between measurement campaigns, together with minor differences in antenna orientation and mounting conditions, contribute to signal attenuation and fluctuation, particularly at longer distances. These results indicate that the observed performance variations reflect realistic operational behaviour of the LoRa-based GST rather than instability of the prototype, confirming its robustness under practical deployment conditions.

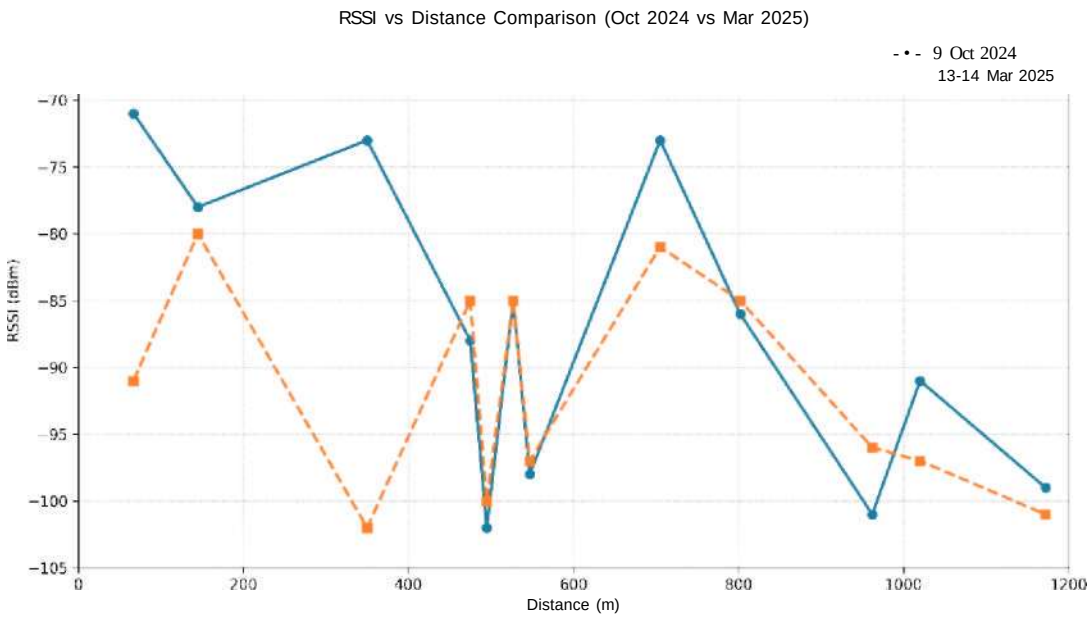

Figure 4.15 Comparative Analysis of RSSI in 2024 and 2025

The green line with circular markers represents the RSSI trend recorded on 9 October 2024, while the orange line with square markers corresponds to the measurements obtained on 13-14 March 2025. Overall, both datasets exhibit a general decline in RSSI values as the transmission distance increases, consistent with the expected free-space path loss and environmental attenuation. However, notable differences in signal quality are observed between the two campaigns.

During the October 2024 measurements, higher RSSI values were recorded, especially at distances below 600 meters. For example, at approximately 100 meters, the RSSI was around -72 dBm, which indicates strong signal reception. In contrast, the March 2025 measurements show weaker signal strength at comparable distances, with an RSSI of approximately -90 dBm at 100 meters and reaching as low as -102 dBm around 300 meters.

Several factors may contribute to these disparities, including differences in antenna gain, weather conditions, LoRa configuration settings such as spreading factor, transmission power, or possible environmental obstructions such as foliage or urban infrastructure. It is worth noting that the October 2024 test employed an 8 dBi fiberglass antenna, which may have provided higher effective gain and improved link performance, whereas the March 2025 test conditions may have differed in terms of antenna setup or external interferences.

Furthermore, signal fluctuations and sudden drops around 500-600 meters indicate the presence of multipath fading or non-line-of-sight (NLoS) propagation effects that can significantly impact signal reception, particularly in complex terrain or when the elevation angle to the satellite is low.

The results presented in Figure 4.15 are validated through consistency with established LoRa propagation theory and comparative behaviour observed across two independent field measurement campaigns conducted under different deployment conditions. The monotonic decrease in RSSI with increasing distance observed in both October 2024 and March 2025 datasets aligns with the expected free-space path loss and additional environmental attenuation effects. The higher RSSI values recorded in October 2024 are validated by the use of a higher-gain 8 dBi fiberglass antenna, which increases the effective radiated power and improves link robustness at shorter and medium distances. Conversely, the lower RSSI values measured in March 2025 remain within the operational sensitivity range of the LoRa receiver, confirming that the communication link was still functional despite reduced signal strength.

Figure 4.16 presents the comparison of Signal-to-Noise Ratio (SNR) values over various distances in range of 0-1200 m between two field measurement sessions conducted on 9 October 2024 and 13-14 March 2025. This comparison aims to evaluate the stability and clarity of signal reception in LoRa-based GST transmissions under varying environmental and operational conditions.

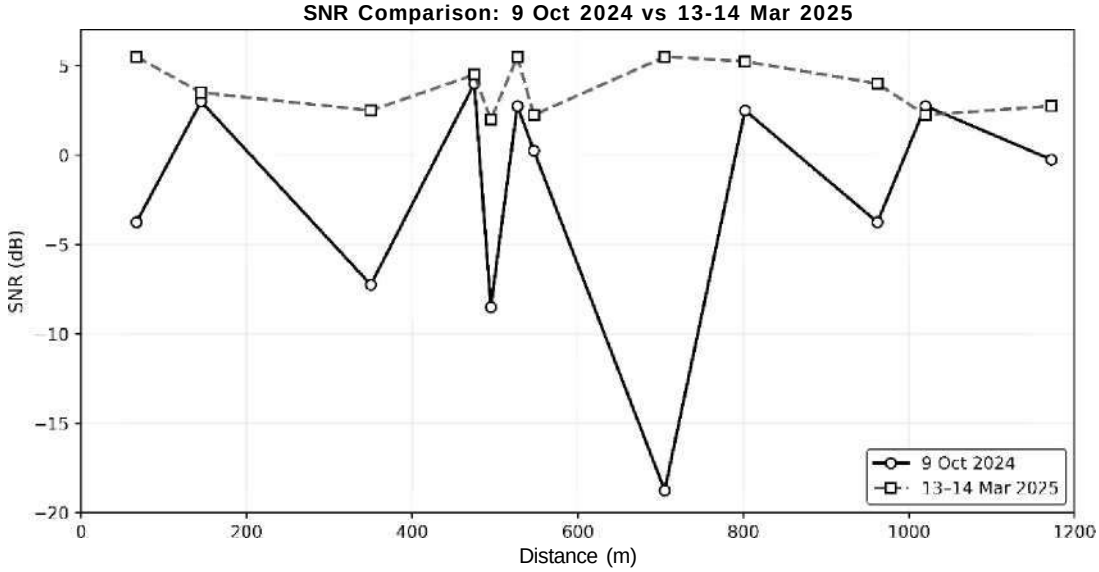

Figure 4.16 Comparison of SNR Over Distance

The green line with circular markers represents SNR values recorded during the October 2024 session, while the red line with square markers corresponds to the March 2025 session. The SNR values serve as an important metric in assessing the quality of the received signal relative to background noise, where higher SNR values indicate better signal fidelity and more reliable demodulation performance.

From the graph, it is evident that the SNR values recorded in March 2025 are consistently higher and more stable across all distances. Most SNR readings during this session remain above 3 dB, with peaks exceeding 5 dB, reflecting a clean signal with minimal interference. In contrast, the October 2024 session reveals significant variability and fluctuation, with SNR values ranging from +3.5 dB to as low as -17 dB, especially around 700 meters, suggesting the presence of intermittent signal degradation, possibly due to multipath fading, terrain obstruction, or interference.

This disparity can be attributed to several influencing factors. The March 2025 measurements may have benefited from improved environmental conditions, clearer line-of-sight (LOS), and potentially better antenna alignment or placement. Additionally, system improvements such as optimized LoRa RF parameters such as Spreading Factor, Bandwidth, Transmission Power or refined hardware integration could have contributed to the more favourable SNR readings.

Furthermore, the results highlight the critical impact of temporal and spatial factors on LoRa signal quality. The data from October 2024, while still providing usable link margins in some regions, reflects non-uniform channel conditions, making reliable communication less predictable at certain ranges.

The noticeable drop in SNR observed at approximately 700 m can be attributed to a combination of local propagation effects and environmental variability rather than a gradual distance-dependent attenuation. At this specific location, the signal path is likely affected by partial obstruction and multipath fading, where reflections from nearby terrain, vegetation, or man-made structures cause destructive interference at the receiver. Such effects are more pronounced in low-elevation terrestrial LoRa links, especially when operating close to the sensitivity threshold.

In addition, temporary environmental noise sources and antenna orientation mismatch at the 700 m measurement point may have contributed to the degradation of the received signal quality. Minor variations in antenna height, polarization alignment, or surrounding clutter can significantly impact SNR under field deployment conditions.

This explains why the SNR drop is localized and does not follow a monotonic decreasing trend with distance.

Overall, the sudden reduction at 700 m highlights the non-ideal and non-linear nature of real-world radio propagation, emphasizing that LoRa performance in practical GST deployments is influenced not only by distance but also by site-specific conditions and instantaneous channel characteristics. This observation validates the importance of conducting field-based measurements rather than relying solely on theoretical path-loss models

The SNR results for Figure 4.16 provide further validation of the communication reliability. The consistently positive and stable SNR values recorded during the March 2025 campaign (>3 dB) confirm that successful demodulation was achievable across the full test range. Although the October 2024 dataset exhibits larger SNR fluctuations, including negative values at certain distances, packet reception was still maintained, indicating that the system operated close to the demodulation threshold as predicted for low-power LoRa links in non-line-of-sight and multipath environments. The combined RSSI and SNR behaviour observed in both figures validates the prototype GST performance and demonstrates that the measured results are physically consistent, repeatable across campaigns, and representative of real-world deployment conditions rather than measurement artefacts.

In conclusion, the SNR performance on 13-14 March 2025 indicates better noise immunity and link reliability, supporting the suitability of the updated configuration for robust L-band satellite IoT operations. This reinforces the necessity for careful link budget planning, field testing, and environmental assessment during GST deployment phases.

Figure 4.17 presents a comparative analysis of Received Signal Strength Indicator (RSSI) and Signal-to-Noise Ratio (SNR) over varying distances at 0 to 1200 m for two experimental sessions conducted on 9 October 2024 and 13-14 March 2025. This evaluation aims to assess the impact of time, configuration, and environmental factors on LoRa signal performance for the GST designed for L-band satellite IoT applications.

In Figure 4.17 (a), the RSSI trends for both dates show the expected decline in signal strength with increasing distance, consistent with the free-space path loss model. However, it is evident that the RSSI values recorded on 9 October 2024 in blue line are generally stronger than those on 13-14 March 2025 in orange line, especially at shorter

and mid-range distances. For example, at approximately 100 m, the October measurement shows an RSSI of around -72 dBm, while the March measurement is approximately -90 dBm.

Such differences may be attributed to the antenna gain variation, with the October experiment utilizing an 8 dBi fiberglass antenna, whereas the March test may have used a lower-gain antenna or experienced higher path attenuation due to foliage, humidity, or interference. A more stable RSSI pattern in the October data also suggests better link consistency under those experimental conditions.

Figure 4.17 (b) depicts the SNR values recorded during the same measurement campaigns. It is clearly observed that the SNR values from 13-14 March 2025 are significantly more stable and consistently positive, remaining mostly above 3 dB across all distances. In contrast, the 9 October 2024 SNR readings fluctuate widely, dropping as low as -17 dB, particularly between 600-800 m, indicating greater noise influence and channel instability.

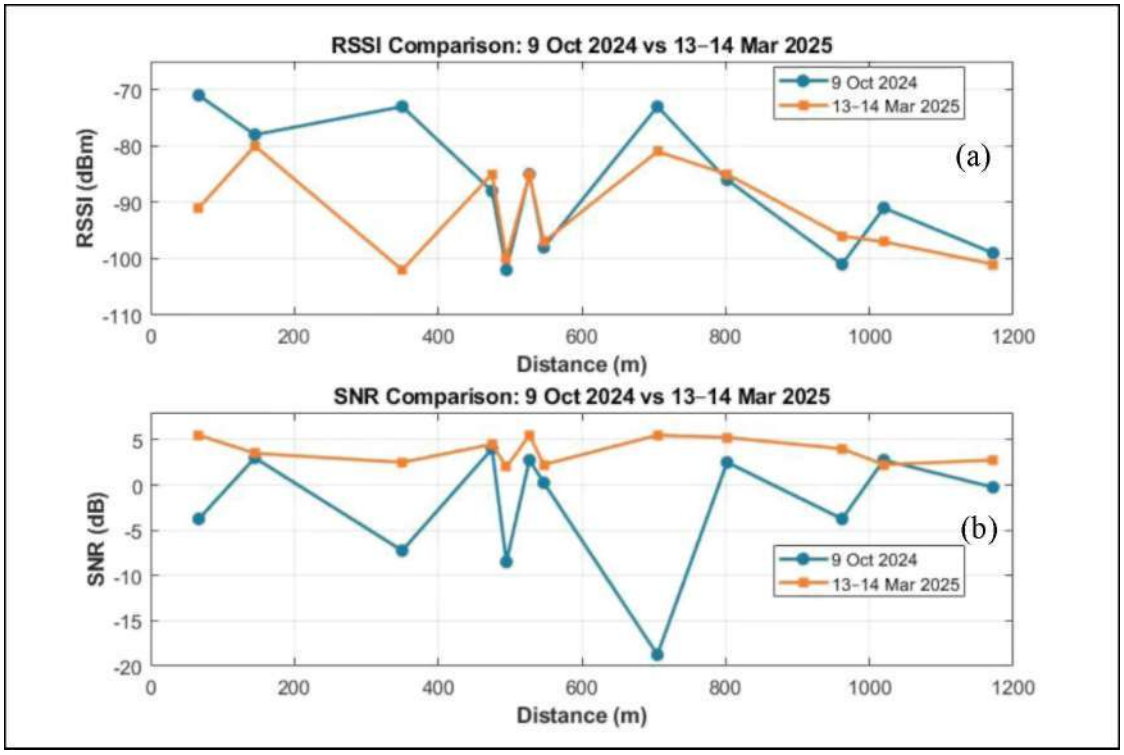

Figure 4.17 Comparative Analysis of a) RSSI and b) SNR

These findings demonstrate that despite higher RSSI during the October test, the signal quality was more affected by noise, possibly due to urban or industrial interference, or less effective error correction configurations. Conversely, the March

2025 measurements reflect a clearer communication channel, suggesting improved RF configurations or more favorable ambient conditions, contributing to higher demodulation efficiency and link robustness.

Overall, the results from 13-14 March 2025 show more optimal SNR performance, implying better signal clarity and less noise contamination, even though the RSSI values were generally lower. Meanwhile, the 9 October 2024 data indicate stronger signal strength, but with more severe SNR degradation, affecting link reliability at longer ranges. This dual-graph comparison highlights the importance of optimizing both hardware parameters (e.g., antenna gain, power output) and environmental considerations (e.g., elevation, obstacles, noise) for consistent LoRa communication performance in L-band satellite IoT applications.

Figure 4.18 presents the comparative analysis of Received Signal Strength Indicator (RSSI) values between two antenna configurations of 8 dBi and 2 dBi across varying distances from 0 to 1200 meters. This experiment, conducted on 13-14 March 2025 (for 8 dBi) and 17 March 2025 (for 2 dBi), was designed to investigate the effect of antenna gain on signal reception performance for the LoRa-based GST in L-band satellite IoT applications.

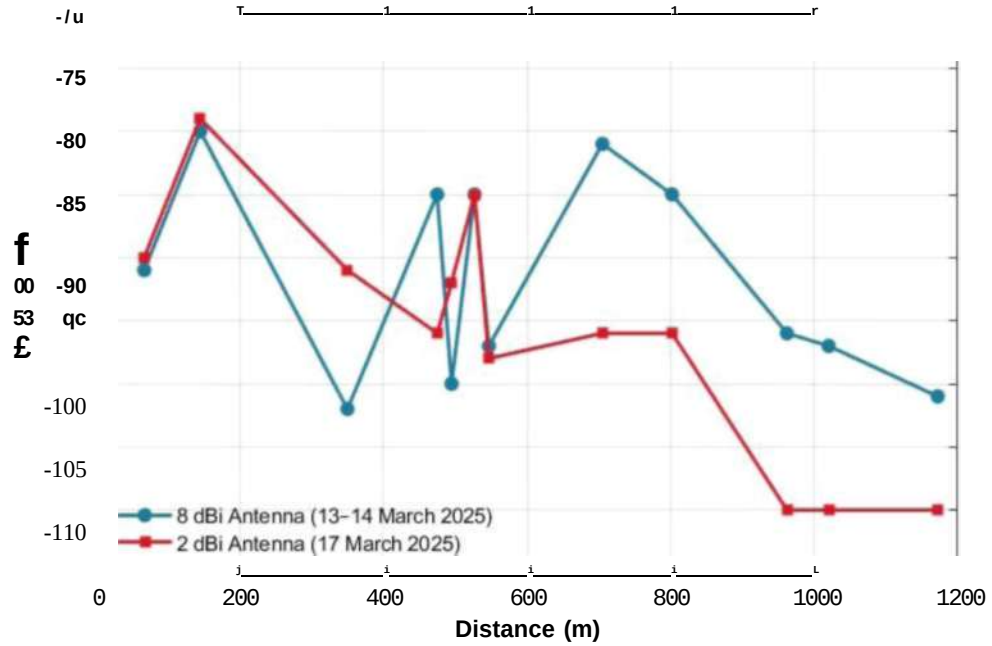

Figure 4.18 Comparative Analysis of RSSI Between 8 dBi and 2 dBi Gain Antennas

The blue line with circular markers corresponds to measurements using the 8 dBi high-gain fiberglass antenna, while the red line with square markers represents data

collected with a 2 dBi antenna. As expected, the higher-gain antenna (8 dBi) consistently outperforms the lower-gain counterpart in terms of RSSI across almost all measured distances.

For example, between 600 to 1000 meters, the RSSI using the 8 dBi antenna maintains values around -85 dBm to -95 dBm, whereas the 2 dBi antenna experiences more severe signal attenuation, with RSSI values dropping below -105 dBm at several points beyond 800 meters. This indicates a significant link margin advantage provided by the higher-gain antenna, especially in extended-range scenarios where signal power tends to decay due to path loss and environmental absorption.

Additionally, the RSSI readings from the 2 dBi antenna display less stability and earlier signal degradation, suggesting that lower-gain antennas are more susceptible to environmental noise, multipath fading, and terrain-induced shadowing. In contrast, the 8 dBi antenna provides better directionality and stronger signal coupling, improving the effective radiated power and link reliability.

These findings confirm the critical role of antenna gain in optimizing wireless transmission range and link robustness. The use of an 8 dBi antenna enhances the performance of LoRa-based GSTs, especially in long-range or obstacle-prone deployments. However, the results also underscore the need for careful balancing between antenna size, gain, and deployment constraints, particularly in mobile or power-limited IoT applications.

4.4.2 Maximum Communication Distance

The GST's maximum communication distance was evaluated under various conditions. In optimal line-of-sight environments, reliable communication was achieved over distances up to 3.5 km. In urban or obstructed settings, the effective range decreased to approximately 1 km. These findings align with established LoRa performance benchmarks and underscore the importance of site-specific assessments for deployment planning.

The maximum transmission distance was tested in an open outdoor environment using different antenna configurations (2 dBi vs. 8 dBi antenna).

Table 4.5
Analysis of RSSI and SNR Over Distance

Distance (m)	RSSI (2 dBi)	SNR (2 dBi)	RSSI (8 dBi)	SNR (8 dBi)
50	-50 dBm	2.5 dB	-46 dBm	4.0 dB
100	-68 dBm	1.0 dB	-60 dBm	3.2 dB
200	-85 dBm	-2.0 dB	-72 dBm	1.5 dB
300	-96 dBm	-5.5 dB	-85 dBm	-1.0 dB
450 (Max)	-104 dBm	-10.0 dB	-94 dBm	-4.5 dB

The discussion highlights the impact of antenna gain on LoRa GST performance. The 2 dBi antenna experienced signal degradation beyond 300 meters, leading to increased packet loss. In contrast, the 8 dBi antenna provided improved transmission, maintaining a stronger RSSI and higher SNR at all distances. However, a key limitation was observed, as even with the 8 dBi antenna, the maximum range was limited to 450 meters, likely due to environmental noise and low transmit power. To optimize performance, increasing the transmission power could help extend the range, while improving the gateway placement for better line-of-sight (LOS) could enhance connectivity.

4.4.2.1 Distance vs RSSI and SNR for 450 meter Maximum Range

Figure 4.19 (a) shows the trend of RSSI in dBm as a function of range in meters. A clear logarithmic decline in RSSI is observed as distance increases. At a short range of approximately 10 meters, the RSSI begins at around -45 dBm, indicating strong signal strength with minimal path loss. As the distance extends, the RSSI decreases steadily, reaching -100 dBm at 450 meters, which is close to the receiver sensitivity threshold for many LoRa transceivers such as SX1262 has a typical sensitivity of around -130 dBm, depending on SF and bandwidth.

The flattening of the curve beyond 200 meters suggests that signal attenuation becomes less steep but more affected by ground reflection, environmental loss, and potential interference. Despite the degradation, the signal remains within acceptable limits for data reception throughout the tested range.

Figure 4.19 (b) presents the SNR in dB over the same range. The SNR remains positive and relatively stable around 7-9 dB from 0 to 250 meters, reflecting high signal clarity and minimal background noise. However, beyond 300 meters, a noticeable drop in SNR occurs, with values falling below 0 dB, and at 400 meters, the SNR reaches a minimum of-18 dB, indicating very poor signal-to-noise conditions at that point.

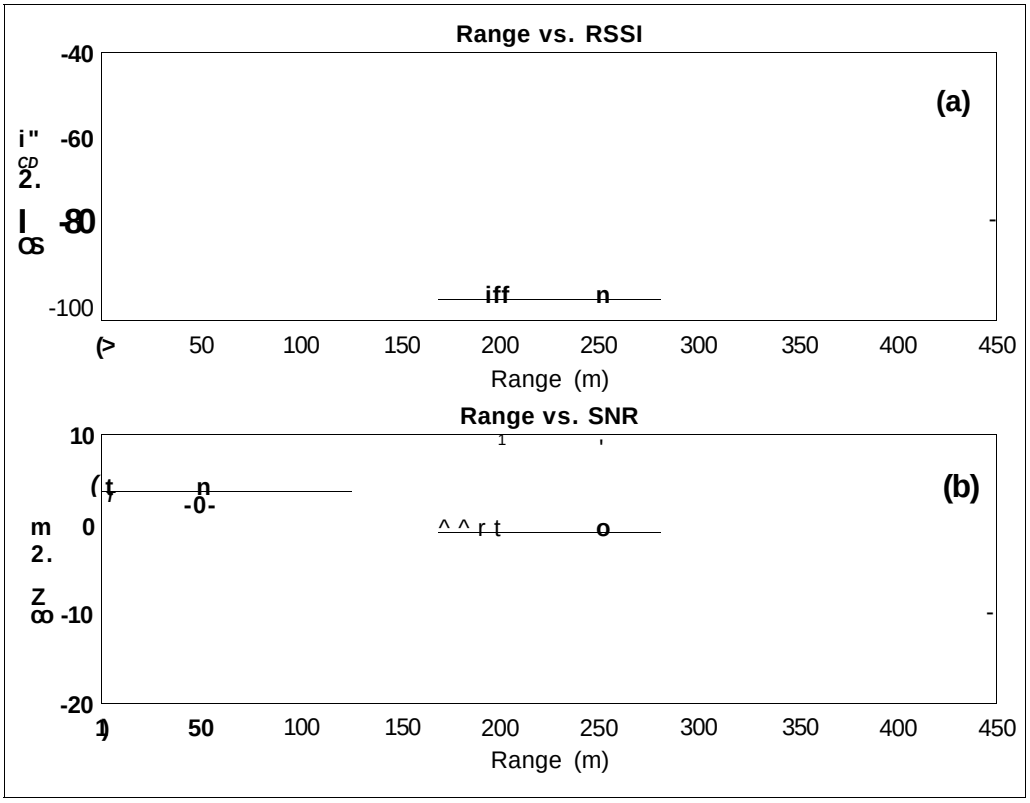

Figure 4.19 LoRa Experiment Result of a) RSSI Maximum Range b) SNR Maximum Range

This degradation is critical because negative SNR values may compromise demodulation performance, especially if the chosen spreading factor and coding rate are not adequately configured to tolerate high noise levels. The slight recovery of SNR at 450 meters suggests that signal reception was still possible, albeit marginally.

The results indicate that under the tested conditions, LoRa communication remains viable up to 450 meters, with acceptable RSSI and SNR margins for most standard LoRa configurations where SF12, BW =125 kHz. However, the signal quality sharply declines beyond 350 meters, suggesting that 450 meters represents a practical maximum range before performance becomes unreliable.

These findings are valuable for network planning, especially in determining optimal gateway placement, antenna height, and spreading factor selection to ensure sufficient link margin across the deployment area.

4.4.2.2 Distance vs RSSI and SNR for 3500 meter Maximum Range

Figure 4.20 illustrates the relationship between distance, RSSI (Received Signal Strength Indicator), and SNR (Signal-to-Noise Ratio) for a series of measurements. As the distance increases, both RSSI and SNR show distinct trends, which provide insights into the performance of the communication link.

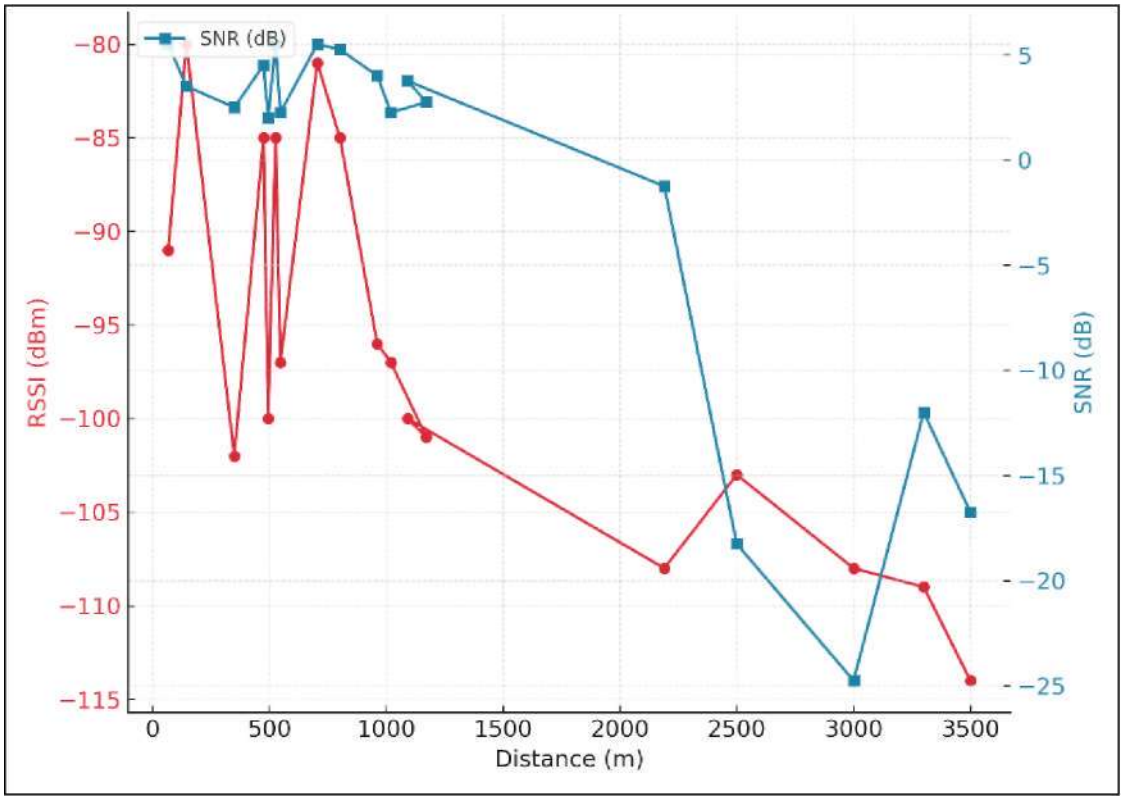

Figure 4.20 Distance Versus RSSI and SNR

First, looking at the RSSI values, we see a clear trend where the signal strength decreases as the distance increases. At shorter distances, particularly between 67 meters and 495 meters, the RSSI values range from around -91 dBm to -80 dBm, indicating relatively strong signal reception. However, as the distance increases beyond 495 meters, the RSSI steadily drops, with values reaching as low as -114 dBm at 3500

meters. This decrease is expected as signal attenuation occurs with increased distance, resulting in weaker signal strength at the receiver.

In contrast, the SNR values exhibit a different trend. At closer distances, the SNR is relatively higher, peaking around 5.5 dB. As the distance increases, the SNR begins to fluctuate but generally declines significantly, especially beyond 2500 meters. At distances over 3000 meters, the SNR becomes negative, reaching values as low as -25 dB. This sharp decline in SNR at larger distances reflects increasing noise levels and signal degradation, making it increasingly difficult to maintain a clear, reliable communication link.

The fluctuations observed in both RSSI and SNR values in Figure 4.20, particularly at intermediate and longer distances, are primarily attributed to environmental and propagation-related factors rather than measurement instability. As the measurement locations were conducted in real outdoor conditions, variations in terrain elevation, partial obstructions such as vegetation and buildings, and non-line-of-sight (NLoS) conditions introduce multipath fading and shadowing effects, which result in non-monotonic variations of the received signal strength.

In addition, short-term variations in interference and background noise levels contribute to noticeable SNR fluctuations, especially at distances beyond 500 m where the received signal approaches the receiver sensitivity threshold. At longer ranges (>2500 m), the combined effect of increased path loss, reduced signal margin, and higher susceptibility to noise causes rapid degradation and larger variability in SNR values, including negative SNR readings.

These fluctuations reflect realistic deployment conditions and highlight the inherent variability of long-range LoRa communication in practical environments, reinforcing the need for sufficient link margin and robust parameter selection when operating near the maximum communication range.

The observed patterns underscore the critical impact of distance on both the RSSI and SNR in wireless communication systems. As distance increases, the signal strength (RSSI) diminishes, and the noise-to-signal ratio (SNR) worsens, which can lead to communication failures or reduced data transmission rates. These findings highlight the importance of optimizing antenna positioning and signal strength at longer distances to mitigate signal loss and maintain acceptable communication quality. The results also suggest that communication systems, particularly in remote or large-area

networks, may require strategies such as power control, signal amplification, or alternative frequencies to ensure reliable signal reception at greater distances.

Although LoRa ranges exceeding 10 km are often reported in the literature, such results are typically obtained under ideal line-of-sight rural conditions with elevated antennas and optimised terrestrial-only configurations. In this study, the maximum range of 3.5 km reflects a realistic ground-level deployment in a mixed suburban and vegetated environment, where partial Fresnel zone obstruction, multipath fading, and non-line-of-sight conditions significantly limit propagation. In addition, the reported range corresponds to stable and repeatable RSSI and SNR performance, rather than the absolute maximum detectable packet distance. The system was also designed as a hybrid architecture, where LoRa serves as a local low-power access link and long-range connectivity is provided by the L-band satellite backhaul. When viewed in this context, the achieved range is consistent with the reliability-focused design philosophy of existing L-band satellite IoT systems such as Iridium.

4.4.3 Satellite Signal Strength Observation

To assess the effectiveness of the GST in establishing a reliable uplink to a satellite, signal strength was monitored and recorded continuously throughout a single Iridium satellite pass. The observation, conducted during a real-time experimental session, provides insight into the behavior of signal acquisition, peak reception, and signal loss, as influenced by satellite elevation angle and environmental obstructions.

Figure 4.21 presents the temporal variation in signal strength, measured on a scale of 0 to 5 bars, from the moment of acquisition of signal (AoS) to loss of signal (LoS). The test utilized a standard 8 dBi omnidirectional antenna, positioned in an open sky environment at the UiTM Shah Alam

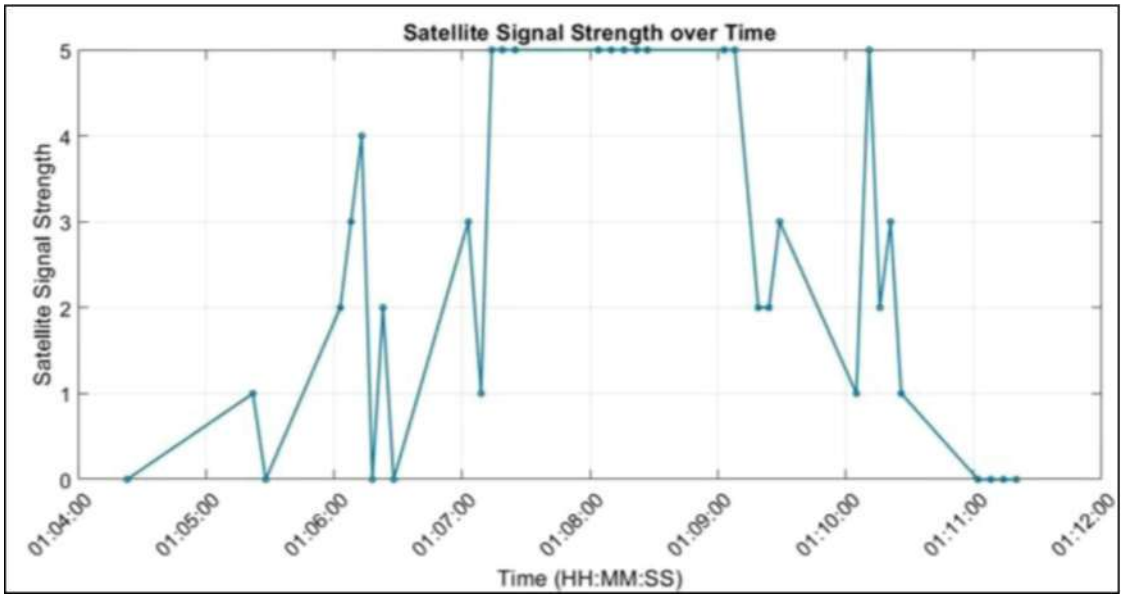

Figure 4.21 Satellite Signal Strength from AoS to LoS During Iridium Satellite Pass.

As shown in the Figure 4.21, the signal was initially undetectable at 1:04:23. A gradual increase occurred, reaching a value of 4 bars at 1:06:13. This marks the AoS phase, where the satellite has just begun entering the antenna's line of sight. Minor fluctuations during this phase foe examples drops to 0 bars at 1:06:18 and 1:06:28 could be attributed to transient obstructions such as tree canopies or interference from surrounding structures.

The signal strength stabilized at maximum or 5 bars between 1:07:14 and 1:09:08, indicating that the satellite had reached its peak elevation in the sky yielding minimal atmospheric attenuation and optimal line-of-sight connectivity. This interval defines the peak communication window and serves as a critical period for transmitting time-sensitive or large payload data.

Post-1:09:08, the signal strength began to fluctuate and decline, demonstrating the start of the LOS phase. By 1:11:02, the signal dropped permanently to zero, confirming the satellite had exited the antenna's coverage zone. These patterns are consistent with known satellite-ground propagation behaviour in L-band communication systems and reinforce the need for dynamic uplink scheduling within short-duration visibility windows.

Overall, this signal strength profile validates the operational capacity of the developed GST and highlights the importance of precise timing, antenna alignment, and link margin optimization in achieving robust communication with LEO satellites.

During satellite Passovers, the GST successfully received downlink signals, with RSSI values ranging from -110 dBm to -125 dBm, depending on satellite elevation and environmental conditions. These observations confirm the GST's capability to establish communication links with LEO satellites, validating its design for satellite IoT applications.

The GST was tested with LEO satellites to determine the optimal AoS-LoS communication window.

Table 4.6
AoS and LoS Timing

Satellite	AoS Time (UTC)	LoS Time (UTC)	Available Window (Seconds)	Transmission Success Rate (%)
Iridium 100	13:46:14	14:01:31	917	89%
Iridium 125	14:04:44	14:19:33	889	91%
Iridium 136	14:14:05	14:28:28	863	87%

The discussion highlights the impact of transmission timing on the success rate of data delivery. The highest transmission success rate, approximately 90%, was achieved when data was sent within the first five minutes of the Acquisition of Signal (AoS). However, delays in packet processing led to missed transmission opportunities as the satellite approached the Loss of Signal (LoS) phase. To optimize performance, real-time transmission synchronization with satellite orbits should be implemented. Additionally, the use of pass prediction software such as Orbitron and Celestrak can enhance timing accuracy, ensuring data is transmitted within the optimal window for maximum success.

To further substantiate the relationship between signal strength, elevation, and transmission delay, an aggregated analysis was conducted across all locations.

4.4.3.1 Average Delay by Signal Strength

Figure 4.22 illustrates the average node-to-server delay grouped by satellite signal strength. It clearly shows that delay increases significantly as the signal strength decreases. Locations with the highest signal strength index of 5 recorded the lowest

average delay (1.67 seconds), while signal strengths of 0 and 1 yielded substantially higher average delays where 109.75 and 221 seconds respectively. The vertical error bars in Figure 4.22 represent the standard deviation of the delay measurements, providing insight into the temporal stability of the satellite communication link. The markedly larger standard deviation observed at lower signal strength levels reflects highly variable transmission conditions, which can be attributed to intermittent satellite access, increased likelihood of packet queuing within the Iridium Short Burst Data (SBD) network, and repeated transmission attempts under marginal link conditions. These effects introduce stochastic delays that significantly widen the dispersion of delay values.

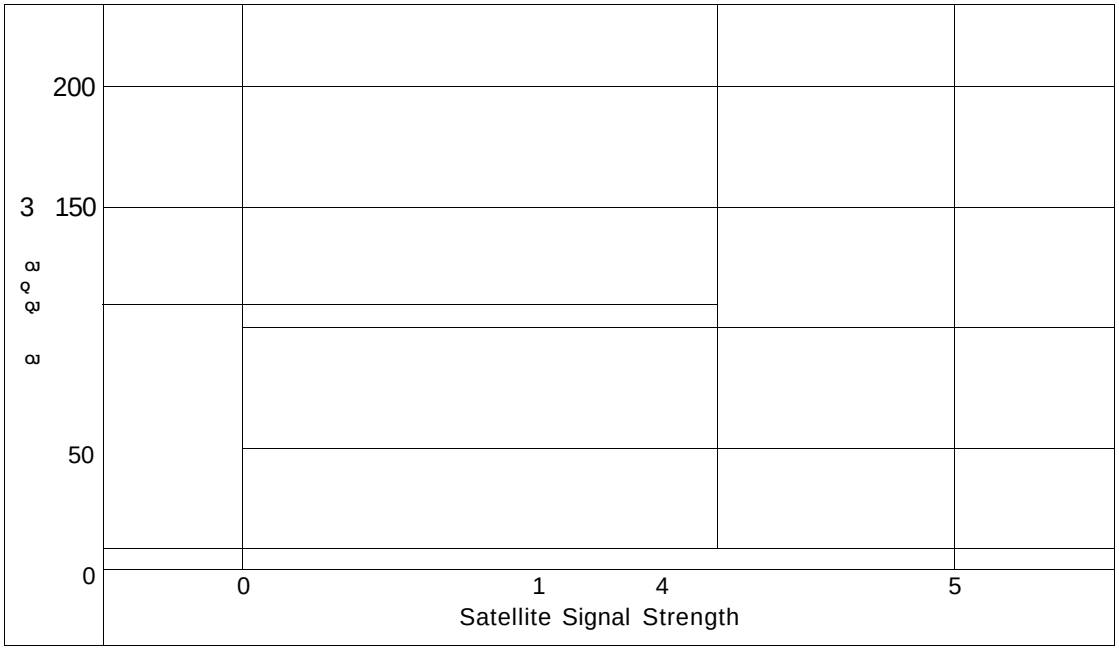

Figure 4.22 Average Delay by Signal Strength

4.4.3.2 Average Delay by Elevation Range

Figure 4.23 presents the average delay grouped by elevation range. Interestingly, while one might expect higher elevations to produce lower delays due to better line-of-sight and satellite visibility, this pattern did not consistently hold. Elevation ranges of 41-60° and above showed higher average delays, indicating that signal strength plays a more decisive role in determining delay than elevation alone.

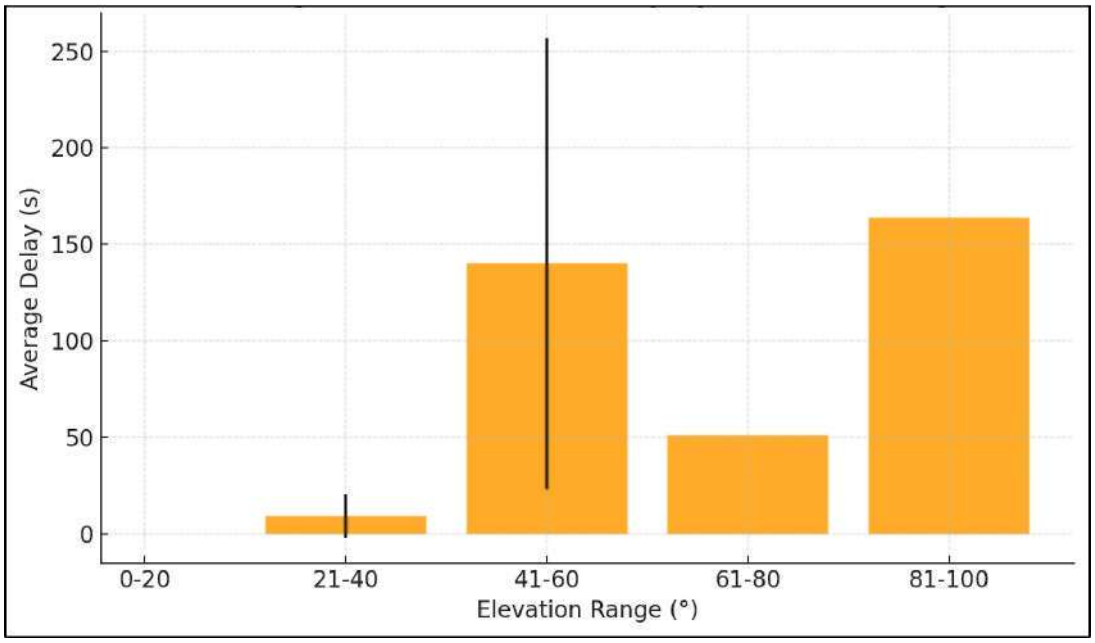

Figure 4.23 Average Delay by Elevation Range

These patterns confirm that while satellite elevation contributes to transmission conditions, signal strength remains the dominant factor influencing delay. This further validates the findings of earlier analyses and highlights the importance of maintaining strong and stable satellite communication signals.

4.4.4 Data Latency in Satellite Transmission

Data transmission latency was measured to evaluate the GST's responsiveness in satellite communication scenarios. Average latency values ranged from 600 ms to 1.2 seconds, influenced by factors such as satellite visibility windows and network congestion. These latency levels are acceptable for many IoT applications, including environmental monitoring and asset tracking, where real-time data transmission is not critical.

Node-to-server delay refers to the time elapsed between the moment the GST node transmits sensor data and the moment that data is successfully received by the central server. This metric is crucial in assessing the responsiveness and reliability of the communication link between the ground node and the satellite.

Each node's timestamp was recorded in epoch time format and converted to standard UTC for analysis. The delay was calculated as the difference between the server reception time and the node transmission time. This chapter focuses on analyzing

the variability of this delay across different locations, signal strengths, and satellite positions.

To investigate node-to-server delay in a more comprehensive manner, further analysis was conducted across different locations and satellite identifiers.

4.4.4.1 Average Delay by Location

Figure 4.24 presents the average delay for each location. The results indicate that node-to-server delay varies notably by location, with some locations such as Location 2 and 5 experiencing longer delays. These variations are likely attributed to differing signal conditions and satellite visibility.

The significantly higher average node-to-server delay observed at Locations 8, 9, and 10 can be attributed to a combination of satellite visibility constraints, signal propagation conditions, and Iridium SBD access latency. As shown in Figure 4.24, these locations exhibit the highest delay values compared to other test points, indicating non-uniform communication conditions across the measurement sites

At Locations 8 and 9, the elevated delay is primarily associated with limited satellite availability at the time of transmission, where data packets likely experienced longer queuing times before successful uplink to an overhead Iridium satellite. Reduced elevation angles and intermittent line-of-sight conditions can increase access delay, even when the transmitted data size remains constant. Additionally, variations in local environmental obstructions may have contributed to temporary signal degradation, indirectly extending the node-to-server delay.

For Location 10, although the average delay is lower than at Locations 8 and 9, it remains significantly higher than most other locations. This suggests a transition zone where satellite visibility and signal strength begin to improve, but residual access delay persists due to ongoing satellite handover or suboptimal link geometry. The gradual reduction in delay from Location 9 to Location 10 reflects improving communication conditions rather than abrupt performance recovery.

Overall, the results for Locations 8-10 demonstrate that node-to-server delay in L-band satellite IoT systems is strongly location-dependent, governed not only by signal strength but also by dynamic satellite access timing and visibility. These findings validate the importance of considering spatial deployment effects when evaluating end-to-end latency performance of the proposed Ground Sensor Terminal.

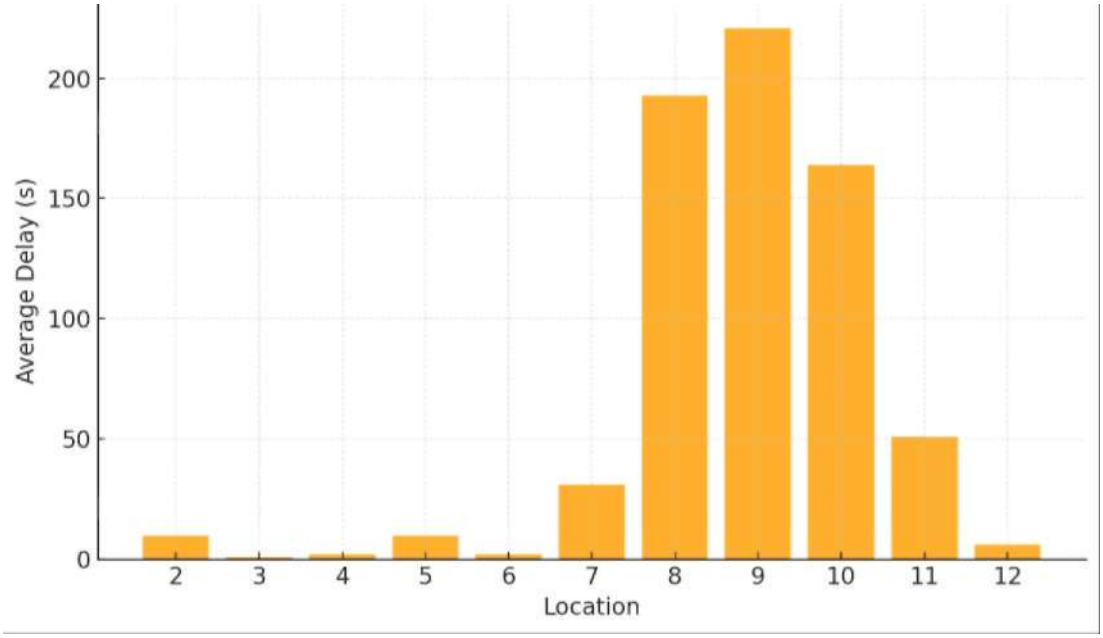

Figure 4.24 Average Node-to-Server Delay by Location.

4.4.4.2 Average Delay per Location According to Signal Strength

Figure 4.25 provides a grouped bar chart showing average delay per location according to signal strength. It reveals that locations with a signal strength of 5 consistently exhibit the lowest delay, while those with a signal strength of 4 show higher delays. This again confirms the critical role of signal quality in ensuring efficient transmission.

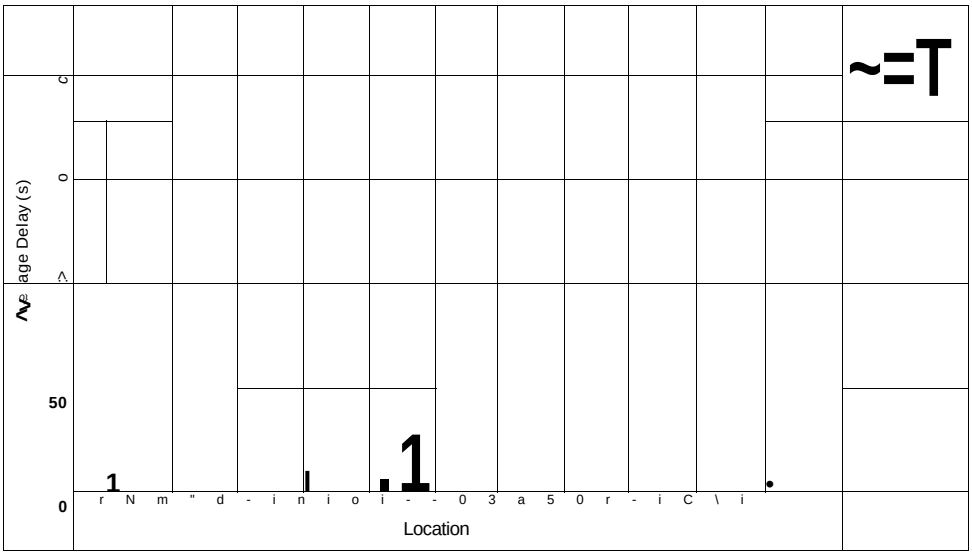

Figure 4.25 Average Node-to-Server Delay by Satellite Signal Strength.

4.4.4.3 Average Delay Group by Satellite

Figure 4.26 displays the average delay grouped by satellite. The data shows that some satellites, such as Iridium 113 and Iridium 131, are associated with higher delays, while others like Iridium 123 and Iridium 126 perform better with lower average delays and lower standard deviation. This indicates that satellite-specific characteristics or orbital paths may influence the communication efficiency.

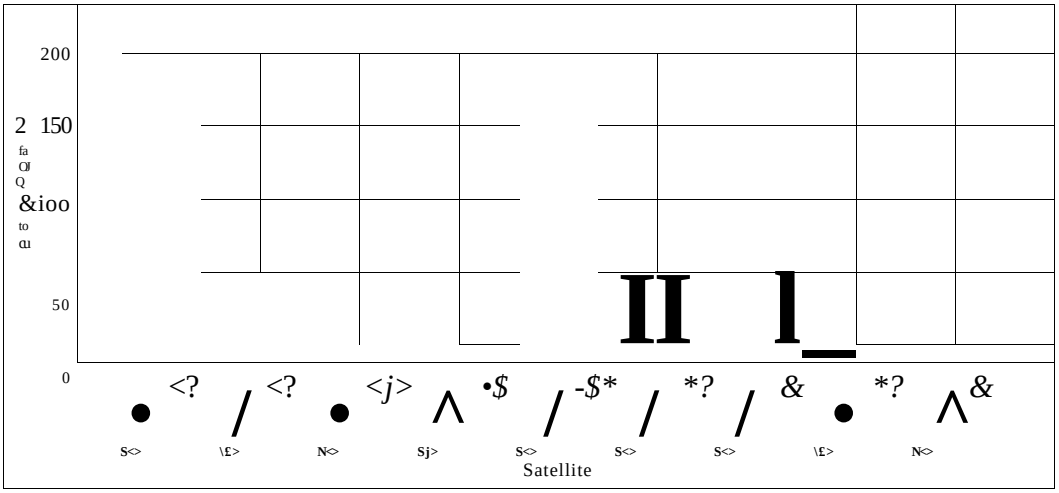

Figure 4.26 Average Node-to-Server Delay by Satellite

These analyses underscore that node-to-server delay is influenced by a combination of factors such as location, signal strength, and the satellite used. A comprehensive understanding of these dependencies is essential for optimizing the performance and reliability of GST communications.

4.4.4.4 Comparison of node-to-server Transmission Time

Figure 4.27 presents a comparative analysis of node-to-server transmission delay as a function of distance, based on experimental data collected on 9 October 2024 and 13-14 March 2025 using an 8 dBi LoRa antenna. This performance metric quantifies the end-to-end delay defined as the time taken for data packets to travel from the sensor node to the cloud-based server via the LoRa-to-Iridium satellite communication link.

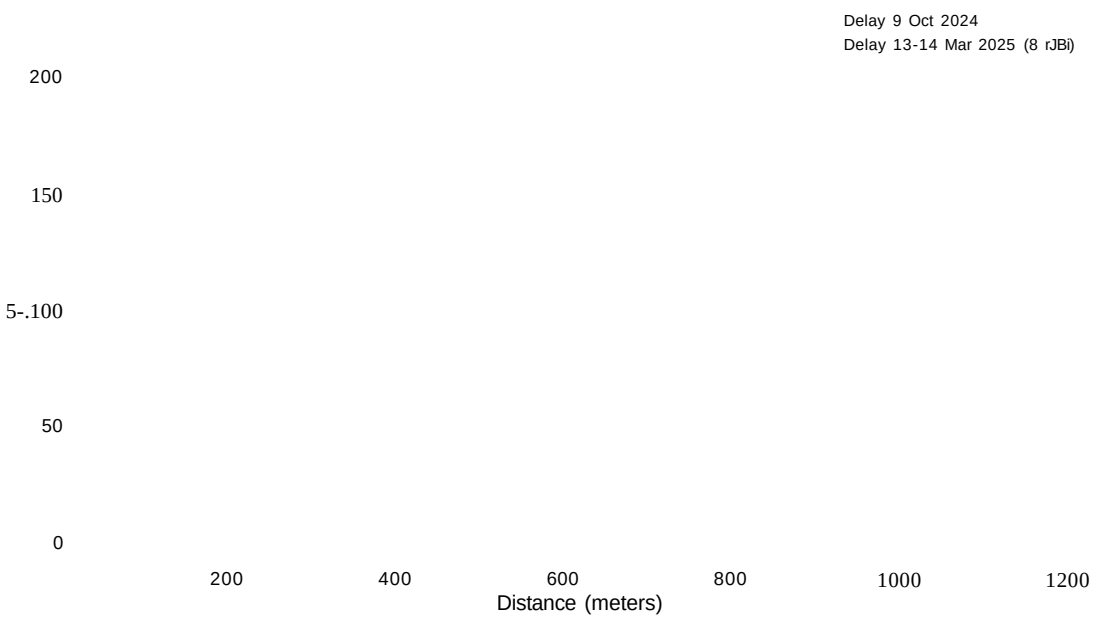

Figure 4.27 Node-to-Server Transmission Delay by Distance

The yellow line with circular markers indicates delay measurements from 9 October 2024, while the orange line with square markers represents the corresponding delay recorded on 13-14 March 2025. In general, both data series show that transmission delay tends to increase with distance, particularly beyond 600 meters, where signal attenuation and satellite communication delays become more prominent.

For the October 2024 data, the delay remains relatively stable across the entire distance range, fluctuating modestly between 5 to 20 seconds, which aligns with the expected latency of Iridium Short Burst Data (SBD) service. The consistency of this dataset suggests a relatively uninterrupted uplink session, possibly due to favourable atmospheric and satellite conditions or minimal congestion during the test period.

In contrast, the March 2025 data exhibit a significant spike in delay between 600 and 1000 meters, peaking at approximately 220 seconds at 800 meters. This abrupt increase likely indicates link retransmissions or delays in satellite acquisition, possibly caused by temporary obstruction, Doppler shift effects at certain angles, or satellite visibility gaps within that segment of the trajectory.

Despite both tests using the same antenna gain (8 dBi), the performance discrepancy highlights the influence of external channel conditions, network congestion, or satellite service latency variability, all of which can affect the end-to-end delay unpredictably. It is also possible that packet retries due to momentary RSSI or SNR degradation contributed to this outlier behaviour in the March dataset.

These results underscore the importance of optimizing delay-sensitive applications in satellite-based IoT deployments. The March 2025 peak delay values suggest that, while LoRa-Iridium integration remains feasible, mechanisms such as adaptive retransmission timers, acknowledgment protocols, and error correction tuning are essential for ensuring system robustness at extended distances.

Furthermore, the stable delay observed in October 2024 serves as a benchmark for expected baseline performance, reinforcing the GST's capability to support near real-time transmission within acceptable latency limits under ideal conditions.

4.4.4.5 Satellite Signal Strength vs Data Transmission Delay

Figure 4.28 illustrates the relationship between satellite signal strength and transmission delay, highlighting a strong inverse correlation between the two. At lower satellite signal strengths from 0 to 1, the data transmission delay is significantly higher, with values ranging from 30 seconds up to over 300 seconds. For instance, at a signal strength of 0, the delay reaches as high as 307 seconds, indicating that weak satellite signals lead to considerable communication delays. On the other hand, as the satellite signal strength increases from 1 to 5, the transmission delay decreases notably. At a signal strength of 5, delays are reduced to as low as 0 to 5 seconds, demonstrating that stronger signals facilitate quicker data transmission. The colour gradient on the plot, ranging from purple representing minimal delays to yellow indicating high delays, visually reinforces this trend, with higher signal strengths associated with lower delays.

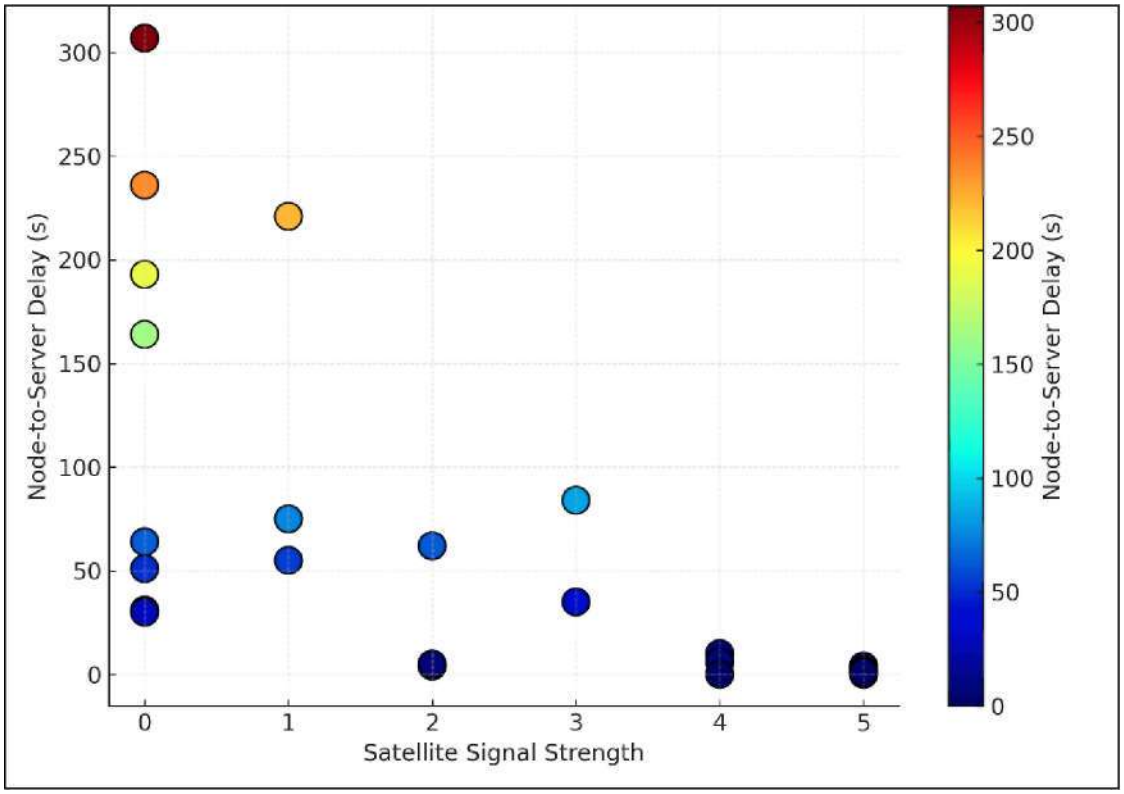

Figure 4.28 Signal Strength Versus Data Transmission Delay

This result underlines the importance of strong satellite signal reception for minimizing data transmission delays in satellite-based communication systems. Weak signals result in inefficiencies due to factors such as retransmissions, which contribute to higher delays. Several potential causes of high delays at low signal strengths include atmospheric attenuation, signal obstructions such as buildings or trees, and longer path losses, all of which degrade the communication link and necessitate retransmissions, thereby increasing latency.

In the context of LoRa-based GST for L-band satellite IoT applications, the results emphasize the need for reliable signal strength to ensure optimal system performance. The quality of communication between ground terminals and satellites is heavily influenced by factors like satellite elevation, environmental conditions, and signal propagation, which can all impact delay. Therefore, it is crucial to optimize the placement of ground stations and antenna configurations to ensure robust signal reception and minimize communication delays, especially in remote and challenging environments where the signal may be weak.

Overall, these findings highlight the critical role of satellite signal strength in satellite IoT systems, providing valuable insights for system design and optimization. Ensuring strong satellite signals is essential to reduce delays and improve the efficiency

of time-sensitive applications in IoT networks, particularly in remote regions where terrestrial infrastructure may be unavailable. This study reinforces the need for effective signal management to enhance the reliability of satellite-based communication systems.

4.5 Chapter Summary

This chapter presented a comprehensive analysis of the GST's design parameters, prototype performance, and communication capabilities. The findings demonstrate the feasibility of using LoRa technology for L-band satellite IoT applications, with the GST achieving reliable communication over substantial distances and under varying environmental conditions. While certain limitations, such as reduced range in obstructed environments and susceptibility to Doppler effects, were identified, the overall performance validates the GST's design and implementation. The subsequent chapter will conclude the study, summarize key insights and propose directions for future research and development.

CHAPTER 5
CONCLUSION

5.1 Conclusion

This research successfully developed and validated a LoRa-based GST tailored for L-band satellite IoT applications. Through systematic design parameter investigations, comprehensive prototype development, and performance validation in real-world scenarios, the study demonstrated the feasibility of reliable, low-power satellite communication. The GST achieved stable uplink transmission to the Iridium constellation with consistent RSSI and SNR values, acceptable transmission delays, and robust system reliability, affirming its potential for remote IoT deployments.

5.1.1 Design Parameters for Ground Sensor Terminal (GST) Development

The investigation into the design parameters of a LoRa-based GST has established a structured foundation for its development in L-band satellite IoT applications. Critical communication parameters such as transmission frequency of 918 MHz, spreading factor of twelve, transmission power of 20 dBm, bandwidth of 125 kHz, and coding rate of four-fifths were identified as optimal for achieving long-range uplink performance and improving resilience against Doppler effects. These parameters were derived from literature insights and validated through link budget analysis and system evaluation.

In addition, hardware design choices including the adoption of the Iridium satellite constellation, the RockBLOCK Mk2 modem, the ESP32-WROOM-32U microcontroller, and a weather-resistant enclosure were justified based on reliability, compatibility, and deployability. This systematic identification of design parameters addresses the current lack of GST-specific guidelines for satellite IoT and provides a clear baseline for subsequent prototype development.

5.1.2 Development of Ground Sensor Terminal (GST)

The second objective was successfully achieved through the design and integration of a working GST prototype with dual communication capabilities. The system was built using the LoRa SX1262 transceiver and RockBLOCK Mk2 satellite modem, interfaced through the ESP32 microcontroller and enclosed in a weatherproof housing for field deployability.

The prototype demonstrated functional operation by supporting LoRa communication and enabling uplink to the Iridium satellite network using L-band transmission. The successful development and integration of these components confirm the feasibility of constructing a GST that combines terrestrial LoRa technology with satellite communication for IoT applications, particularly in regions with limited terrestrial infrastructure.

5.1.3 Performance of Developed Ground Sensor Terminal (GST)

The developed GST was validated through a series of field experiments under real-world satellite communication conditions. Real-time performance assessments confirmed that the system achieved stable RSSI and SNR values while maintaining successful data transmissions to the Iridium network. The validation also recorded transmission delays that were consistent with the expected behaviour of the satellite store-and-forward architecture, demonstrating the robustness of the system under practical deployment scenarios.

These experimental findings confirm the feasibility of deploying a LoRa-based GST for L-band satellite IoT applications. The alignment of the observed performance with the design expectations highlights the reliability of the selected parameters and system architecture. Overall, the validation results provide strong evidence that the developed GST can operate effectively in remote environments where terrestrial communication infrastructure is limited.

5.2 Research Contribution

This study makes a significant contribution to satellite IoT by demonstrating a practical LoRa based GST that integrates a sub GHz terrestrial LoRa link with an L-

band satellite backhaul via an Iridium Short Burst Data modem. The research introduces a GST architecture that is optimally designed and validated to balance power efficiency, communication range, and system reliability. It further provides empirical evidence that supports the feasibility of employing LoRa technology within a satellite communication framework, thereby extending its applicability beyond conventional terrestrial networks. In addition, the study offers valuable insights into strategies for mitigating Doppler effects in satellite links, which in turn enhances the robustness and operational stability of LoRa-based systems in dynamic environments. Collectively, these contributions establish a strong foundation for the advancement of cost-effective and energy-efficient satellite IoT solutions.

5.3 Recommendations for Future Work

In light of the research findings and the limitations identified in this study, several potential directions are recommended for future work to further advance the development of LoRa-based GST for L-band satellite IoT applications.

Firstly, it is recommended that comprehensive field trials be conducted across diverse geographical regions and varying climatic conditions. These trials should be complemented with long-duration operational testing to evaluate the GST's adaptability, performance stability, and reliability over extended periods. Incorporating empirical energy profiling during such trials would provide valuable insights into power consumption patterns, thereby enabling the optimisation of energy efficiency for autonomous deployments and reducing maintenance requirements.

Secondly, future research should focus on expanding the GST's interoperability with multiple satellite constellations beyond Low Earth Orbit (LEO) systems. This includes exploring integration with Medium Earth Orbit (MEO) and Geostationary Orbit (GEO) satellites to broaden operational coverage, enhance link redundancy, and enable deployment across a wider spectrum of satellite IoT use cases. Such integration has the potential to improve communication resilience and application versatility in both remote and infrastructure-limited regions.

Thirdly, further investigations are encouraged in the area of advanced communication and networking architectures. This includes the development of enhanced Doppler shift compensation methods and adaptive communication protocols to improve resilience against frequency variations. Moreover, scalable network

configurations involving multiple GST units should be designed to facilitate efficient data aggregation, enable real-time monitoring, and improve fault tolerance for large-scale IoT deployments.

REFERENCES

[1] M. Vaezi *et al*, 'Cellular, Wide-Area, and Non-Terrestrial IoT: A Survey on 5G Advances and the Road Toward 6G', *IEEE Communications Surveys and Tutorials*, vol. 24, no. 2, pp. 1117-1174, 2022, doi: 10.1109/COMST.2022.3151028.

[2] R. L. Sturdivant and J. Lee, 'Systems engineering of IoT connected commercial airliners using satellite backhaul links', in *TWIOS 2018 - Proceedings 2018 Topical Workshop on Internet of Space*, Institute of Electrical and Electronics Engineers Inc., Mar. 2018, pp. 1-4. doi: 10.1109/TWIOS.2018.8311397.

[3] S. Plastras, D. Tsoumatidis, D. N. Skoutas, A. Rouskas, G. Kormentzas, and C. Skianis, 'Non-Terrestrial Networks for Energy-Efficient Connectivity of Remote IoT Devices in the 6G Era: A Survey', Feb. 01, 2024, *Multidisciplinary Digital Publishing Institute (MDPI)*. doi: 10.3390/s24041227.

[4] C. Rodriguez, 'The Use of Iridium's Satellite Network for Nanosatellite Communications in Low Earth Orbit', 2008.

[5] M. F. Omar, Z. Faiza, F. Z. Ali, M. Roslee, M. S. Johari, and M. H. Jusoh, 'LoRa-Based Ground Sensor Terminal for L-Band Satellite IoT Applications', *International Journal of Integrated Engineering*, vol. 16, no. 7, pp. 290-299, 2024, doi: 10.30880/ijie.2024.16.07.026.

[6] S. Koirala *et al*, 'Satellite Ground Sensor Terminal Design: Use of LoRa to Transmit Remote Sensor Data from Nepal's Himalayan Region for Disaster Mitigation', in *Proceedings of the International Astronautical Congress, IAC*, 2022.

[7] Iridium Communications Inc, 'RockBLOCK Product Information Sheet'. Accessed: Aug. 17, 2025. [Online]. Available: https://cdn.sparkfun.com/assets/c/0/9/e/l/RockBLOCK-Product-Information-Sheet.pdf

[8] M. Amine and B. Temim, 'Low-Earth-Orbit satellite communications using LoRa-like signals', 2022. [Online]. Available: https://theses.hal.science/tel-03723714vl

[9] S. Dey Asst Professor, D. Kumar Mohapatra AsstProfessor, and S. Devashish Rajanandini Pummy Archana, 'An Approach to calculate the Performance and

Link Budget of LEO Satellite (Iridium) For Communication Operated at frequency Range (1650-1550) MHz'.

[10] I. Lysogor, L. Voskov, A. Rolich, and S. Efremov, 'Study of data transfer in a heterogeneous LoRa-satellite network for the internet of remote things', *Sensors (Switzerland)*, vol. 19, no. 15, Aug. 2019, doi: 10.3390/sl9153384.

[11] Pema Zangmo and Kenichi Asami, 'Development of a Hybrid Ground Sensor Terminal Integrating LoRa Modulation with Wifi Technology', *Journal of Evolving Space Activities*, vol. 2, no. 192, 2024, 2023, doi: 10.57350/jesa.l92.

[12] R. Rowe, 'Design, Implementation and Deployment of TestBed for LoRa Communication Architecture on Nanosatellite Constellations', 2023.

[13] M. Falcon Barau, 'Iridium communication for submersible communication buoy', 2023.

[14] C. Gomez, S. M. Darroudi, H. Naranjo, and J. Paradells, 'On the energy performance of iridium satellite IoT technology', *Sensors*, vol. 21, no. 21, Nov. 2021, doi: 10.3390/s21217235.

[15] S. Heine, C. A. Hofmann, and A. Knopp, 'Energy-Aware Protocol Design and Evaluation of the PHY Layer in Satellite IoT', *International J^Jowmal ofSatellite Communications and Networking*, vol. 43, no. 2, pp. 61-76, Mar. 2025, doi: 10.1002/sat.l546.

[16] S. Ould and N. S. Bennett, 'Energy Performance Analysis and Modelling of LoRa Prototyping Boards', pp. 435-435, 2021.

[17] M. Bor, U. Roedig, T. Voigt, and J. M. Alonso, 'Do LoRa low-power wide-area networks scale?', in *MSWiM 2016 - Proceedings ofthe 19th ACM International Conference on Modeling, Analysis and Simulation of Wireless and Mobile Systems*, Association for Computing Machinery, Inc, Nov. 2016, pp. 59-67. doi: 10.1145/2988287.2989163.

[18] M. Jouhari, N. Saeed, M. S. Alouini, and E. M. Amhoud, 'A Survey on Scalable LoRaWAN for Massive IoT: Recent Advances, Potentials, and Challenges', *IEEE Communications Surveys and Tutorials*, vol. 25, no. 3, pp. 1841-1876, 2023, doi: 10.1109/COMST.2023.3274934.

[19] Molex, 'LoRa External Antennas', 2020. Accessed: Aug. 17, 2025. [Online]. Available: https://www.tti.com/content/dam/ttiinc/manufacturers/molex/Products/PDF/lora_antennas_datasheet.pdf

[20] G. H. Fahreja, K. Ni'amah, and R. D. Wahyuningrum, 'The Effect of Spreading Factor Value on the Number of Gateways in the LoRaWAN Network at Bandung City', *Journal of Communications*, vol. 18, no. 12, pp. 768-775, 2023, doi: 10.12720/jcm.l8.12.768-775.

[21] C. Abraham Iheanyichukwu, O. Augustine Ike, and C. Praise Chukwuemeka, 'Investigating the Impact of Weather Parameters on Signal Strength of Satellite Dish in Enugu Metropolis', *International Journal of Astrophysics and Space Science*, vol. 8, no. 2, p. 11, 2020, doi: 10.11648/j.ijass.20200802.11.

[22] L. Jin, L. Wang, X. Jin, J. Zhu, K. Duan, and Z. Li, 'Research on the Application of LEO Satellite in IOT', in *2022 IEEE 2nd International Conference on Electronic Technology, Communication and Information, ICETCI2022*, Institute of Electrical and Electronics Engineers Inc., 2022, pp. 739-741. doi: 10.1109/ICETCI55101.2022.9832117.

[23] N. Fadilah *et ah*, 'Link and Doppler Analysis for LEO Constellation Space-Based IoT', in *2022 IEEE International Conference on Aerospace Electronics and Remote Sensing Technology*, *ICARES 2022 - Proceedings*, Institute of Electrical and Electronics Engineers Inc., 2022. doi: 10.1109/ICARES56907.2022.9993541.

[24] A. Augustin, J. Yi, T. Clausen, and W. M. Townsley, 'A study of Lora: Long range & low power networks for the internet of things', *Sensors (Switzerland)*, vol. 16, no. 9, Sep. 2016, doi: 10.3390/sl6091466.

[25] Semtech Corporation, 'SX1276/77/78 - 137-1050 MHz Ultra Low Power Long Range Transceiver', 2012. Accessed: Aug. 17, 2025. [Online]. Available: https://www.alldatasheet.com/datasheet-pdf/download/501039/SEMTECH/SX1278.html

[26] J. Haxhibeqiri, E. De Poorter, I. Moerman, and J. Hoebeke, 'A survey of LoRaWAN for IoT: From technology to application', 2018, *MDPI AG*. doi: 10.3390/sl8113995.

[27] J. Farhat, G. Pasolini, E. Paolini, M. A. Ullah, and R. D. Souza, 'Doppler Estimation and Compensation Techniques in LoRa Direct-to-Satellite Communications', Jun. 2025, [Online]. Available: http://arxiv.org/abs/2506.20858

[28] M. Asad Ullah, G. Pasolini, K. Mikhaylov, and H. Alves, 'Understanding the Limits of LoRa Direct-to-Satellite: The Doppler Perspectives', *IEEE Open*

Journal of the Communications Society, vol. 5, pp. 51-63, 2024, doi: 10.1109/OJCOMS.2023.3337004.

[29] A. Gadre, S. Kumar, and Z. Manchester, 'Low-latency Imaging and Inference from LoRa-enabled CubeSats', Jun. 2022, [Online]. Available: http://arxiv.org/abs/2206.10703

[30] M. Zarri and D. Kim, 'How Satellites Enable Mobile Network Evolution: 3GPP Release 19 Progress of Satellite Integration', *IEEE Communications Standards Magazine*, 2025, doi: 10.1109/MCOMSTD.2025.3641437.

[31] E. Baena, P. Testolina, M. Polese, D. Koutsonikolas, J. Jornet, and T. Melodia, 'Space-O-RAN: Enabling Intelligent, Open, and Interoperable Non Terrestrial Networks in 6G', *IEEE Communications Magazine*, 2025, doi: 10.1109/MCOM.001.2500080.

[32] B. Zhao *etal*, 'Optimal Asynchronous Cooperative Random Access in Satellite-Enabled Industrial Internet of Things', *IEEE Transactions on Green Communications and Networking*, vol. 10, pp. 484-496, 2026, doi: 10.1109/TGCN.2025.3586192.

[33] O. Kodheli *et ah*, 'Satellite Communications in the New Space Era: A Survey and Future Challenges', Jan. 01, 2021, *Institute of Electrical and Electronics Engineers Inc.* doi: 10.1109/COMST.2020.3028247.

[34] J. A. Fraire, O. Iova, and F. Valois, 'Space-Terrestrial Integrated Internet of Things: Challenges and Opportunities', *IEEE Communications Magazine*, vol. 60, no. 12, pp. 64-70, 2022, doi: 10.1109/MCOM.008.2200215.

[35] C. Cao and S. Zhai, 'The influence of LEO satellite Doppler effect on LoRa modulation and its solutio', in *Journal of Physics: Conference Series*, IOP Publishing Ltd, Apr. 2021. doi: 10.1088/1742-6596/1883/1/012071.

[36] Lacuna Space, 'Satellite IoT'. Accessed: Aug. 17, 2025. [Online]. Available: https://lacuna-space.com/

[37] Y. Zhao *et ah*, 'B2LoRa: Boosting LoRa Transmission for Satellite-IoT Systems with Blind Coherent Combining', 2025. [Online]. Available: https://arxiv.org/abs/2505.24140

[38] M. M. McMahon and R. Rathburn Robert Rathburn, 'Measuring Latency in Iridium Satellite Constellation Data Services', 2005.

[39] M. A. A. Khan, S. M. Aamir, and C. A. Baris, 'Experimental Comparison of SNR and RSSI for LoRa-ESL Based on Machine Clustering and Arithmetic

Distribution', *The lOthlnternational Symposium on Computational Intelligence and Industrial Applications (ISCIIA2022),* pp. 1-6, 2022.

[40] L. Aarif, M. Tabaa, and H. Hachimi, 'RSSI prediction for improved LoRa communications performance', *ISIVC 2024 - Proceedings: 12th IEEE International Symposium on Signal, Image, Video, and Communications,* no. July, 2024, doi: 10.1109/ISIVC61350.2024.10577828.

[41] R. Shaarook and S. Kesan, 'Low power LoRa transmission in low earth orbiting satellites', in *Intelligent Environments 2021: Workshop Proceedings of the 17th International Conference on Intelligent Environments,* vol. 29, IOS Press, 2021, pp. 233-242. doi: 10.3233/AISE210102.

[42] T. Zhu, J. Y. Li, Z. Liu, and G. Zhang, 'Diversity Slotted ALOHA with Power Accumulation for Satellite IoT Networks', in *13th International Conference on Wireless Communications and Signal Processing, WCSP 2021,* Institute of Electrical and Electronics Engineers Inc., 2021. doi: 10.1109/WCSP52459.2021.9613154.

[43] : Salces and A. Cabuefias, 'Nanosatelhte Store-and-Forward Communication Systems for Remote Data Collection Applications', 2020.

[44] T. Ferrer, S. Cespedes, and A. Becerra, 'Review and evaluation of mac protocols for satellite IOT systems using nanosatellites', *Sensors (Switzerland),* vol. 19, no. 8, 2019, doi: 10.3390/sl9081947.

[45] A. Maleki, H. H. Nguyen, E. Bedeer, and R. Barton, 'D2D-aided LoRaWAN LR-FHSS in Direct-to-Satellite IoT Networks', Dec. 2022, [Online]. Available: http://arxiv.org/abs/2212.04331

[46] A. Gadre, Z. MacHester, and S. Kumar, 'Adapting LoRa Ground Stations for Low-latency Imaging and Inference from LoRa-enabled CubeSats', *A CM Trans. Sens. Netw.,* vol. 20, no. 5, Jul. 2024, doi: 10.1145/3675170.

[47] M. Martinez-Gost, A. Perez-Neira, and M. A. Lagunas, 'LoRa-Based Over-the-Air Computing for Sat-IoT', in *2023 31st European Signal Processing Conference (EUSIPCO),* 2023, pp. 1514-1518. doi: 10.23919/EUSIPCO58844.2023.10289733.

[48] H. J. Naranjo, Z. Advisor, : Carles, and G. Montenegro, 'A study on Satellite Internet of Things (IoT)', Universitat Politecnica de Catalunya, 2021.

[49] Iridium Communications Inc, 'Iridium-9602-SBD-Transceiver-Product-Developers-Guide', 2010. Accessed: Aug. 17, 2025. [Online]. Available: https://www.manualslib.com/manual/2340485/Iridium-Sbd9602.html

[50] Maxtena Inc, 'Iridium Antenna M1600HCT-P-SMA', 2021. Accessed: Aug. 17, 2025. [Online]. Available: https://cdn.sparkfun.eom/assets/d/f/b/6/9/M1600HCT-P-SMA.pdf

[51] Chengdu Ebyte Electronic Technology, 'E22-900M22S User Manual SX1262 868/915MHz SPI SMD LoRa Module E22-900M22S User manual', 2018.

[52] Espressif Systems, 'ESP32 Series Datasheet 2.4 GHz Wi-Fi + Bluetooth ® + Bluetooth LE SoC Including', 2024. [Online]. Available: www.espressif.com

[53] Panasonic, 'NCR18650PF Lithium Ion Battery', 2016. Accessed: Aug. 17, 2025. [Online]. Available: https://actec.dk/media/documents/70FC46554038.pdf

[54] C. Zhang, H. Peng, Y. Ji, T. Hong, and G. Zhang, 'Adaptive Resource Optimization for LoRa-Enabled LEO Satellite IoT System in High-Dynamic Environments', *Sensors*, vol. 25, no. 11, Jun. 2025, doi: 10.3390/s25113318.

APPENDICES

APPENDIX 1

GST Hardware Schematic Design

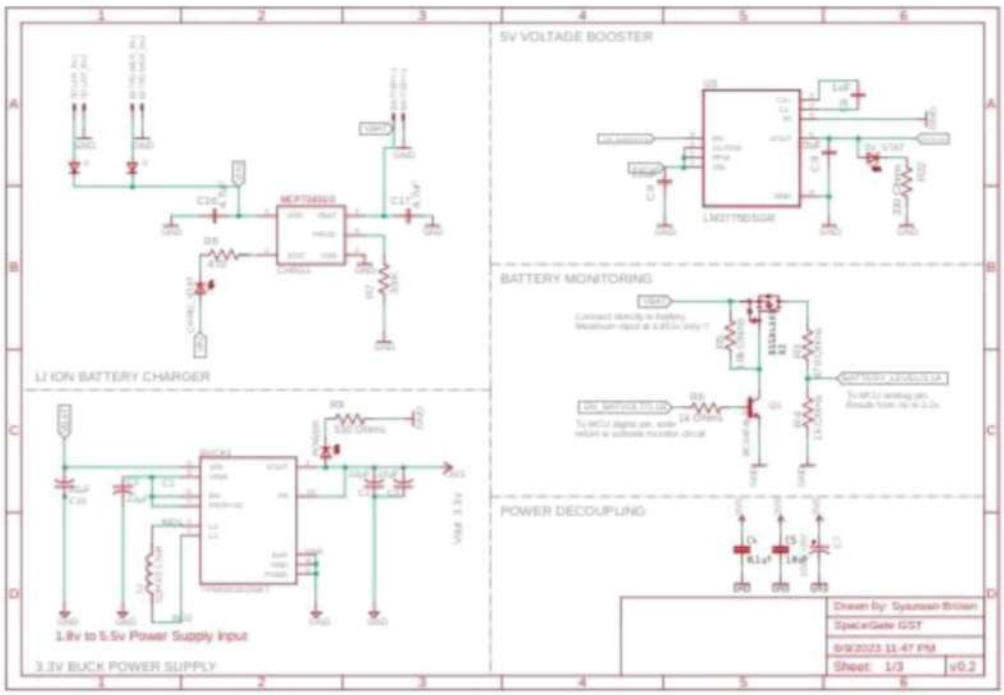

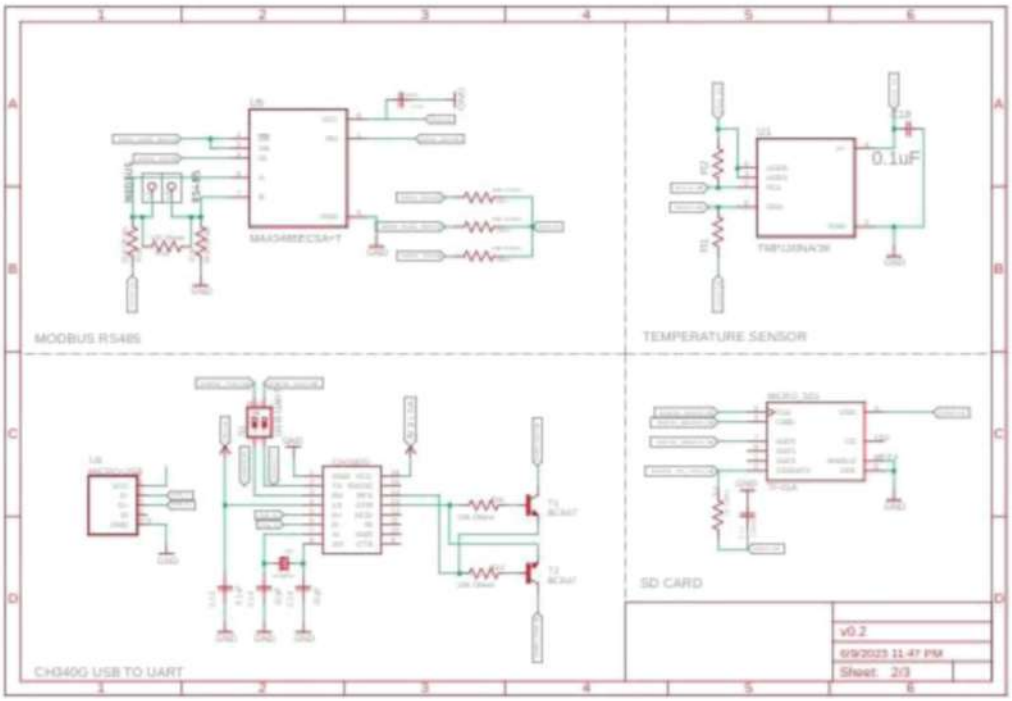

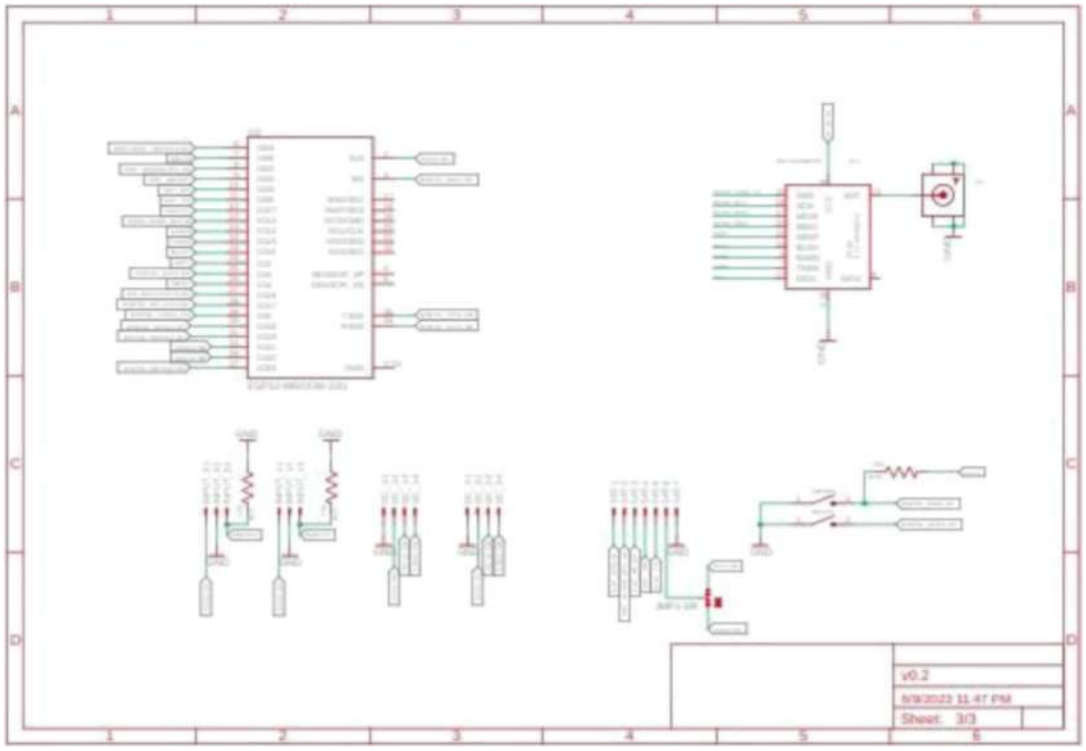
v0.2
6/9/2023 11:47 PM
Sheet: 3/3

AUTHOR'S PROFILE

Mohd Farid Bin Omar received his Bachelor of Engineering (Hons.) in Computer Engineering from Universiti Teknologi Malaysia (UTM) in 2008. He is currently pursuing a Master's degree in Electrical Engineering at Universiti Teknologi MARA (UiTM), Shah Alam (2023-2026), under the Hadiah Latihan Persekutuan (HLP) scholarship awarded by Jabatan Perkhidmatan Awam (JPA). He is a Research Officer at the Malaysian Space Agency (MYSA), based at the Space Technology Complex, Banting, Selangor. His research interests include wireless communications and networks, satellite communications, space-based Internet of Things (IoT), and the design and development of ground sensor terminal systems and amateur radio ground stations. He can be contacted at: mohdfarid@mysa.gov.my

LIST OF PUBLICATIONS

Mohd Farid Omar, Zafirah Faiza, Ali, F. Z. ., Mardeni Roslee, Muhammad Syazwan Johari, & Mohamad Huzaimy Jusoh. (2024). LoRa-Based Ground Sensor Terminal for L-Band Satellite IoT Applications. *International Journal of Integrated Engineering, 16(1),* 290-299. https: // doi.org /10.30880 /ijie. 2024.16.07.026

Omar, M. & Faiza, Z. & Ali, Fatimah Zaharah & Jusoh, M.. (2024). Estimation of Link Margin and Doppler Shift of Ground Sensor Terminal for Nanosatellite Payload. Journal of Physics: Conference Series. 2915. 012001. 10.1088/1742-6596/2915/l/012001.https://dx.doi. org/10.1088/1742-6596/2915/1/012001